

# **Liquid Crystallinity and Alignment of Ionic Self-Assembly Complexes**

Dissertation  
zur Erlangung des akademischen Grades  
“doctor rerum naturalium”  
(Dr. rer. nat.)  
in der Wissenschaftsdisziplin “Physik weicher Materie”  
 (“Soft Matter Physics”)

eingereicht an der  
Mathematisch-Naturwissenschaftlichen Fakultät  
der Universität Potsdam

von  
Yuriy Zakrevskyy

Potsdam 2006



# Table of Contents

<b>1. Introduction and aim of the work.....</b>	<b>1</b>
1.1. What is a liquid crystal?.....	1
1.2. Liquid crystal phases.....	2
1.3. Types of liquid crystals.....	4
1.4. Alignment of liquid crystals.....	6
1.4.1. Director and types of director orientation.....	6
1.4.2. Anchoring energy and mechanisms of surface alignment.....	7
1.4.3. Methods of LC alignment.....	8
1.5. Ionic self-assembly complexes.....	12
1.6. Aim of the work.....	16
<b>2. Materials and experimental techniques.....</b>	<b>17</b>
2.1. Materials and sample preparation.....	17
2.2. Experimental techniques.....	19
2.2.1. Differential scanning calorimetry.....	19
2.2.2. Polarized light microscopy.....	19
2.2.3. X-ray scattering measurements.....	19
2.2.4. Transmission null ellipsometry.....	20
2.2.5. UV-Visible spectral measurements.....	21
2.2.6. IR spectral measurements.....	21
2.2.7. Temperature dependent UV-Visible and IR spectral measurements.....	22
2.2.8. Irradiation conditions.....	24
<b>3. Liquid crystallinity, phase behavior and alignment of benzene-based ISA complexes.</b>	<b>25</b>
3.1. Phase characterization.....	26
3.2. Alignment properties.....	29
3.2.1. Characterization with transmission null ellipsometry.....	29
3.2.2. Characterization with SAXS in reflection mode.....	31
3.3. Ordering within the complex.....	35
3.3.1. Angular-dependent polarized UV spectroscopy investigations.....	35
3.3.2. Angular-dependent polarized IR spectroscopy measurements.....	37
3.4. Ordering within the complex at different temperatures.....	42

3.5. Other complexes.....	49
3.6. Conclusions.....	51
<b>4. Liquid crystallinity and alignment of perylenediimide-based ISA complexes.....</b>	<b>53</b>
4.1. Thermotropic liquid crystalline phase.....	54
4.1.1. Phase characterization.....	54
4.1.2. Alignment in the thermotropic phase.....	59
4.2. Lyotropic liquid crystalline phase.....	62
4.2.1. Phase characterization.....	62
4.2.2. Alignment in the lyotropic phase.....	63
4.3. Conclusions.....	68
<b>5. Liquid crystallinity and photo-alignment of azobenzene-based ISA complexes.....</b>	<b>71</b>
5.1. Phase characterization.....	72
5.2. Aggregation and film-forming properties.....	77
5.3. Photo-alignment properties.....	85
5.4. Conclusions.....	97
<b>6. Summary and conclusions.....</b>	<b>99</b>
<b>Appendix.....</b>	<b>101</b>
<b>Abbreviations and notations.....</b>	<b>109</b>
<b>List of publications.....</b>	<b>111</b>
<b>References.....</b>	<b>114</b>

## Acknowledgments

Here I would like to express my sincere acknowledgments to the people, whose full backing made this thesis possible. First of all I would like to thank to Dr. Stumpe and Fraunhofer Institute for Applied Polymer Research for the financial support. The first person in the list is my adviser Dr. Stumpe, thank you for giving me opportunity, for the assistance, for all discussions, for the personal favors, for the freedom to work on my own and to develop my own ideas. I would like to thank Dr. Faul (Max Planck Institute of Colloids and Interfaces, Potsdam, Germany), the person introduced me into the field of ionic self-assembly, provided materials, helped me with DCS and X-ray measurements and analysis of the data, critically discussed results and interpretation, and spend a lot time correcting my English. I feel obliged to mention the other members of Dr. Faul research group – Dr. Ying Guan and Danielle Franke. Your collaboration with me was my pleasure and honor. Special acknowledgments to Dr. Bernd Smarsly (Max Planck Institute of Colloids and Interfaces, Potsdam, Germany) for some special X-ray measurements and hard work on finding correct models to fit results.

I would like to thank to my wife Svitlana. Thank you for the patience, for the understanding and for the criticism. During last 4 years your support and faith were the most important driving force for me.

At last but not least I would like to thank to all people from the department of polymer photochemistry in the Fraunhofer IAP for the great parties and for a unique atmosphere in the group.

Summer 2006

Yuriy Zakrevskyy



## 1. Introduction and aim of the work

### 1.1. What is a liquid crystal?

It is well known that during the melting of a molecular crystal, which in general is composed of anisotropic molecules, there can occur prior to the formation of the isotropic fluid a stage involving the formation of intermediate phase (or mesophase). For example, the crystals can lose stability with respect to the orientational degree of freedom, i.e. they can lose orientational order in the distribution of the molecules, while still retaining their translational order. In this case the molecules rotate freely while remaining on their original positional sites in the crystal lattice. Such a mesophase is called a plastic crystal and is characteristic of materials whose molecules do not exhibit pronounced anisotropy, e.g. solid methane. The exact opposite will occur if a crystal loses translational order in at least one direction while remaining orientational order. In this case the mesophase remains the anisotropy of almost all its physical properties. Such a mesophase is called a liquid crystal (LC), and is generally characteristic of materials with molecules which are highly anisotropic in shape. Subsequent heating of the mesophase will lead to the break-up of its residual ordering (translational ordering for the plastic crystal and orientational ordering for the liquid crystal), and the material converts to an isotropic liquid.

In literature one can find a little bit other definition of LC phase: there are certain substances which do not directly pass from crystalline solid to isotropic liquid and vice versa but adopt the intermediate structure which flows like a liquid but still possesses the anisotropic physical properties similar to crystalline solids. This definition does not include some types of liquid crystalline materials, e.g. polymeric liquid crystals or liquid crystals involving secondary interactions like hydrogen bonding and metal coordination, which do not really flow like a liquid. When discussing LCs and especially introducing new types of LC materials, one should use exact definition of LC state.

In this work new type of LC materials is introduced. Presence of mesophases in these materials is identified using the definition of a LC state done at the beginning of this section.

## 1.2. Liquid crystal phases

The mesophases can be obtained by imposing no positional order, or imposing positional order in one or two rather than in three directions (see Fig. 1.1):

- ☑ The first case obviously corresponds to a liquid but, there is orientational order, this is not an isotropic liquid. This mesophase is called nematic phase.
- ☑ The second case describes one-dimensional order in three dimensions: the system can be viewed as a set of two-dimensional liquid layers stacked on each other with a well defined spacing. The corresponding phases are called smectic phases.
- ☑ The third case corresponds to two-dimensionally ordered systems in three dimensions. They can be described as a two dimensional array of liquid tubes and are called columnar phases.

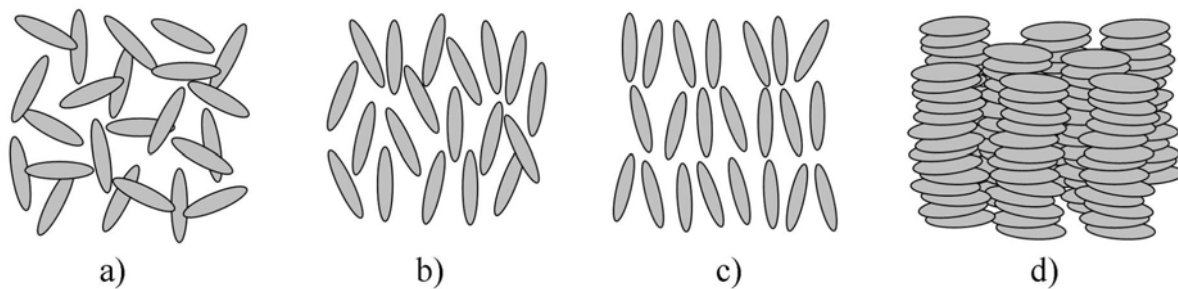


**Fig. 1.1. Schematic representation of (a) isotropic phase, (b) nematic, (c) smectic and (d) columnar liquid crystalline phases.**

Depending on the shape and symmetry there are some additional subclasses of the mentioned phases. The cholesteric mesophase can be considered as a modified form of the nematic, insofar as it has similar molecular packing over intervals of the order of tens and hundreds of molecular dimensions. Depending on the shape of molecules nematic phases can be nematic calamitic (N) and nematic discotic ( $N_D$ ). In the first case molecules are rod-shaped and in the second they are disk-shaped.

Depending on molecular packing within the layers of smectics they are classified as (see Fig. 1.2 for details of order within layers):<sup>[1]</sup> Smectic A (SmA), B (SmB), C (SmC), E (SmE), F (SmF), H (SmH), I (SmI).

Columnar phases are classified depending on packing of columns and ordering within the columns (see Fig. 1.3): nematic columnar ( $N_{col}$ ), disordered hexagonal columnar ( $Col_{hd}$ ),



ordered hexagonal columnar ( $\text{Col}_{\text{ho}}$ ), disordered rectangular columnar ( $\text{Col}_{\text{rd}}$ ), ordered rectangular columnar ( $\text{Col}_{\text{ro}}$ ), tilted columnar phases ( $\text{Col}_{\text{ht}}$  or  $\text{Col}_{\text{rt}}$ ).

These liquid crystalline phases are the mostly happening in nature. However, depending on the structure of building blocks (molecules or molecular aggregates) there is possibility to get a specific packing and a new phase. Detailed nomenclature and classification of liquid crystalline phases is done in <sup>[2(Volume 1, Chap. II)]</sup> with further details in appropriate chapters of the book.

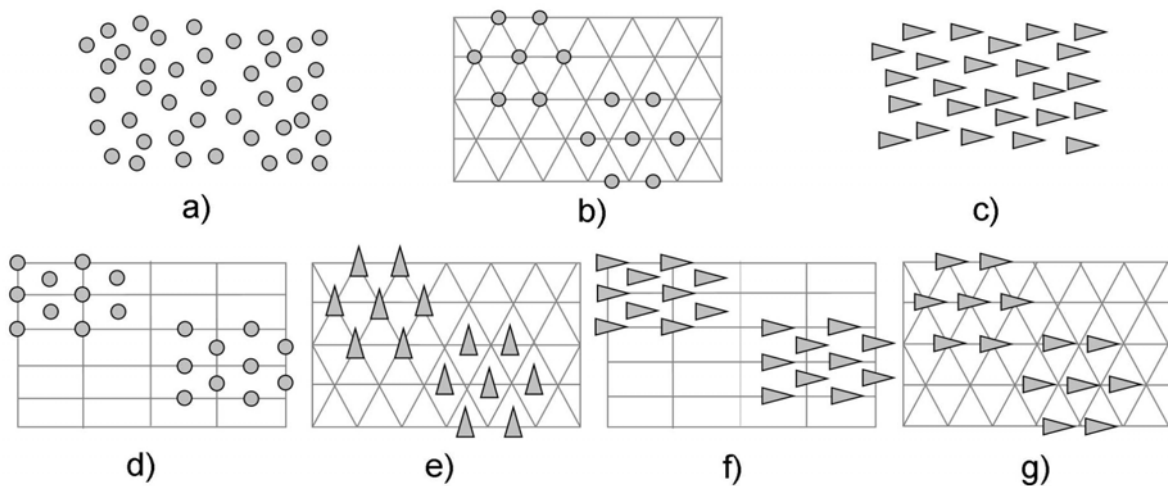


**Fig. 1.2.** Plan view of (a) Smectic A, (b) Smectic B, (c) Smectic C, (d) Smectic E, (e) Smectic F, (f) Smectic H and (g) Smectic I liquid crystalline phases.

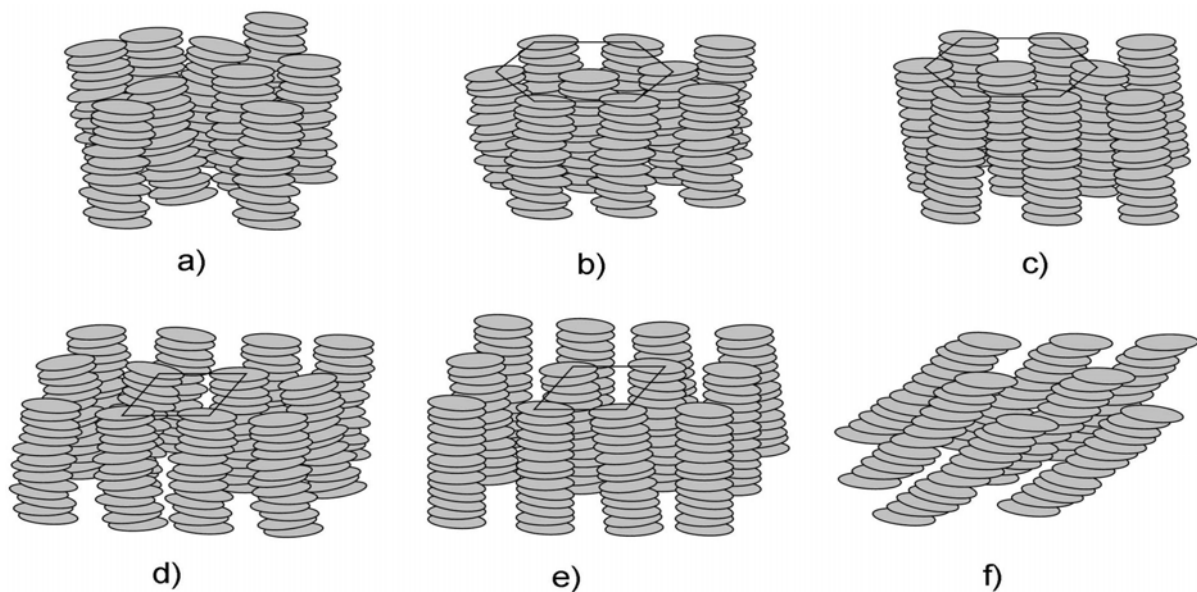


**Fig. 1.3.** Schematic representation of (a) nematic columnar, (b) disordered hexagonal columnar, (c) ordered hexagonal columnar, (d) disordered rectangular columnar, (e) ordered rectangular columnar and (f) tilted columnar liquid crystalline phases.

### 1.3. Types of liquid crystals

As was briefly mentioned in section 1.1 to generate a liquid crystal (LC) one must use anisotropic molecular structure. This concept is already firmly established in literature.<sup>[29(Vol. 1, Chap. VI.)]</sup> The classical way to achieve this is to use elongated (rod- and lath-like) molecules. This type of molecules forms nematic and smectic LC phases. Some other nematic and most columnar phases are often made of disk-like molecules.<sup>[3]</sup> The clear dependence of the mesomorphic properties on the geometrical shape of the molecules and on the combination of repulsive and attractive interactions of the van der Waals type has allowed the derivation of satisfactory models for describing LC systems theoretically.<sup>[4(Vol. 1, Chap. 2)]</sup> In compounds containing strongly polar groups (e.g.  $-\text{CN}$ ,  $-\text{NO}_2$ ) the interaction of permanent and induced electrical dipoles plays a remarkable role in phase formation.<sup>[5]</sup> The reduced symmetry of molecules, that imparts form chirality, leads to a variety of interesting phases that are manifested in the formation of helical ordering of the constituent mesogens.<sup>[6(Chap. 6)]</sup>

Further modifications and complications of the shape of the molecules lead to a variety of different LC phases; to this class belong non-conventional LC materials. The first subgroup is laterally substituted and swallow-tailed liquid crystals.<sup>[29(Vol. 2B, Chap. XI), 7]</sup> Lateral substitution produce a drastic decrease in the mesophase stability, that is, a lowering of the clearing temperatures is observed as the volume of lateral groups increases. The second subgroup is hybrid molecules with a long rod-like rigid core ending with two half-disk moieties.<sup>[8]</sup> To the third subgroup belong liquid-crystalline dimers and oligomers.<sup>[9]</sup> The molecules of such compounds consist of two or more mesogenic groups linked by a flexible spacer. The phase transition properties of these compounds are markedly different to those of conventional low molar mass LCs containing a single mesogenic group and strongly depend on the length and odd-even properties of the flexible spacer. The boundaries between these different types of LC materials are not necessarily always so clear, and sometimes the same compound can be related to two groups at the same time.

A further type of LC materials are the high molecular weight liquid crystals, so-called main-chain and side-chain LC polymers.<sup>[29(Vol.3)]</sup> Any of above-discussed low molecular weight LCs may act as mesogenic group in this type of LCs. A remarkable feature of these compounds is high viscosity, causing a transition to a glassy instead of to a crystalline state.

All types of LCs described above are thermotropic in nature, with liquid crystallinity generated by changes in temperature. Another possible way to generate LC states is by the addition of an appropriate solvent (the most conventional is water) in appropriate amounts,

that is, lyotropic LC materials. Influence of temperature gives additional degree of freedom, but is of secondary importance. The classical representatives of this type of LCs are lyotropic surfactant liquid crystals.<sup>[10]</sup>

In contrast to conventional surfactant mesogens (consisting of distinct hydrophilic and hydrophobic regions within the mesogen) liquid-crystalline chromonic dyes do not exhibit significant surfactant properties.<sup>[11,12]</sup> The molecules are disk-like or plank-like as opposed to rod-like, are aromatic rather than aliphatic, and the hydrophilic ionic or hydrogen-bonding solubilizing groups are arranged around the peripheries of the molecules and not at the ends. The molecules can be regarded as being insoluble in one dimension, and the basic structural unit of all chromonic phases is a molecular stack of some kind, rather than a micelle.

Amphotropic LCs show both thermotropic and lyotropic mesophase formation.<sup>[13]</sup> Nearly all amphotropic compounds possess, beside their conventional form anisotropy, hydrophilic (polar) parts that are well segregated from lipophilic (apolar) moieties.

Furthermore, a variety of new phases with interesting properties can be obtained by introducing specific interactions between molecules. For example, metal-containing LCs, also known as metalomesogens<sup>[14,15,16]</sup>, combine the physical properties exhibited by LCs with the variety and range of metal-based coordination chemistry due to the presence of one or more metals. Geometries and shapes not easily found in organic chemistry can result from the coordinated metal species. Many metal complexes are in an oxidation state that gives coloured compounds, and many have unpaired electrons and exhibit paramagnetism. Charge-transfer<sup>[17]</sup> and hydrogen-bonding interactions are further examples of specific interactions between molecules that influence and even induce the formation of LC phases. Investigations into hydrogen-bonded systems were stimulated since it is a key interaction in chemical and biological processes in nature. A wide variety of structures of molecular liquid-crystalline complexes has been prepared through intermolecular hydrogen bonds.<sup>[29(Vol. 2B, Chap. XVII),18]</sup>

## 1.4. Alignment of liquid crystals

### 1.4.1. Director and types of director orientation

The phenomenon of orientation of liquid crystals by surfaces has been known nearly as long as have liquid crystals themselves.<sup>[19]</sup> The phenomenon has mainly been studied in low-molecular-weight nematic liquid crystals, both because of simplicity of their structure and because of the use of this type of liquid crystal in displays.

In macroscopic physics, the structure of liquid crystalline phases is usually characterized by so-called director  $\vec{n}$ , a unit vector which shows an average orientation of the molecular axes in some macroscopic bulk. The solid surface which is in contact with the mesophase is usually considered to be flat on the macroscopic scale, and the position of the director is determined by polar  $\theta$  and azimuthal  $\varphi$  angles (see Fig. 1.4).

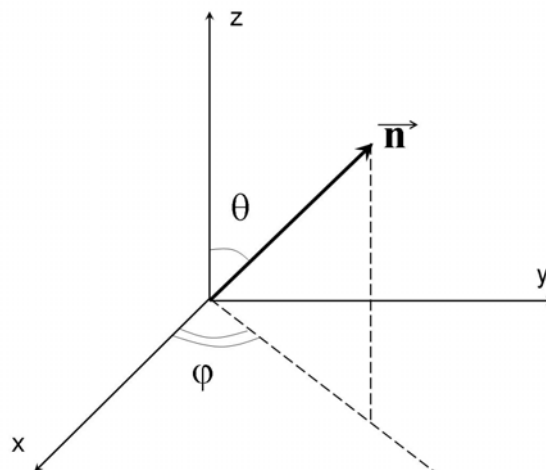


**Fig. 1.4:** Orientation of the director of a liquid crystal at the interface. *xy*-plane is a plane of an interface, e.g. substrate.

In most practical applications, and when examining liquid crystals, sandwich-type cells are used. A flat capillary with a thickness of 1-100  $\mu\text{m}$  and above is formed between two glass plates with or without transparent electrodes. This capillary is filled with a liquid crystal. Depending on orientation of the director of a liquid crystal at the interface boundaries different types of alignment are distinguished: planar ( $\theta=90^\circ$ ), homeotropic ( $\theta=0^\circ$ ), or tilted ( $0^\circ < \theta < 90^\circ$ ).

Depending on orientation of the director of a liquid crystal through the bulk of the cell

different types of alignment are distinguished (see Fig. 1.5): homogeneous (parallel), ( $\theta=90^\circ$ ,  $\varphi=const$ ), homeotropic ( $\theta=0^\circ$ ,  $\varphi=const$ ), twisted ( $\theta=90^\circ$ ,  $\varphi=2\pi z/L$ , where  $z$  – distance from a substrate,  $L$  – pitch of the twist), and hybrid alignment ( $\varphi=const$ , polar angle of the director varies from  $\theta=0^\circ$  at one interface to  $\theta=90^\circ$  at another interface).

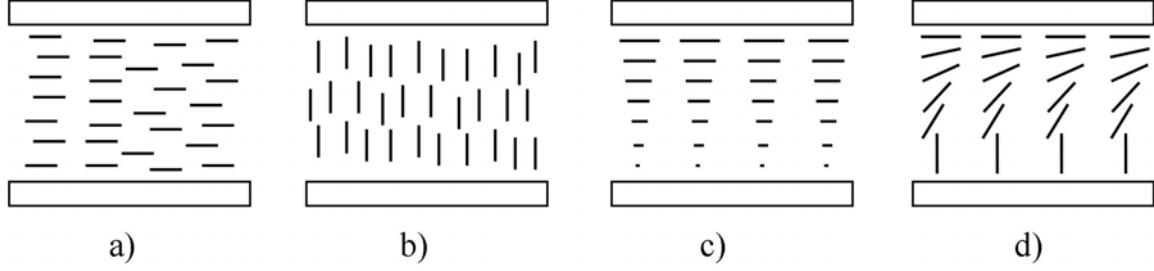


**Fig. 1.5: Types of the alignment in a liquid crystal cell: (a) homogeneous or planar; (b) homeotropic; (c) twisted with  $45^\circ$  twist; and (d) hybrid alignment.**

#### 1.4.2. Anchoring energy and mechanisms of surface alignment

A nematic LC deposited on an aligning substrate spontaneously develops an equilibrium, or easy orientation, at the interface characterized by the polar angle  $\theta=\theta_0$  and the azimuthal angle  $\varphi=\varphi_0$  (see Fig. 1.4). The polar and azimuthal anchoring energies,  $F_p(\theta)$  and  $F_a(\varphi)$ , specify the energy required to deviate the director from  $\theta_0$  and  $\varphi_0$  respectively. These are expressed in their most simple form by the Rapini-Papoular approximation as

$$F_p(\theta) = W_\theta \sin^2(\theta - \theta_0) \quad (1-1)$$

$$F_a(\varphi) = W_\varphi \sin^2(\varphi - \varphi_0) \quad (1-2)$$

where  $W_\theta$  ( $W_\varphi$ ) is the polar (azimuthal) part of the anchoring energy with  $\varphi_0$  ( $\theta_0$ ) fixed. The polar anchoring energy is typically an order of magnitude greater than the azimuthal anchoring energy. For example,  $W_\theta > 10^{-3} \text{ J m}^{-2}$  and  $W_\varphi > 10^{-4} \text{ J m}^{-2}$  for strongly rubbed polyimide.<sup>[20]</sup>

The substrate–LC interactions is phenomenologically described by the ratio of the surface tensions of the surface ( $\gamma_s$ ) and the LC ( $\gamma_{LC}$ ). If  $\gamma_s > \gamma_{LC}$ , the intermolecular LC forces are larger than the surface–LC forces and homeotropic alignment results. Homogeneous alignment is archived when the surface anchoring forces are dominant. The nature of the LC–surface interaction is complex and includes dispersive (Van der Waals),

polar and steric terms as well as orderelastic and ionic terms. Topological factor should also be included. A unique azimuthal orientation normally requires surface treatment of the alignment layer.

### 1.4.3. Methods of LC alignment

To get uniform alignment of a liquid crystal in the cell different methods were applied. The simplest method to get planar orientation is mechanical rubbing of the surface of the glass with paper or cloth. The rubbing creates microrelief in the electrode coating or glass in the form of ridges and troughs, which promotes the orientation of the molecules along these formations. It is very simple, but unfortunately it does not provide a sufficiently strong anchoring of the director to the surface.

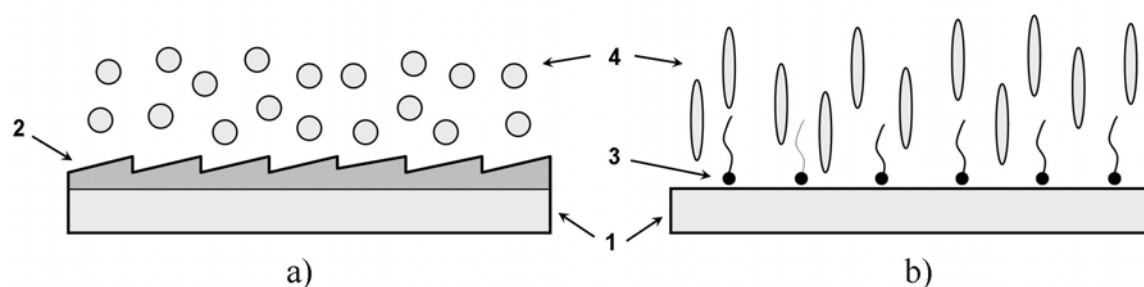


**Fig. 1.6: Illustration of the mechanism for: (a) planar alignment by an obliquely evaporated thin film of a metal, and (b) homeotropic alignment by a monolayer of surfactant molecules. 1 – substrate; 2 – obliquely evaporated film; 3 – molecules of the surfactant material; 4 – nematic liquid crystal molecules.**

Better results of alignment were obtained by evaporation of metals or oxides (e.g. SiO) onto the surface at oblique incidence.<sup>[21]</sup> The mechanism of the planar orientation of nematic liquid crystals by means of obliquely evaporated thin film of metal is illustrated in Fig. 1.6a. Molecules of a nematic liquid crystal align along the obtained grooves. A surface of different geometrical form obtained by photolithographic method was also tested for alignment of liquid crystals. When a nematic LC is in contact with a rectangular surface relief, or a relief in a form of a trapezoid, a homogeneous alignment of the director along the grooves is obtained. In order to explain why longitudinal grooves are conducive to a homogeneous alignment the interaction of a nematic LC with such surface from the view point of continuum theory was studied by Berreman.<sup>[22]</sup>

To achieve a homeotropic orientation of the director, deposition of different surfactants on the substrate is most often used. The mechanism of homeotropic orientation by

a monomolecular layer of a surfactant is demonstrated in Fig. 1.6b. An orienting monolayer can be achieved by withdrawing the substrate from the solution, by polymerization of the organosilicon films directly onto the substrate, and, in particular, by using a plasma discharge. Moreover, surface-active impurities can be introduced directly into the liquid crystal (e.g., lecithin or alkoxybenzoic acid). Treatment of the walls with organometallic complexes also produces a stable homeotropic alignment of LCs.

The orientation of molecules at a given angle to the surface was achieved using layers of SiO produced by oblique evaporation at a very large angle (80-90°) between the normal to the surface and the direction to the source. In this case, the quasi-one-dimensional surface structure is achieved which is oriented at an angle to the surface. This induced a tilt of the nematic LC molecules in the same direction.<sup>[23]</sup>

Alignment of LCs can be obtained by applying strong external electric or magnetic fields.<sup>[24]</sup> Depending on their dielectric or diamagnetic anisotropy, the LC molecules tend to orient themselves in directions parallel or perpendicular to the field. Usually orientation in external fields is utilized in combination with treatment of the substrates.

Hydrodynamic flow also greatly influences the orientation of the nematic director. At the first moment of filling a plane-parallel glass capillary (LC cell) with a LC, capillary forces initiate flow of the liquid. The elongated form LC molecules usually tend to orient their long axes along the direction of the hydrodynamic flow. The disk form LC molecules usually tend to orient their planes along the direction of the hydrodynamic flow. Only when the cell is completely filled with the LC, does the flow disappear and the orientation is then mainly determined by the action of the substrates. Similar effects of alignment can also be achieved by shearing of the substrates (shear force alignment). If a liquid crystal is very viscous the obtained alignment can preserve after flow or shear force is stopped.

One should note that all methods mentioned in this section work well for nematic phase LCs. Alignment of smectic and columnar phase LCs is influenced by their internal ordering. For example, it is very difficult to obtain uniform homeotropic orientation of a smectic LC even on very flat and thoroughly purified surfaces. Due to specific elastic properties of smectic LC phases solid surface inhomogeneities initiate disturbances in the smectic layers, which penetrate into the bulk of the mesophase at very large distance (~1 μm). However it is easy to obtain planer homogeneous alignment of a smectic LC. In this case the layered structure is undisturbed. Columnar LC phases are usually much more viscous than nematic and smectic ones. So, the alignment of columnar phases requires stronger surface interaction or external fields.

The most reliable technique for alignment of LCs nowadays is rubbed polyimide layers.<sup>[20]</sup> The aligning layer are archived by rubbing of polyimide layer with a cloth. This method still remains the large-scale method for alignment of liquid crystals in production of LC displays (LCDs). Alignment of LCs can also be obtained by rubbing techniques on other polymers (e.g. polyvinylalcohol).

Although the rubbing of polyimide layers remains the current method of choice for the large-scale production of LCDs, there is a widespread interest in viable alternative technologies. The rubbing of polyimide, carried out with large rolling machines, generates dust and static electricity. Both electrostatic charging and mechanical damage lower the yield of LCDs with active matrix addressing, which contain an underlying array of thin-film transistors on a silicon substrate.

One of the most attractive alternative to rubbing is the generation of a surface anisotropy of an alignment film by photochemical means. LCs are extremely sensitive to interface properties and the director on the surface orients along the easy axis of alignment layer. Research into photo-induced alignment began in 1988 when the illumination of surface monolayer of azobenzene with unpolarized light was shown to change the alignment of the adjacent LC from perpendicular to parallel to the monolayer.<sup>[25]</sup> The rod-shaped *E* configuration and bent-shaped *Z* configurations are considered to promote homeotropic and planar alignment, respectively (see Fig. 1.7). Changing the wavelength of irradiation alters their relative distributions. The photo-induced homogeneous alignment is unstable because of the relaxation to the more stable *E* configuration.

Polarized UV exposure was found to induce an in-plane anisotropy in a polymer doped with an azobenzene-containing dye and, hence, a preferred in-plane alignment direction to the overlying LC.<sup>[26]</sup> Later on the azobenzene chromophores were covalently attached as side chains to the polymer backbone.<sup>[27]</sup> Recently, it was found that surface relief gratings can be formed on azobenzene-containing polymer films irradiated with two laser beams at different incident angles. The mechanism of the groove formation is unclear, but LC alignment has been achieved and explained on the basis that elastic strain is minimized when the LCs lie parallel to the grating grooves.<sup>[28]</sup>

Photo-alignment was also obtained on photo-crosslinkable materials (e.g. polyvinylcinnamate),<sup>[29,30]</sup> on the materials capable to undergo photo-degradation (e.g. polyimide)<sup>[31]</sup>. This area is now reaching technological maturity with the development of high-quality materials giving strong LC anchoring with good long-term stability.<sup>[32]</sup> Prototype displays have been manufactured using photo-alignment technology, but the technique is not



yet used on a large commercial scale. Alignment can also be achieved by photo-alignment in the bulk.<sup>[33]</sup> In this case the LC system should consist of molecules which are capable to undergo photo-reactions. For example, azobenzene containing side-chain LC polymers can be aligned under irradiation with linearly polarized light.<sup>[34,58]</sup>

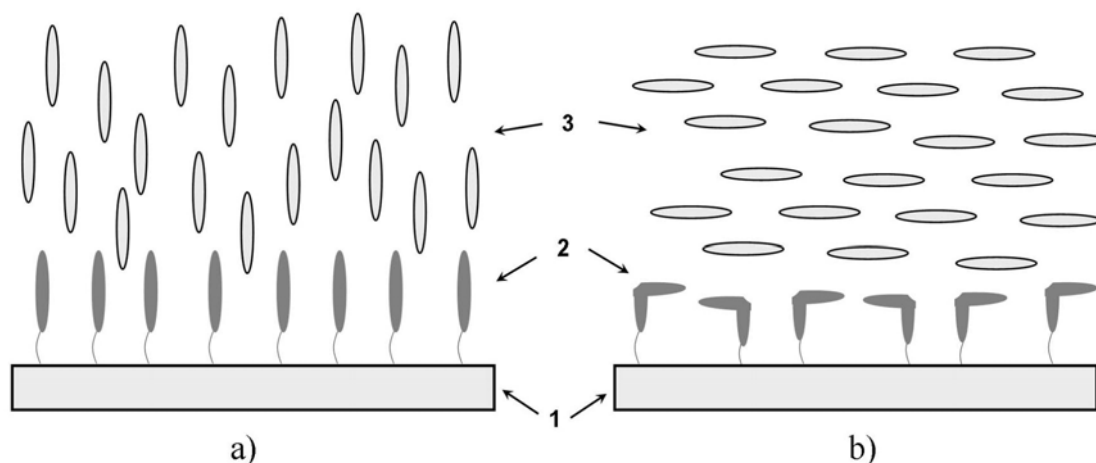


**Fig. 1.7: Illustrative representation of photo-alignment control of LC molecules. 1 – substrate, 2 – monolayer of azobenzene molecules in (a) *trans* and (b) *cis* configurations, 3 – liquid crystal. Switching between homeotropic and planar modes of alignment triggered by *trans-cis* and *cis-trans* photo-isomerization upon alternative irradiation with nonpolarized UV and Visible light, respectively.**

New methods were also developed for the alignment of other 'nonclassical' LC systems (such as lyotropic LCs or highly ordered discotic LCs that form columnar phases) for the production of various functional components. These methods include shear force alignment from lyotropic phases of different dyes for organic thin-film polarizers,<sup>[35,36,37,38,39]</sup> surface alignment of discotic materials for negative retardation films<sup>[40,41]</sup> for the improvement of the viewing angle of LC displays, and alignment by a so-called zone-casting process of semiconducting discotic materials.<sup>[42]</sup>

Alignment of nonclassical LC systems is not a trivial task because each material requires an individual approach for its alignment. However, development and introduction of new functional LC materials into the market demand reliable methods for their alignment. This remains the biggest problem before the application of such materials can be realized.

## 1.5. Ionic self-assembly complexes

Considerable research effort is currently focused on the interplay between molecular architecture, intermolecular interactions, order and macroscopic properties.<sup>[43,44,45]</sup> The construction of materials with different functionalities, easy processing, high anisotropy and stability through self-assembly and self-organization processes, in which molecules associate spontaneously into ordered aggregates as a result of noncovalent interactions and/or entropic factors, is becoming one of the primary frontiers of materials research. In order to achieve this goal, several strategies, such as H-bonding,<sup>[46]</sup> metal-coordination,<sup>[47]</sup> charge-assisted H-bonding<sup>[48]</sup> and, more recently, ionic self-assembly<sup>[49]</sup> have been investigated. A quite large number of these activities is directed to generate mesophases where the mesogenic units are formed by intermolecular interactions. Manipulation of structural and macroscopic order in films and bulk solids, however, remains a major challenge for all of these approaches.

The mutual order is encoded not only in the shape and chemical functionality of the objects involved, but also in the strength and directionality of the secondary interactions used. In classical supramolecular chemistry these interactions are usually hydrogen bridges or coordinative metal binding. However, fit-interactions and amphiphilic association should also be considered. In Table 1.1 the most important interactions playing main role in organization of organic materials are summarized.

*Table 1.1: Interactions and some of their properties.*

<b>Interaction</b>	<b>Strength (kJ mol<sup>-1</sup>)</b>	<b>Range</b>	<b>Character</b>
van der Waals	~ 50	short	non-selective, non-directional
H-bonding	5 – 65	short	selective, directional
coordination binding	50 – 200	short	directional
fit-interactions	10 – 100	short	very selective
amphiphilic	5 – 50	short	non-selective
<b>ionic</b>	<b>50 – 250 *</b>	<b>long</b>	<b>non-selective</b>
covalent	350	short	irreversible
* data are for organic media, dependent on solvent and ion solution			

There is one secondary interaction which is largely underestimated in systematic use in supramolecular chemistry, namely the coulombic interaction. Employment of coulombic

interactions for the self-organization of tectonic units is so-called Ionic Self Assembly (ISA). To differentiate ISA from the simple coulombic binding of salts, it was shown that ISA is usually accompanied by a cooperative binding mechanism, i.e. that the first bonds stimulate further binding which propagate towards the final self-assembly structures (Fig. 1.8).<sup>[50,51]</sup>

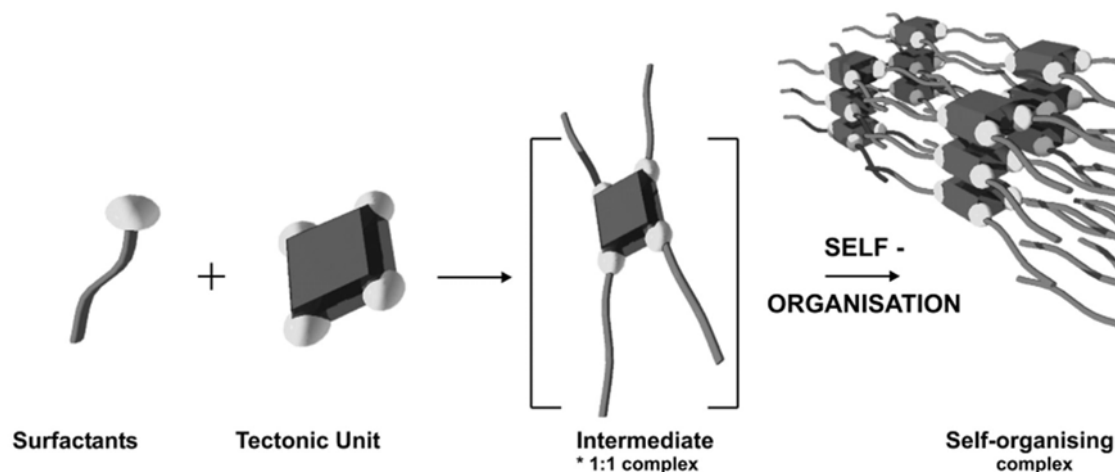


**Fig. 1.8: Ionic self-assembly (ISA) process.**

Using the ISA strategy, in principle, a whole variety of binding blocks can be mutually bound and arranged, as described in Fig. 1.9. The existing tectons are assigned (partly arbitrary) in this diagram to four different classes. It is interesting to note that some combinations, including the ionic binding within each tecton class, are already well examined and are regarded as very promising cases of soft supramolecular chemistry.<sup>[49]</sup>

In order to differentiate salts from ionic self-assembly, let's make small overview of both classes. Salts are characterized by presence of opposite molecular and/or atomic ions which are in combination with steric, van der Waals and sometimes  $\pi$ - $\pi$  interactions bind these fragments together. Usually when salt is placed into water (the most polar solvent) separate ions are surrounded by molecules of water forming a shell around it. In this case there is complete solubility of the material in water. There are a variety of organic materials in addition to nonorganic ones (like NaCl or charged inorganic clusters) which can be named salts. They can also be found in Fig. 1.9. These are, for example, supramolecular salts which may also form liquid crystalline phases. Usually these materials are called ionic liquid crystals.<sup>[52]</sup> Chromonic materials (usually disc-like and forming lyotropic columnar LC phases<sup>[11,12]</sup>), surfactants (known as classical lyotropic LCs<sup>[10]</sup>) and even polyelectrolytes (main and side chains polyelectrolytes<sup>[52]</sup>) can be classified as water soluble salts.

There is a separate class of materials which do not already behave as water soluble salts. It is polyelectrolyte supported LCs using prolonged<sup>[53,54]</sup> and disc-like molecules<sup>[55]</sup> which both show liquid crystalline behavior. It was not investigated if these materials possess cooperatively – combining of molecules and precipitation of the material from water solution. However, it was shown that complexes of surfactant with polyelectrolytes and dye-surfactant complexes possess strong cooperativity.<sup>[49]</sup> In the ISA complexes, one of the building blocks is often a surfactant and the other building block can be oppositely charged ionic dye, polyelectrolytes, or metal complex. The cooperativity of the ionic binding process is presumably a central theme of ISA, and the reason for the simplicity of synthesis, stability, as well as for the strict fulfillment of the 1:1 stoichiometry in the resulting supramolecular structures.

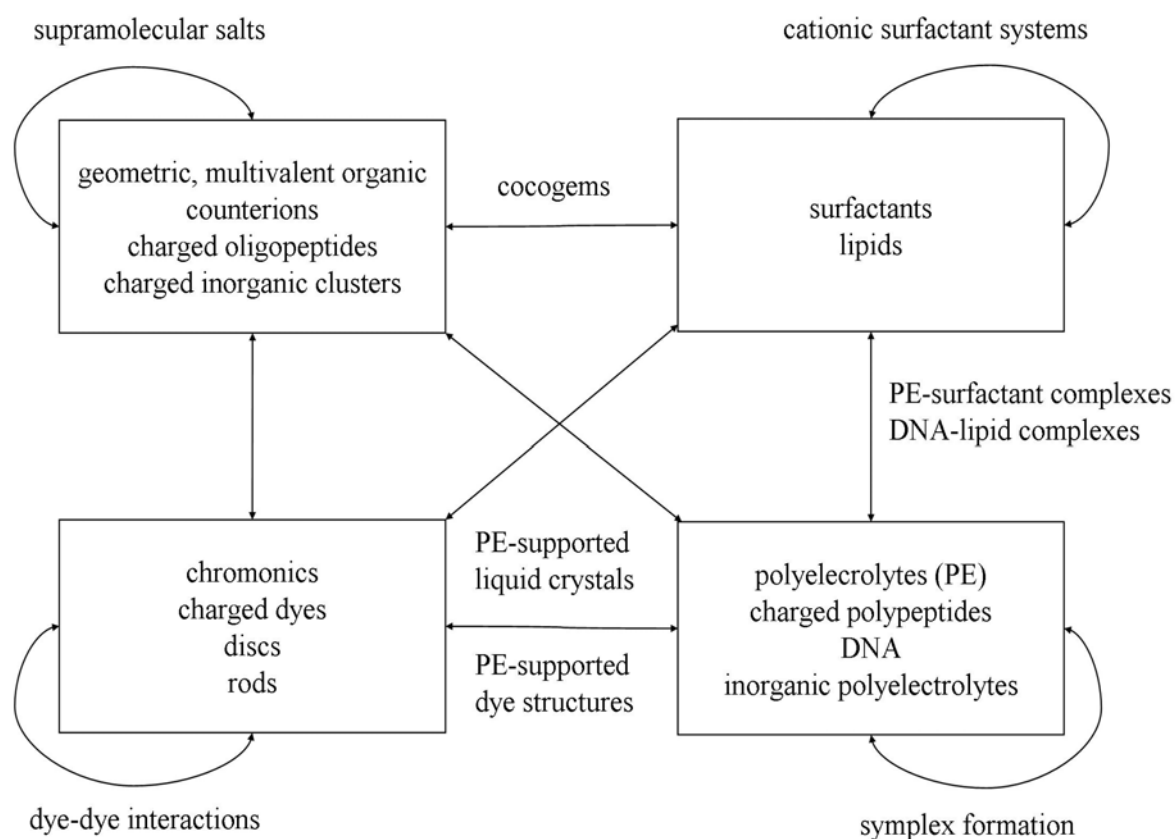


**Fig. 1.9: The potential sample space of Ionic Self Assembly (ISA). Taken from Ref. 49.**

Formation of complexes between chromonics (charged dyes, discs or rods) and surfactants had not been investigated until the beginning of this century. For the first time, formation of dye-surfactant complexes was shown and investigated in the ISA group of Dr. C. F. J. Faul.<sup>[51,56,57]</sup> The complexes are formed and precipitated on mixing of two water

solutions of dye and surfactant. The resulting complexes are insoluble in water; however, they are soluble in organic solvents. All the complexes are highly ordered but liquid crystalline behavior of these complexes had not been studied.

Nowadays, a wide variety of secondary interactions in addition to van der Waals and fit-interactions known from supramolecular chemistry, as described above in section 1.3, have been investigated to influence and to be responsible for the formation of LC phase. Using these interactions the following types of liquid crystals have been obtained:

- ☑ Surfactants – classical lyotropic LCs<sup>[10]</sup>;
- ☑ Chromonic LCs<sup>[11,12]</sup>;
- ☑ Hydrogen-bonding LCs<sup>[18]</sup>;
- ☑ Metalomesogens<sup>[14-16]</sup>;
- ☑ Ionic LCs<sup>[52]</sup>;

However, one interaction strategy for the construction of mesogens has not been considered: ionic interactions. It could be disputed that ions are responsible for the formation of lyotropic phases of surfactants, chromonic materials, and ionic LCs but these ions do not act as the binding interaction within supramolecular self-assembly replacing, for example, hydrogen bonds. The simplest example of pure ionic interactions would be the application of two oppositely charged ions between a rigid core and flexible tails in any classical nematic liquid crystal. Liquid crystallinity should be induced, or influenced, without presence of a third component, e.g. solvent. The ISA liquid crystals might be considered as subclass of Ionic LCs. However, the cooperatively binding mechanism makes them different from known ionic LCs.<sup>[52]</sup> One can say that the ISA LCs is a new type of liquid crystals.

The presence of liquid crystallinity in low molecular ISA complexes has been shown for the first time and investigation of their properties was performed and are the subject of this work. The attention is mostly focused on disc- or rod-like charged molecules (including dyes) with oppositely charged surfactants. Alignment of different liquid crystalline ISA complexes by different methods known from the field of liquid crystals has been also investigated.

## 1.6. Aim of the work

In this work the first observation of new type of liquid crystals is presented. These are ionic self-assembly (ISA) liquid crystals formed by introduction of oppositely charged ions between different low molecular tectonic units. As practically all conventional liquid crystals consist of rigid core and alkyl chains, attention is focused on the simplest case where oppositely charged ions are placed between a rigid core and alkyl tails.

The aim of this work is to understand liquid crystalline and alignment properties of these materials. This aim was achieved by applying detailed experimental investigations of influence of ionic interactions on:

- ☑ Ordering in the ISA complex and formation of liquid crystalline phases;
- ☑ Phase transitions of the ISA complexes;
- ☑ Alignment properties of the ISA complexes.

The investigations of these properties were prepared on the simplest ‘model’ ISA complex in which the benzene ring with six ionic peripheral groups complexed with six oppositely charged surfactants. In order to show potentials for application perylenediimide and azobenzene containing ISA complexes investigation of the following properties of these materials were carried out:

- ☑ Liquid crystalline and phase transition properties of perylenediimide-surfactant ISA complexes;
- ☑ Alignment properties of perylenediimide-surfactant ISA complexes; ordering in aligned films of the complexes;
- ☑ Liquid crystalline and phase transition properties of azobenzene-surfactant ISA complexes;
- ☑ Photo-alignment of azobenzene-surfactant ISA complexes; ordering in aligned films of the complexes;

Surfactants with different length, shape and number of alkyl tails were used for these investigations. These investigations were carried out applying combination of differential scanning calorimetry, polarized light microscopy, X-ray scattering, transmission null ellipsometry, UV-Visible and IR (both polarized, non-polarized, polarized incidence-angle dependent, and temperature dependent) spectral measurements.

## 2. Materials and experimental techniques

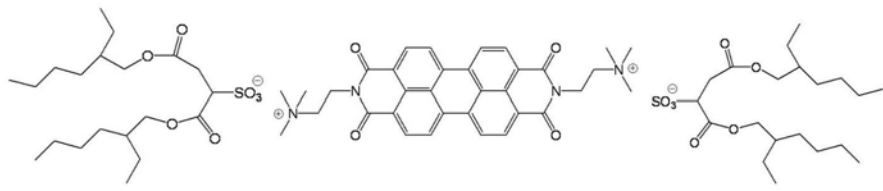
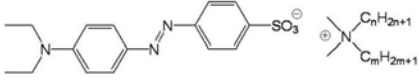
### 2.1. Materials and sample preparation

For the preparation of all complexes the water soluble (1g/l) tectonic units (functional tectons and surfactants) were complexed in a one to one charge ratio. The precipitated complexes were removed from water by centrifugation, washed with water to remove produced salt and possible non-complexed precursors, and dried under vacuum. Elemental analyses confirmed that the complexes were 1:1 (charge ratio) adducts. All initial materials for complexation process were provided by the ISA group of Dr. C. F. J. Faul (Max Planck Institute of Colloids and Interfaces, Research Campus Golm, Potsdam, Germany) or ordered from Sigma-Aldrich. Chemical structures and abbreviations of the complexes used in all investigations are shown in Table 2.1.

For the most investigations the samples were prepared by spin-coating or casting method from the solution of appropriate complex in chloroform. In some cases the samples were prepared by pressing of a complex between two substrates in appropriate viscous state. Details about preparation of each sample are present in appropriate section.

Table 2.1: Chemical structure of the investigated complexes.

Name	Chemical structure
BHC – (C <sub>10</sub> D) <sub>6</sub> (n = m = 10) BHC – (C <sub>12</sub> D) <sub>6</sub> (n = m = 12) BHC – (C <sub>14</sub> D) <sub>6</sub> (n = m = 14) BHC – (C <sub>16</sub> D) <sub>6</sub> (n = m = 16) BHC – (C <sub>16</sub> S) <sub>6</sub> (n = 16, m = 1)	
1 – DHDP	

Name	Chemical structure
1 - AOT	
EO - C <sub>12</sub> D (n = m = 12)  EO - C <sub>16</sub> D (n = m = 16)	



## 2.2. Experimental techniques

### 2.2.1. *Differential scanning calorimetry*

The phase behavior of the complexes was investigated by differential scanning calorimeter (DSC). All DSC measurements were performed on a Netzsch DSC 200. The samples were examined at a scanning rate of 10 K min<sup>-1</sup> by applying several heating and cooling cycles.

### 2.2.2. *Polarized light microscopy*

Optical textures of the complexes were investigated with polarized light microscopy. Photomicrographs were taken using a ZEISS Axioplane 2 microscope with strain-free objectives and a ZEISS AxioCam camera.

### 2.2.3. *X-ray scattering measurements*

To determine molecular order in the complexes small- and wide-angle X-ray scattering measurements were performed. The resulting data were analyzed and models of molecular packing were proposed.

Small-Angle X-ray Scattering (SAXS) measurements were carried out with a Nonius rotating anode ( $U = 40$  kV,  $I = 100$  mA,  $\lambda = 0.154$  nm) using image plates. With the image plates placed at a distance of 40 cm from the sample, a scattering vector range of  $s = 0.07$ - $1.5$  nm<sup>-1</sup> was available. 2D diffraction patterns were transformed into 1D radial averages.

Wide-Angle X-ray Scattering (WAXS) measurements were performed using a Nonius PDS120 powder diffractometer in transmission geometry. A FR590 generator was used as the source of Cu-K<sub>α</sub> radiation. Monochromatization of the primary beam was achieved by means of a curved Ge crystal. Scattered radiation was measured using a Nonius CPS120 position-sensitive detector. The resolution of this detector in  $2\theta$  is  $0.018^\circ$ .

Simultaneous WAXS and SAXS were also performed at beamline A2, Hasylab, DESY, Germany.

For the in-situ temperature dependent SAXS and WAXS experiments a Nonius generator (Cu-K<sub>α</sub>) was used, applying a position-sensitive detector (Inel). The samples were heated in an Anton Paar (Austria) heating chamber. The SAXS experiments in symmetric reflection were carried out on a Bruker D8 instrument with Cu-K<sub>α</sub> radiation, using Goebel mirrors and a scintillation counter as a detector. In this setup the sample is fixed horizontally

and the X-ray tube and detector moved.

#### 2.2.4. Transmission null ellipsometry

Information about optical anisotropy in aligned samples of the complexes was obtained performing a transmission null ellipsometry.<sup>[58]</sup> The optical scheme of the method is presented in Fig. 2.1. The setup was self-built using He-Ne laser, Glan-Thompson polarizers, quarter wave plate, photo-diode and precision stepper motor provided by Newport.

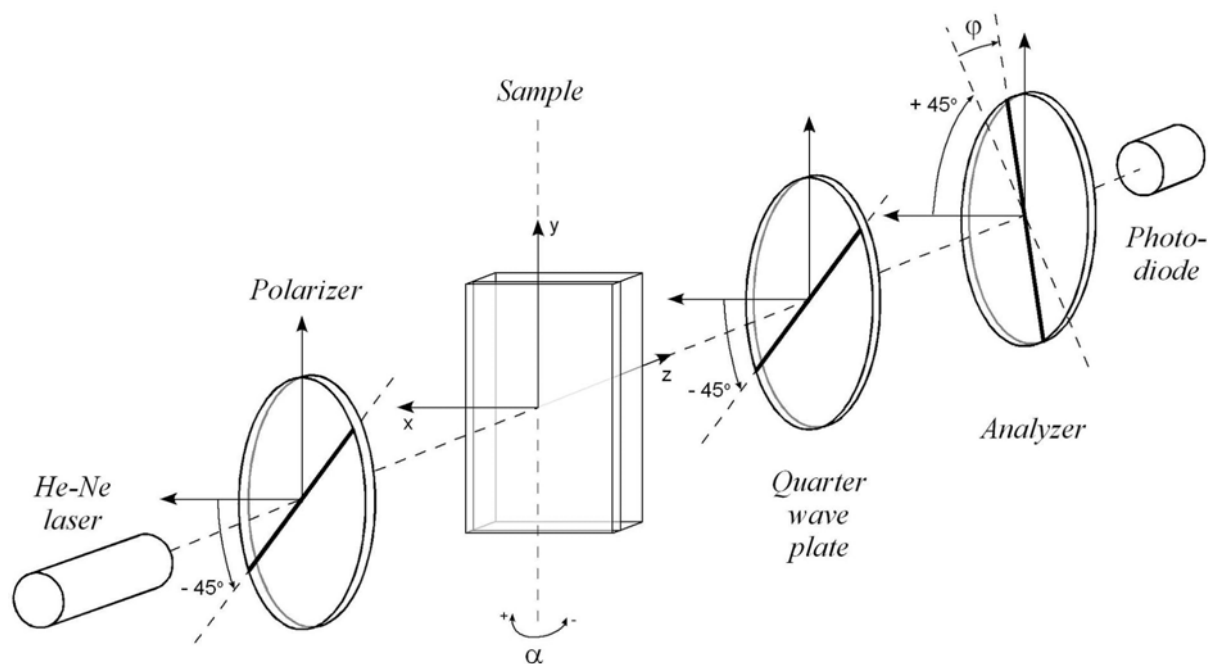


**Fig. 2.1:** Experimental setup for the transmission null ellipsometry measurements.

In the setup the sample is mounted between the polarizer and the quarter wave plate. This configuration provides measurements of the phase shift between two polarizations (vertical and horizontal, if they are eigenpolarizations) of the sample. The light from He-Ne laser ( $\lambda = 632,8$  nm) propagating through the polarizer becomes linearly polarized at  $-45^\circ$  with respect to the x-axis. The sample converts the polarization from linear to elliptical. The polarization is further transformed into almost linear polarization by the quarter wave plate placed at  $-45^\circ$  with respect to the x-axis. It can be compensated to the minimum light leakage by rotating the analyzer by the angle  $\varphi$  that encodes information of the phase shift by the sample. Dependence of  $\varphi$  on the tilt angle  $\alpha$  of the sample (it was rotated around vertical axis) for two mutually orthogonal positions of one was measured. Solving Maxwell's equations for light propagation in a biaxial medium numerically by using 4x4 matrix method<sup>[59]</sup> the dependence of  $\varphi$  on  $\alpha$  for the most probable configuration was fitted. The details of this method are given in the Appendix. Using this technique one can estimate only

in-plane  $(n_x - n_y)d$  and out-of-plane  $(n_x - n_z)d$  retardation of the film. Measuring the thickness of the film and average refractive index of nonoriented film (or  $n_x$  of oriented sample) independently it was possible to find the principal refractive indices of the film. The thickness of an investigated film was determined by measuring a scratch profile with AFM (“SMENA” Scanning Probe Microscope, NT-MDT, Russia). The thickness of a cell was determined by measuring and modeling interference visible spectrum of the sample in parts without material (air gap). The average refractive index of nonoriented film was obtained from the measurements and fitting of reflection of polarized light by an isotropic film on a glass substrate.<sup>[60, Chap. 4]</sup> In some cases the refractive index measurements were done with Carl Zeiss Abbe-refractometer.

### 2.2.5. UV-Visible spectral measurements

The UV-Visible spectra were measured with a Lambda 2 UV-Visible spectrometer (Perkin Elmer). The UV-Visible polarized spectra were measured with a Lambda 19 UV-Visible spectrometer (Perkin Elmer) or a Tidas UV-Visible spectrometer (J&M) equipped with Glan-Thompson polarizer, driven by computer-controlled stepper motors (DC-500, Owis). Polarized Visible spectra were also measured with a ZEISS Microscope equipped with monochromator and Glan-Thompson polarizer, driven by computer-controlled stepper motors. To prepare measurements of polarized spectra on tilt of a sample a special custom-built sample holder was used to tilt the sample.

To characterize the order in the system from maximum  $A_{max}$  and minimum  $A_{min}$  absorbance (or absorbance parallel  $A_{\parallel}$  and perpendicular  $A_{\perp}$  to the director of a liquid crystal) of the samples the following parameters were calculated:

$$\text{dichroic ratio:} \quad DR = \frac{A_{max}}{A_{min}}, \text{ or } DR = \frac{A_{\parallel}}{A_{\perp}}; \quad (2.1)$$

$$\text{dichroism:} \quad D = \frac{A_{max} - A_{min}}{A_{max} + A_{min}} = \frac{DR - 1}{DR + 1}; \quad (2.2)$$

$$\text{spectroscopic order parameter:} \quad S = \frac{A_{\parallel} - A_{\perp}}{A_{\parallel} + 2A_{\perp}} = \frac{DR - 1}{DR + 2}. \quad (2.3)$$

### 2.2.6. IR spectral measurements

The IR spectra were measured with Mattson PS-10000 FTIR spectrometer. Polarized spectra were measured by placing KRS-5 wire grid polarizer (Specac, England) in the incident light path in the sample chamber. To prepare measurements of polarized spectra on tilt of a sample a special custom-built sample holder was used to tilt the sample.

In order to obtain information about of out-of-plane absorbance in the sample calculations of angle dependent polarized absorbance have been prepared. In the case of an isotropic distribution of the refractive index the s- and p-polarized components of absorbance will be described by the formulas:<sup>[61]</sup>

$$A_s(\beta) = A_x \frac{d(\beta)}{d(0)} \quad (2.4a)$$

$$A_p(\beta) = [A_y + (A_z - A_y)\sin^2 \beta] \frac{d(\beta)}{d(0)} \quad (2.4b)$$

where  $\frac{d(\beta)}{d(0)} = \frac{1}{\cos \beta}$  considers changes of optical path on tilt of the sample;  $\beta$  is the angle between the electric field vector in the medium and the sample plane and is equal to the angle of refraction of the beam described by Snell's law:  $\sin \alpha = n \sin \beta$ .  $A_x$  and  $A_y$  are components of the absorbance in the plane of the sample.  $A_z$  is the absorbance normal to the sample.

From the change in the s-polarized component of absorbance the ordinary refractive index  $n$  of the sample was determined and was used for calculation of the p-component of absorbance. The obtained out-of-plane absorbance component  $A_z$  was used to calculate dichroic ratio or spectroscopic order parameter.

This method was also applied in the case UV-Visible tilted polarized measurements to obtain qualitative estimation of the order parameter.

### *2.2.7. Temperature dependent UV-Visible and IR spectral measurements*

Temperature dependent UV-Visible and IR spectral measurements were prepared by placing the Linkam THM600 heating stage directly in a sample beam of Lambda 2 UV-Visible spectrometer (Perkin Elmer) and Mattson PS-10000 FTIR spectrometer. Temperature control of the samples was achieved within  $\pm 0.1^\circ\text{C}$ . The heating and cooling rate was  $0.1^\circ\text{C}/\text{min}$ . Before each spectral measurement the sample was hold at appropriate temperature for 5 min to ensure temperature stabilization.

In order to obtain information about order parameter of different fragments in the investigated complexes at different temperatures the obtained IR spectra were processed as follows. All spectra were smoothed, and baseline corrections made. PEAKFIT software was used to find the peak position, to fit peaks to the sum of the Lorentzian and Gaussian functions, and to calculate the integrated areas under the peaks. The integrated intensities of some peaks were used to calculate the dichroic ratio and corresponding order parameter using

Neff's method<sup>[62]</sup> which was successfully applied for investigation of discotic mesophases.<sup>[61,63]</sup>

The orientational order in the mesomorphic phase can be described by an orientational distribution function. The infrared absorption for the single vibration  $i$  a molecule is proportional to  $(\vec{E} \cdot \vec{p}_i)^2$  where  $\vec{E}$  is the electric field of IR radiation and  $\vec{p}_i$  is the transition dipole moment vector. The main advantage of the IR spectroscopy lies in its possibility of studying the orientational distribution of dipoles, for those part of the molecule in which the molecular vibration is localized. This contrasts with other techniques in which the molecular orientation as a whole is investigated.

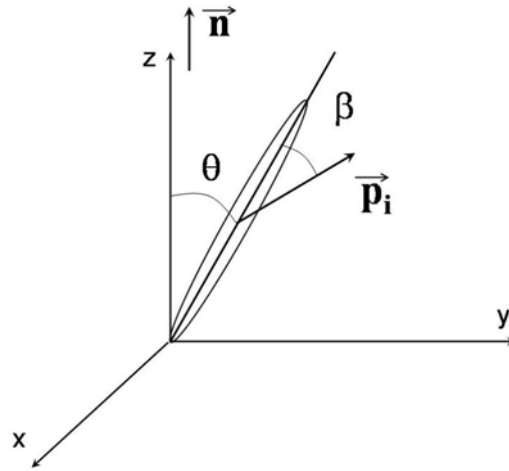


**Fig. 2.2: Schematic diagram showing interaction of an unpolarized IR beam with LC material. z -direction is the direction of propagation of the IR beam.**

The orientational order parameter of LC is given by

$$S = 1/2 \langle 3 \cos^2 \theta - 1 \rangle \quad (2.5)$$

where  $\theta$  is the angle between optical axis (director) of the sample and the orientation position of an individual molecule (Fig. 2.2). The LC sample is assumed to be aligned with the director normal to the substrates. The dichroic ratio for an unpolarized beam is defined as follows:

$$R_i = \frac{I_F}{I_I} \quad (2.6)$$

where  $I_F$  is the integrated absorbance of the band in LC phase, and  $I_I$  is the integrated absorbance in the isotropic phase. Because of broadening of the bands on heating of the sample the integrated absorbance should be used instead of peak intensity. In general, the transition dipole moment of a vibration can be at angle  $\beta$  to the symmetry axis of molecule.

For unpolarized irradiation  $I_F$  can be defined as follows:

$$I_F = \cos^2 \beta \langle \sin^2 \theta \rangle + 0.5 \sin^2 \beta \langle 1 + \cos^2 \theta \rangle \quad (2.7)$$

The angle  $\theta$  is different for different molecules, and its average value determines the order parameter. Taking into account that in the isotropic phase

$$\langle \sin^2 \theta \rangle_I = 2/3; \quad \langle \cos^2 \theta \rangle_I = 1/3 \quad (2.8)$$

Substituting equations (2.8) into equation (2.7) we obtain

$$I_I = 2/3 (\cos^2 \beta + \sin^2 \beta) = 2/3 \quad (2.9)$$

From equation (2.5) order parameter becomes

$$S = 1 - 3/2 \langle \sin^2 \theta \rangle \quad (2.10)$$

or

$$\langle \sin^2 \theta \rangle = 2/3 (1 - S) \quad (2.11)$$

Substituting equations (2.7), (2.9) and (2.11) into equation (2.6) one obtains

$$R_i = \frac{2(1 - S) + 3S \sin^2 \beta}{2} \quad (2.12)$$

Assuming  $\beta = 90^\circ$  or  $\beta = 0^\circ$  one obtains

$$S = 2(R_i - 1) \quad (\text{for } \beta = 90^\circ) \quad (2.13)$$

for vibrations with the transition dipole moment  $\vec{p}_i$  lying perpendicular to the molecular axis and

$$S = 1 - R_i \quad (\text{for } \beta = 0^\circ) \quad (2.14)$$

for vibrations with  $\vec{p}_i$  parallel to the molecular axis.

### 2.2.8. Irradiation conditions

Films of the photosensitive complexes were irradiated with a linearly polarized light of an Ar<sup>+</sup> laser ( $\lambda = 488$  nm). The intensity of the exciting light in the sample position was 50 mW cm<sup>-2</sup>. Intensity of the exciting light was also varied in the range of 10 – 1000 mW cm<sup>-2</sup> but the final results were qualitatively the same and only dependent on the exposure dose.

### 3. Liquid crystallinity, phase behavior and alignment of benzene-based ISA complexes

In order to investigate the influence of the ionic interactions on the ordering properties in the ISA complex, the formation of LC phases and phase transitions the investigation should start with a rather simple molecule with maximum symmetry. Keeping in mind that the first (covalent) discotic systems were prepared from benzene-hexa-*n*-alkanoates in 1977,<sup>[64]</sup> therefore mellitic acid / benzenehexacarboxylic acid (BHC) as tecton was selected for this study. By this choice the idea to replace covalent bonding between rigid core and alkyl chains of the LC molecules was realized. In addition symmetry and small size of the rigid core allowed not to consider steric interactions between these cores. The main idea of this choice is to ensure that the ionic interactions are dominating in the complex.

Benzene derivatives have attracted some attention over the last few years as mesogens for the formation of a variety of columnar phases. Nuckolls *et al.* have investigated the use of crowded hexasubstituted benzene (more specifically alternatingly substituted with alkoxy and amide groups) in the formation of columnar structures in a series of papers.<sup>[65,66,67]</sup> They introduced the possibility for hydrogen bonding through the presence of amide groups, which provided further stabilization (in conjunction with  $\pi$ - $\pi$  interactions). Müllen *et al.*<sup>[68]</sup> have shown that in the case where the central benzene of a hexaaryl-substituted system could be reduced to the hexaanion, a twisted central benzene molecule was produced in solution.

BHC tecton has the possibility to form a complex with six surfactant molecules, and can the covalent bonds between benzene ring and alkyl chains of the original discotic material now be replaced with ionic interactions. Didodecyldimethylammonium bromide (C<sub>12</sub>D) was used as surfactant for the main part of this study. The chemical structure of the BHC-(C<sub>12</sub>D)<sub>6</sub> complex is shown in Table 2.1.

In the study surfactants with various lengths and number of alkyl chains were used. The length and number of surfactants has influence on solubility of initial components in water and further complexation and precipitation properties of the resulting complex from water. Surfactants with very long alkyl tails do not solve readily in water and surfactants with short alkyl tails do not complexate and precipitate from water. The optimum length of alkyl chains for double tail surfactants lays in the range from 10 to 16 of carbon atoms. For single tail surfactant the optimum was 16. In the investigation the surfactants with even number of carbon groups were used. This was restricted by commercial availability of the surfactants.

### 3.1. Phase characterization

The BHC-(C<sub>12</sub>D)<sub>6</sub> complex material shows fan-shaped textures under crossed polarizers when pressed between two glass slides at room temperature (Fig. 3.1). More rare in some parts of the sample, the complex shows Schlieren and marbled textures (probably due to some alignment effects from the preparation procedure). From the observed textures some cautious prediction can already be made that the complex exists in a smectic, most probably A, phase.<sup>[69]</sup> On heating to temperatures higher than 50°C all the textures disappear. On the following cooling and heating cycles the sample appears isotropic when observed in polarized light microscope with crossed polarizers. As will be shown in section 3.2, this was rather due to homeotropic alignment of the material than the absence of anisotropy. When the complex is heated to temperatures higher than 140°C it starts to produce fine gas bubbles. This is not a result of decomposition, since TGA measurements revealed decomposition temperature of the complex of approximately 170°C. This is attributed to evaporation of water trapped in the complex, and does not affect the inner order and macroscopic alignment of the material in any way (even after annealing at 150°C for several hours).

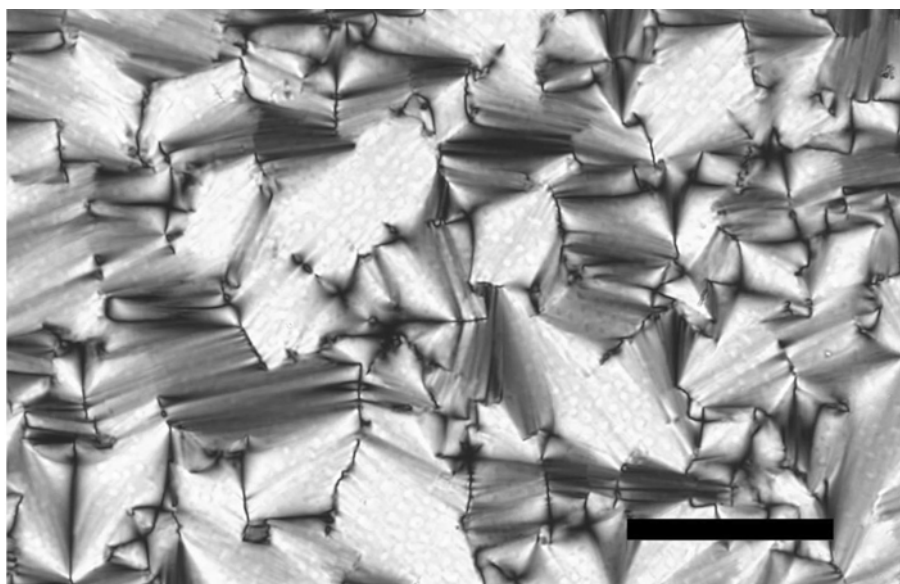


**Fig. 3.1: The fan-shaped texture of the BHC-(C<sub>12</sub>D)<sub>6</sub> complex at 25°C as observed in polarizing microscope (crossed polarizers, bar: 100 μm).**

The DSC investigations showed several transition peaks (Fig. 3.2). All peaks are attributed to transitions of the surfactant alkyl chains (C<sub>12</sub>D). Similar transitions were observed for the noncomplexed surfactant. The most prominent peaks in the range of 20 to



-20°C correspond to crystallization of the surfactant alkyl chains. Below this temperature range the complex is crystalline. It is not possible at the stage to give reasonable explanation of all transitions. This needs more detailed investigations with other methods. Detailed descriptions of all transitions will be given below in the section 3.4 dealing with the temperature-dependent IR spectroscopy investigations.

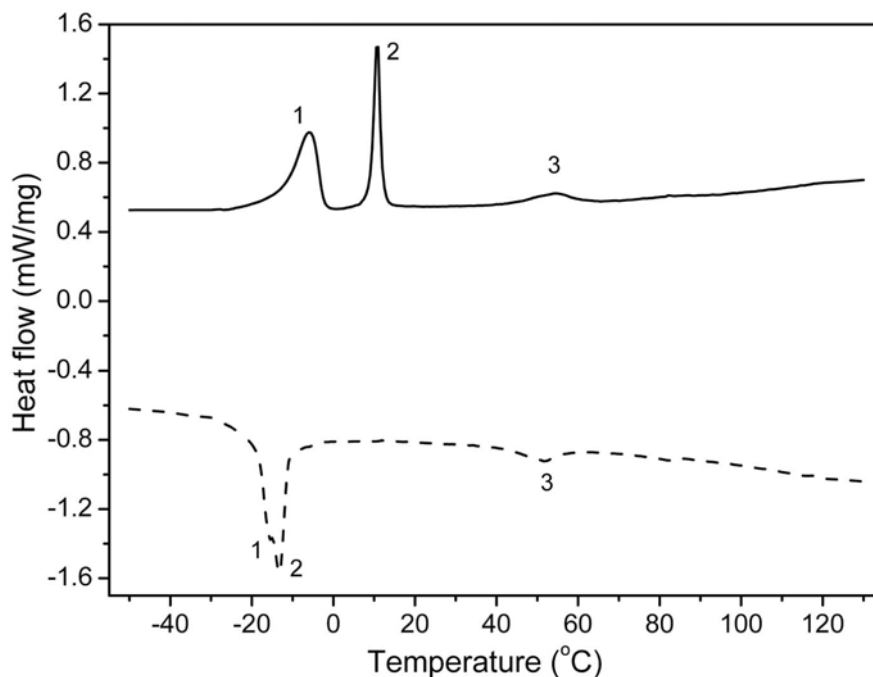


**Fig. 3.2: DSC curves of the BHC-(C<sub>12</sub>D)<sub>6</sub> complex: second cooling circle (dashed curve) and third heating circle (solid curve).**

Temperature-dependent X-ray scattering measurements were performed on annealed complex material in order to identify the LC phases present. WAXS diffractograms measured at 25°C showed a broad peak around  $2\theta = 20^\circ$  similar to that shown by nematic and smectic A mesophases.<sup>[70(Chap. 1)]</sup> This peak is attributed to a noncrystalline arrangement of the surfactant alkyl chains with an average interchain distance of 0.44 nm. The SAXS diffractogram recorded at this temperature (Fig. 3.3) indicated the presence of long-range order on the nanometer scale. The three equidistant reflections correspond to a layered structure with a repeat distance  $d_0 = 3.22$  nm. The small set of reflections noticed at higher scattering vectors ( $s = 0.765, 0.8$  and  $0.84$  nm<sup>-1</sup>) are probably due to some low correlation/internal order originating from the in-plane packing of the BHC molecules. According to generally accepted notation<sup>[29(Vol. 1, Chap. II)]</sup> the present phase is labeled as bilayer smectic A phase SmA<sub>2</sub> (Fig. 3.4). The bilayer structure will be disclosed in the following

sections.

From the SAXS diffractogram measured at 120°C (Fig. 3.3) no specific phase assignment can be made. However it shows that the material still possesses some order on the nanometer scale. Additional proof of the proposed packing of the different fragments within the complex (at different temperatures) will be presented in the following sections.

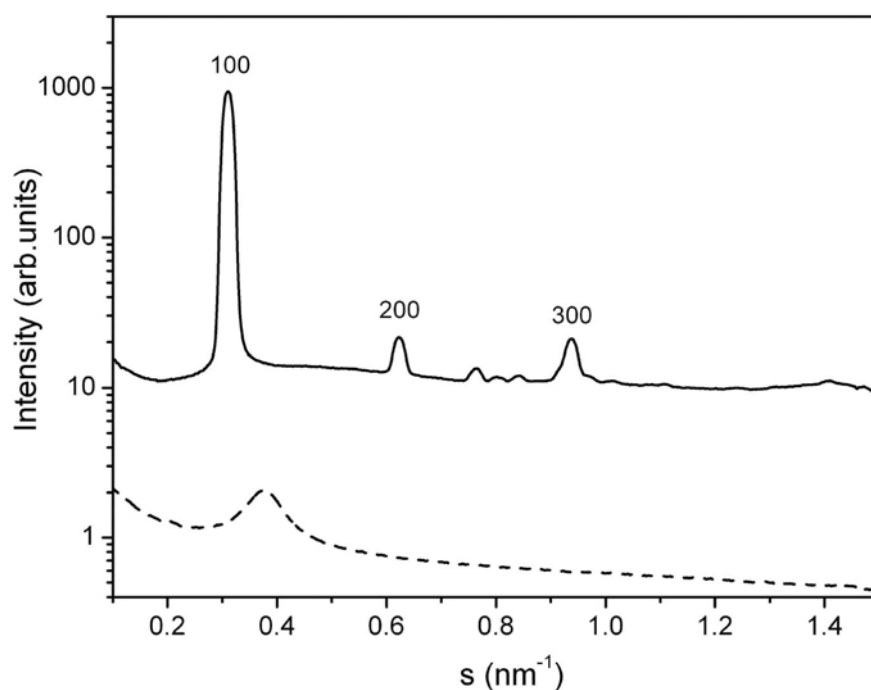


**Fig. 3.3:** SAXS diffractograms (in transmission mode) of the BHC-(C<sub>12</sub>D)<sub>6</sub> complex recorded at 25°C (solid curve) and at 120°C (dashed curve).

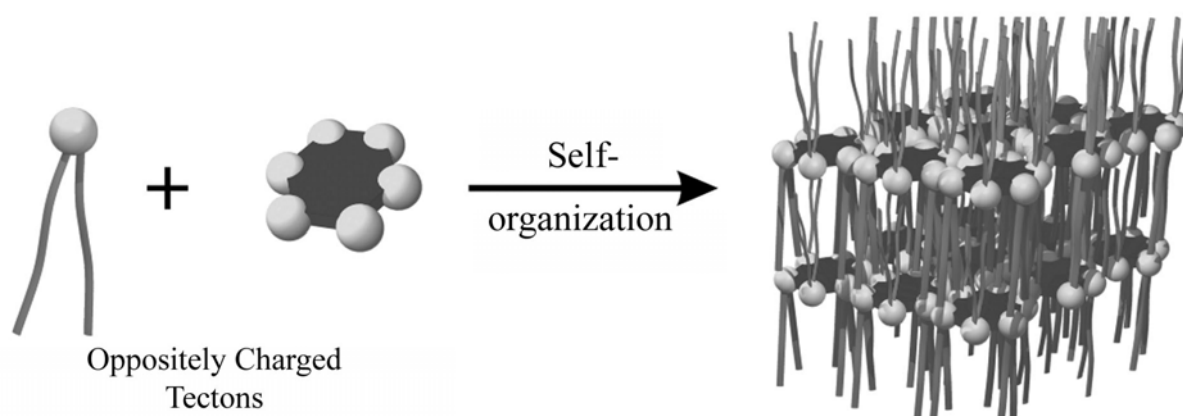


**Fig. 3.4:** ISA process and proposed model of molecular packing in the BHC-(C<sub>12</sub>D)<sub>6</sub> complex.

## 3.2. Alignment properties

As was briefly mentioned in the previous section the complex shows strong tendency to orient between two glass or quartz slides. Aligned samples were prepared by pressing the complex between two slides at 100°C with subsequent slow cooling to room temperature. Glass powder spacers (1 to 90  $\mu\text{m}$ ) were used to control the thickness of the films. Thin films were prepared by casting of the solution of the complex in chloroform (50 mg/ml) and keeping it at room temperature under quiescent conditions to ensure very slow evaporation of the chloroform. The films were then heated to 100°C for 30 minutes with subsequent cooling. It was found that neither the chemical nature (hydrophilic or hydrophobic) nor the presence (or absence) of a second (top) glass slide had any influence on the quality of the alignment.

### 3.2.1. Characterization with transmission null ellipsometry

As was mentioned in the section 3.1 on heating to the temperatures higher than 50°C and on the subsequent cooling and heating cycles the sample appeared isotropic when observed in polarized light microscope with crossed polarizers. However, on tilt of the sample with respect to the testing beam when observing in the polarized light microscope a homeotropically oriented optical axis was observed. To unambiguously determine and characterize the existence of a homeotropically oriented optical axis transmission null-ellipsometry was used. Fig. 3.5a shows the experimentally obtained and modeled dependence of change of angle of polarization  $\varphi$  after the quarter wave plate on the tilt  $\alpha$  of the sample (see section 2.2.4). From this dependence the out-of-plane retardation  $\Delta n \cdot d$  in the film was determined, which was found to be negative. Measuring and modeling the interference visible spectrum of the sample in parts without material (air gap) the thickness of the sample between slides was determined. The thickness of thin films (no top slide) was determined by measuring the scratch profile with AFM. The dependence of the retardation on the thickness (in different samples) is shown in Fig. 3.5b. The dependence is linear, with small deviations found for large thicknesses caused by the appearance of defects (as was also observed in polarized light microscope). The found linear dependence of retardation on the thickness of the sample indicates that the complex is uniformly aligned throughout the sample.

From the slope of the curve in Fig. 3.5b the difference between refractive indexes  $\Delta n = n_e - n_o = -0.02$  was determined. The ordinary refractive index of the film of aligned complex was measured with an Abbe refractometer (utilizing s-polarized light of a He-Ne laser) and found to be  $n_o = 1.490$ . The extraordinary refractive index was calculated to be

$n_e = 1.470$ . These values were determined for  $\lambda = 632.8$  nm.

With this measurements it was unambiguously determined that the complex is uniformly aligned with homeotropically oriented negative optical axis. However, the reasons for negative retardation are unclear. These reasons will be explained in section 3.3.1.

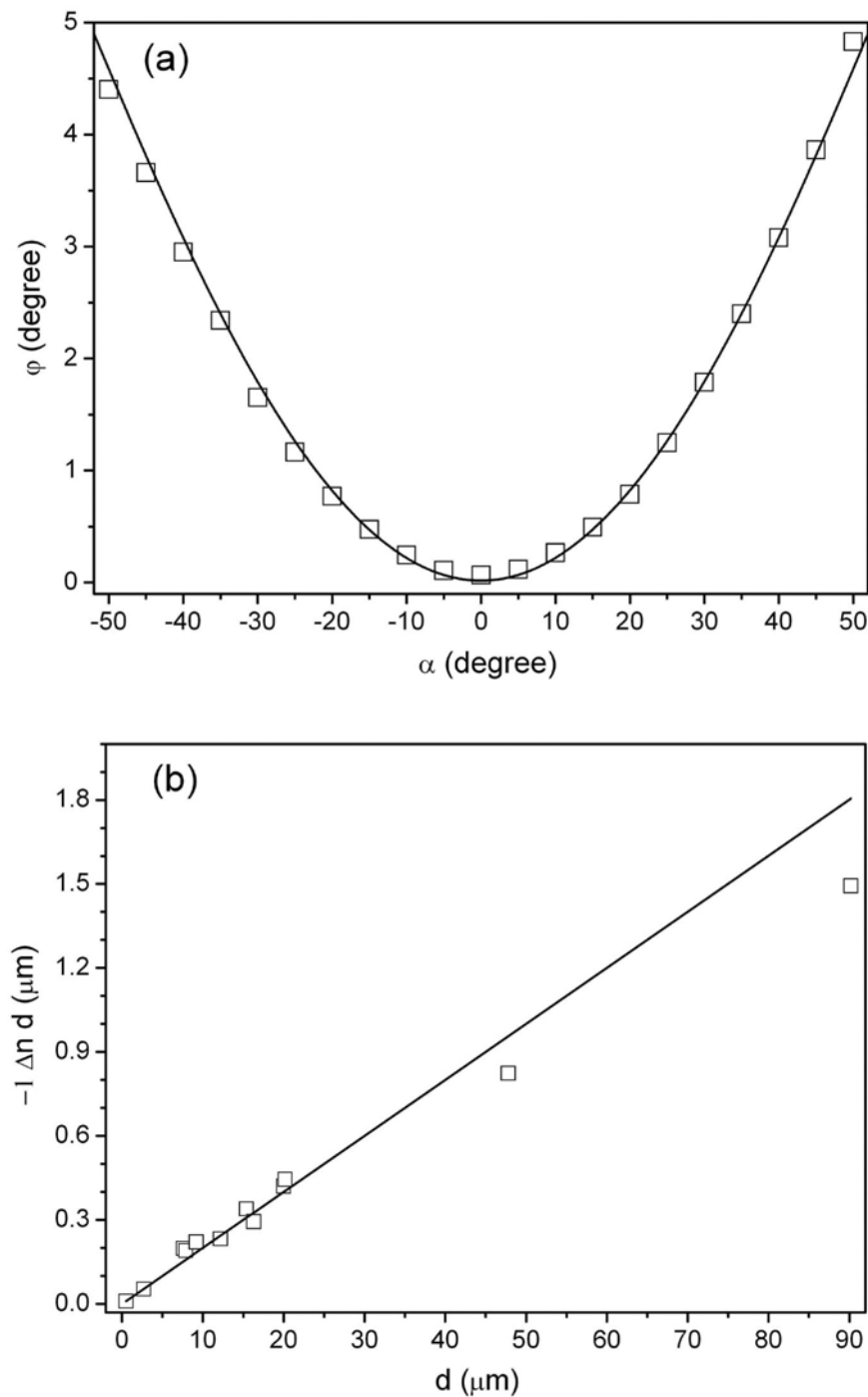


**Fig. 3.5:** (a) Experimental ( $\square$ ) and theoretical (—) dependences of change of the angle  $\varphi$  of polarization after quarter wave plate on tilt angle  $\alpha$  of the sample; (b) dependence of the retardation on thickness of aligned samples.

### 3.2.2. Characterization with SAXS in reflection mode

In order to understand the reasons for negative birefringence in the aligned samples more detailed investigations of the ordering of the complex in the aligned samples should be prepared. The most suitable techniques to get into the internal structure on the nanometer scale is X-ray diffraction techniques. For the system under investigation Small Angle X-ray Scattering (SAXS) on the aligned sample is the best choice.

SAXS was performed in symmetric and asymmetric reflection on an aligned sample (thin film on a Si wafer), to investigate both the mesostructure and the orientation with respect to the substrate. It is seen (Fig. 3.6a) that the sample produces a series of distinct (00k) interferences which are attributable to a layered mesostructure with a long period of  $d_0 = 3.15$  nm. This is in very good agreement with the results from SAXS experiments using a transmission setup (described in section 3.1). Furthermore, compared to the nonaligned bulk sample, the interferences are significantly sharper, and even a fourth order peak is observed.

The appearance of several higher order interferences allowed for quantitative analysis in terms of a model<sup>[71,a]</sup> of two alternating types of layers of different electron densities  $\rho_1$  and  $\rho_2$ , thicknesses  $d_1$  and  $d_2$ , and their variances  $\sigma_1$  and  $\sigma_2$ , taking into account the preferred orientation, a finite instrumental resolution and the absorption correction. If the finite width of the boundaries cannot be neglected, a suitable approach is given by the function  $H_z^2 = \exp(-2\pi d_z^2 s^2)$ <sup>[72]</sup>, where  $d_z$  is the thickness of the interface boundary. The final expression to fit the data is  $J(s) = k A(s)[I(s)H_z^2 + I_B]$ <sup>[71]</sup>, where  $k$  is a scaling constant,  $A(s)$  is the absorption correction,  $I(s)$  is the ideal scattering from a layered two-phase system and  $I_B$  the background scattering from 3D density fluctuations.

This basic model was considered appropriate for several reasons. First, the electron densities of the surfactant tails and the charged units are substantially different and can be estimated to be constant in the respective domain. Second, and more importantly, this model only needs a minimum number of parameters, which are physically meaningful. More detailed models cannot be expected to provide more structure information since the model used here already leads to an excellent fitting of the data. The experimental data could be excellently fitted over almost the whole range of scattering vectors  $s$  (Fig. 3.6a). The obtained values are  $d_1 = 1.41$  nm and  $d_2 = 1.74$  nm ( $\sigma_1 = 0.03$  nm,  $\sigma_2 = 0.04$  nm), thus suggesting that the two layers are quite uniform in thickness, as indicated by the small values for  $\sigma_i$ . The model provides an estimate for the transition region between these two layers,

---

a The modeling was done by Dr. B. Smarsly (Max Planck Institute of Colloids and Interfaces)

which is calculated to be approximately  $d_z = 0.2 \div 0.3$  nm. In addition, the average height of the domains of the layer structure is estimated to be at least 100 nm. An exact value cannot be determined because of the finite resolution of the instrument used. In conclusion, from the modeling of the SAXS data on the aligned samples in reflection mode it can be inferred that a well-defined and extended layer structure, oriented parallel to the substrate, is present with a low degree of structural inhomogeneity. These results fit well with the proposed model of molecular ordering in the complex presented in Fig. 3.4. However, there is still no experimental confirmation about ordering of the tectons of the complex within these layers.

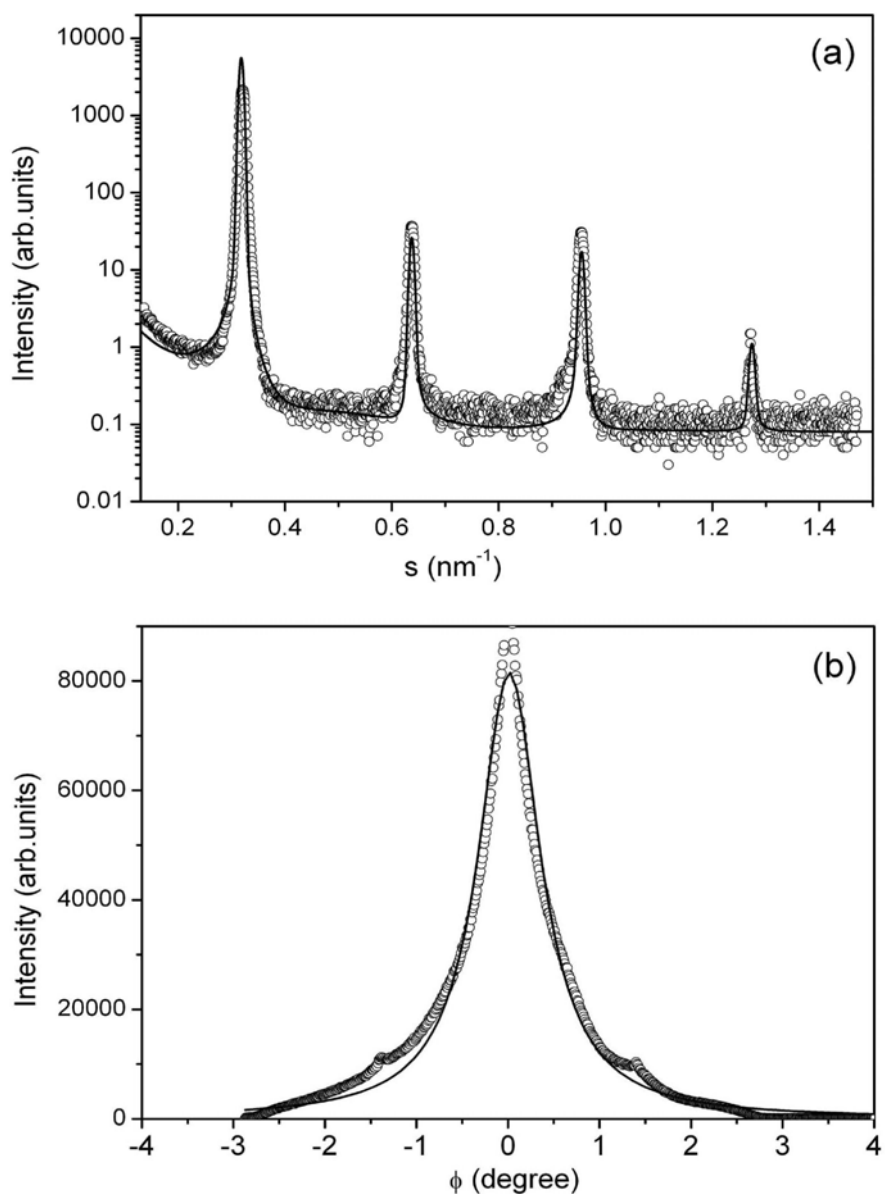


**Fig. 3.6:** (a) Measured ( $\circ$ ) and modeled ( $—$ ) small angle X-ray reflectivity on aligned sample of the complex at 25°C; (b) X-ray measurement in asymmetric reflection on the (001) reflection.

In addition, SAXS experiments were carried out in “asymmetric reflection” mode. By this technique (see reference <sup>[71]</sup>), the degree of orientation with respect to the substrate can be determined. In essence, a fixed value of  $2\theta$  is chosen (here the first Bragg interference) and the X-ray tube and detector are moved (by the angle  $\phi$ ) around this position, thus providing the degree of preferred orientation of the layer structure (Fig. 3.6b). It is observed that the experimental profile can be fitted to a Lorentzian profile with an integral width of only  $0.8^\circ$ .<sup>[73]</sup> First, the observation of a maximum in asymmetric reflection proves the presence of an orientation with respect to the substrate. Second, the small value itself indicates a high degree of orientation, for instance compared to the order parameter  $S$  of liquid crystals. The formal application of the order parameter concept  $S = 0.5\langle 3\cos^2\Theta - 1 \rangle$ , taking into account the experimentally determined orientation distribution (Fig. 3.6b) leads to an averaged value of  $S$  close to 1.

In summary, the SAXS experiments in symmetric and asymmetric reflection prove the existence of a highly ordered and oriented layer structure parallel to the substrate.

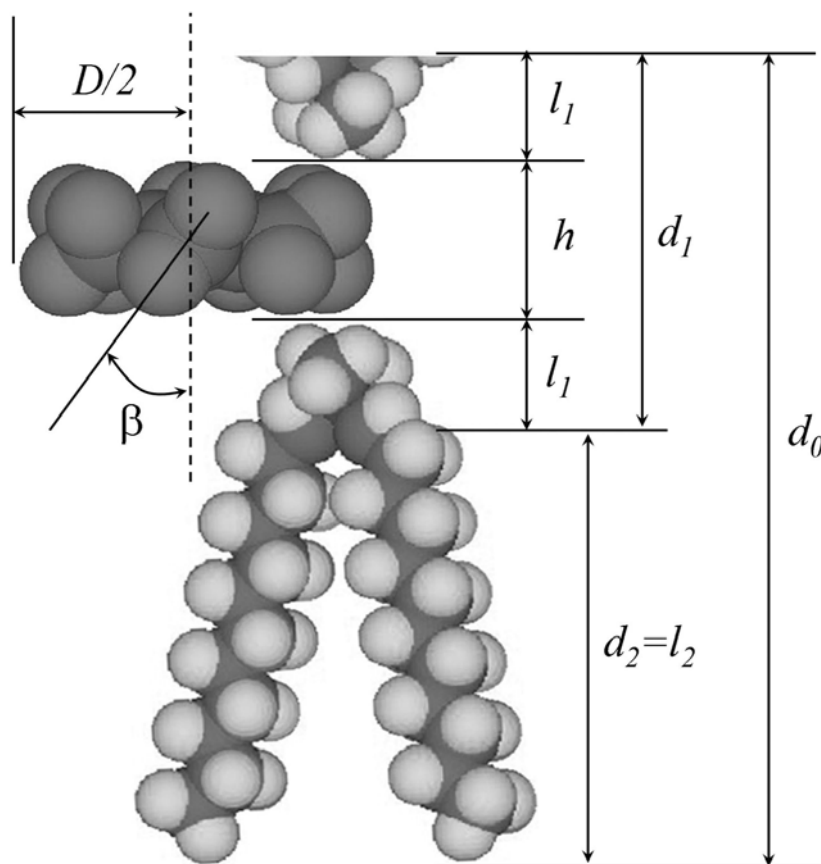


**Fig. 3.7:** Calculated molecular dimensions of the layered repeat unit of the BHC-(C<sub>12</sub>D)<sub>6</sub> complex.

In order to further verify the data obtained from the stacking model, calculations of the molecular dimensions of the molecules were performed using known lengths of the appropriate covalent bonds<sup>[74(Section 9, pp.1-14)]</sup> and Van der Waals radii of elements.<sup>[75(Chap. 4, p. 71)]</sup> Schematic representation of BHC and C<sub>12</sub>D molecules with their molecular dimensions are shown in Fig. 3.7. For the BHC molecule the diameter  $D = 0.98$  nm and height  $h = 0.72$  nm was calculated. The value of the angle  $\beta = 31^\circ$  (the tilt of the carboxylate group with respect to the normal to the BHC molecule plane) used for calculations was obtained from the results of the temperature-dependent IR spectroscopy presented in section 3.4. The surfactant molecule C<sub>12</sub>D was divided into two parts: (1) the dimethylammonium headgroup ( $l_1 = 0.38$  nm) and (2) the stretched alkyl chains ( $l_2 = 1.68$  nm).

According to the X-ray model, one layer has a thickness of 1.41 nm. This would correspond very closely to the combined thickness of the BHC molecules and charged headgroups of the surfactants,  $d_1 = h + 2l_1 = 1.48$  nm. Full interdigitation of the alkyl layers would then fit very well with the thickness of the second layer obtained from the stacked model, with  $d_2 = l_2 = 1.68$  nm. The value  $d_0 = d_1 + d_2 = 3.16$  nm obtained for the  $d$ -spacing from these basic calculations of the molecular dimensions is very close to that obtained from the stacked model and experimentally obtained X-ray data.

Accordingly to the obtained experimental data, modeling and proposed model the complex consists of two sublayers. First sublayer consists of charges (BHC molecules and charged headgroups of the surfactants) and the second sublayer consists of completely interdigitating alkyl tails of the surfactants. Planes of the BHC molecules are considered to be parallel to the layers. Alkyl tails of the surfactant are considered to be perpendicular to the layers.

Although the proposed model fits well with the modeling of the experimental data this is non-direct method for determination of molecular ordering in the complex. To get direct experimental conformation of the proposed molecular packing in the complex angular-dependent polarized UV and IR spectroscopy investigations on the aligned samples were performed. In addition, information about order parameter of different fragments has been obtained. This is a subject of the following section.



### 3.3. Ordering within the complex

In the previous sections it was shown that the complex exists in bilayer smectic liquid crystalline phase at room temperature. One sublayer of the complex consists of charged groups and another consists of alkyl tails. These are results of the proposed model which fits to the results of the modeling of experimental data. However, to propose this model additional information about ordering of different molecular fragments was needed. This information can give UV and IR spectroscopies. Results of this section should be considered as supplementary for the proposed model present in the previous section. These results give also additional information about quality of ordering (i.e. the order parameter) of different molecular fragments.

To obtain information about ordering of different molecular fragments within an aligned sample angular-dependent polarized UV spectroscopy and angular-dependent polarized IR spectroscopy were used. In the following sections the results from each method are present. Each method gives additional useful information about the molecular packing within the layers.

#### 3.3.1. *Angular-dependent polarized UV spectroscopy investigations*

The samples for this measurement were aligned between two quartz substrates by the method described above. The thickness of the sample was 2  $\mu\text{m}$  and controlled with glass powder spacers. As can be seen from Fig. 3.8 the absorbance of the complex is characterized by two maxima in the UV range. The maxima at 290 and 240 nm correspond to the  $S^1$  ( $\pi$ - $\pi^*$ ) and  $S^2$  ( $\pi$ - $\pi^*$ ) transitions, respectively, of the anionic BHC molecule. The dipole moments of these transitions are parallel to the double bonds and lie in the plane of the benzene ring.<sup>[76(Part 3, pp. 247-312)]</sup>

The polarized components of absorbance (s and p) at different angles  $\alpha$  of incidence were measured (Fig. 3.8). As a reference the same quartz substrate, as used for the preparation of the sample, positioned at the same incidence angle, was used. By using this substrate as reference the effect of reflectance of light at the air-quartz interfaces of the substrates could be removed. The reflectance at the interfaces between substrates and aligned complex can be neglected (as seen from the absorbance staying close to zero in the nonabsorbing part of the spectrum). There should be some reflection at these interfaces in the range of the absorbance bands, but to get qualitative results it can be neglected.

In the insert graph in Fig. 3.8 the dependence of normalized absorbance at 260 nm on

the tilt  $\alpha$  of the sample is shown as an example. The absorbance of s-polarized component increases as expected because of an increase of the optical path on the tilt of the sample. In the case of isotropic absorbance, the s and p components should increase simultaneously. However, the absorbance of the p-polarized component decreases dramatically. This is a result of the decrease of absorbance in the out-of-plane direction of the aligned sample. This result shows that the dipole moments of the  $S^1(\pi-\pi^*)$  and  $S^2(\pi-\pi^*)$  transitions of the anionic BHC molecule (and therefore also the planes of benzene rings) are aligned parallel to the substrate. Due to the dispersion of the refractive index, the negative anisotropy of the refractive index in the visible range is caused by anisotropic absorbance in the UV range. These results would therefore also fit with the proposed model (from the X-ray investigations) of the phase morphology of the complex.

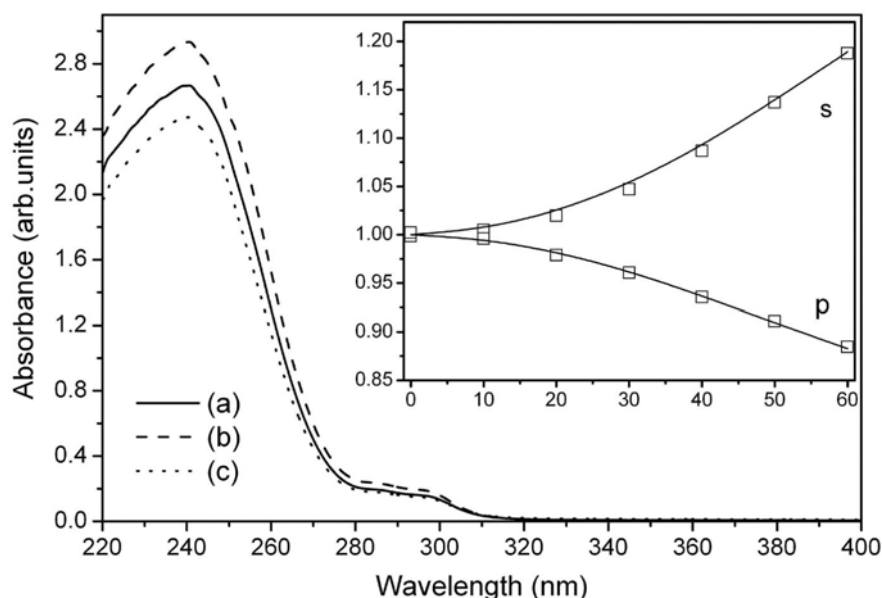


**Fig. 3.8:** Changes in polarized UV absorption spectra on tilt of the aligned sample: (a) Spectrum of aligned sample at normal incidence; (b) Spectrum of s-polarization of aligned sample at tilt angle  $\alpha = 60^\circ$ ; (c) Spectrum of p-polarization of aligned sample at tilt angle  $\alpha = 60^\circ$ . Insert graph: Measured ( $\square$ ) and modeled (—) changes of absorbance of s- and p-polarization components at 260 nm on tilt angle  $\alpha$  of the sample.

To get information about the quality of ordering of the benzene rings (i.e. the order parameter), the change of absorbance on the tilt of the sample has been calculated. These calculations do not consider all effects, with the main simplification being an isotropic distribution of the refractive index, but do provide qualitative results (when considering the anisotropy of the refractive index in these calculations, the calculated order parameter would

have a slightly smaller value). Therefore, using equation 2.4a the change in the s-polarized component of absorbance was fitted to obtain the ordinary refractive index of the sample. This value was used to fit the p-polarized component of absorbance using equation 2.4b from which the out-of-plane absorbance  $A_z$  was determined and used for calculation of dichroic ratio (equation 2.1) and order parameter (equation 2.3).

These calculations were performed for changes of absorbance in the range 240 - 290 nm with steps of 10 nm. For all wavelengths the final results are similar. As an example the modeled curves at 260 nm are shown in the insert graph in Fig. 3.8. On the basis of these calculations the dichroic ratio  $DR = A_z/A_x = 0.12 \pm 0.01$  and corresponding spectroscopic order parameter of benzene rings (transition dipoles)  $S' = -0.42 \pm 0.02$  were obtained. The negative value of the order parameter indicates that the dipole moments of the electronic transitions in the UV range are preferentially oriented perpendicular to the director. The director is determined, similarly to discotic LCs, as the preferential orientation of the normals to the benzene ring planes. There is a simple correlation between the order parameter of normals to the disc planes and order parameter of dipoles which are in the plane of the discs. The order parameter of normals:  $S = 0.5 \langle 3 \cos^2 \Theta - 1 \rangle$ . The corresponding order parameter of the transition dipoles, which are perpendicular to the normals:  $S' = 0.5 \langle 3 \cos^2(90^\circ - \Theta) - 1 \rangle$ . The order parameter of the normals can be obtained from the order parameter of the transition dipoles:  $S = 0.5 - S' = 0.92 \pm 0.02$ . From this value the conclusion can be made with certainty that the benzene rings (i.e. BHC molecules) are highly ordered and the planes of the BHC molecules are aligned mostly parallel to the layers of the bilayer smectic phase. This fits with the results of SAXS in reflection mode (section 3.2.2).

### 3.3.2. Angular-dependent polarized IR spectroscopy measurements

IR vibrational spectroscopy is a powerful tool for investigation of the ordering of liquid-crystalline systems. It was successfully applied to study the ordering of discotic LCs. The same procedure (as for UV spectroscopy) was applied for the IR spectral range. The main difference between the IR and UV measurements is that the absorbance in the IR range is one to two orders of magnitude lower than in the UV range. The anisotropic dispersion of the refractive index can therefore be reasonably neglected in the modeling, giving more accurate values of the order parameter.

To get information about the orientation of the different fragments in an aligned sample of the complex sample was prepared between two CaF<sub>2</sub> slides in exactly the same way as was done for the UV spectra (see section 3.2.1). The measurements were performed at

25°C. The sample thickness was determined to be 2.7  $\mu\text{m}$ . This sample was also investigated with transmission null-ellipsometry, and a negative homeotropically oriented optical axis with the same parameters as between two glass slides was found confirming that the sample is aligned. Changes in the IR absorbance spectra of s- and p-polarized components on tilt of the sample are shown in Fig. 3.10. All bands that appear in the spectra are summarized in Table 3.1 and identified.<sup>[77,78,79]</sup> The band at 721  $\text{cm}^{-1}$  is not presented in these measurements (due to the absorbance of the  $\text{CaF}_2$  slides below 1000  $\text{cm}^{-1}$ ), but will be discussed in the section 3.4 dealing with temperature-dependent IR spectroscopy.

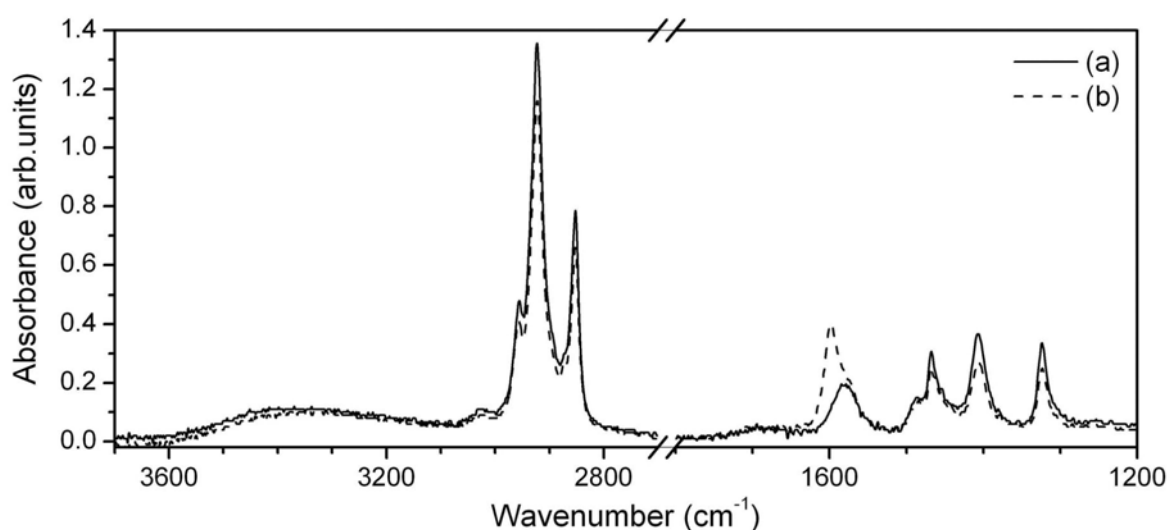


**Fig. 3.9:** Changes in polarized IR absorption spectra on tilt of aligned sample: (a) Spectrum of s-polarization of aligned sample at tilt angle  $\alpha = 50^\circ$ ; (b) Spectrum of p-polarization of aligned sample at tilt angle  $\alpha = 50^\circ$ .

At first the bands of minor importance are considered. The first group consists of those connected to absorbance of water (1690, 3030, 3370) which is present in the complex. The absorbance of these bands increases on tilt of the sample, indicating isotropic distribution of these transition moments. This is reasonable because water is not ‘aligned’. The second group consists of the bands assigned to the absorbance of the  $\text{CH}_3$  groups of the  $\text{C}_{12}\text{D}$  surfactant (1375, 1485, 2872, 2954). The absorbance of these transitions is low because of the low fraction of  $\text{CH}_3$  groups in comparison to other groups in the complex. These bands overlap with other more intense bands, making it difficult to analyze them qualitatively.

The first group of major importance corresponds to transitions of the  $\text{CH}_2$  groups (1466, 2852, 2922). These transitions have an anisotropic distribution with a preference in the plane of the sample, as can be seen from relative value of change of the s- and p-polarized

absorbance components on tilt of the sample. According to the procedure described for the UV measurements the spectroscopic order parameter for each transition is estimated to be:  $S'(1466) = -0.20 \pm 0.02$ ,  $S'(2852) = -0.25 \pm 0.02$ , and  $S'(2922) = -0.25 \pm 0.02$ . Due to overlap with other vibrations at  $1466 \text{ cm}^{-1}$ , the resulting value of the order parameter at this frequency is lower (Fig. 3.9), and will be therefore not considered in the analysis. Taking into account that transition moments corresponding to these vibrations lie in the plane of the  $\text{CH}_2$  group, and that this plane is perpendicular to the alkyl chains, one can conclude that the alkyl chains are aligned perpendicular to the substrates with an order parameter  $S = 0.5 - S' = 0.75 \pm 0.02$ .

Table 3.1: Vibrations appeared in IR spectra of the  $\text{BHC}-(\text{C}_{12}\text{D})_6$ .

$\nu, \text{cm}^{-1}$	Vibration	Tecton
721	$\text{CH}_2$ ( $\rho$ )	$\text{C}_{12}\text{D}$
1260	$\text{CH}_2$ ( $\tau, \omega$ )	$\text{C}_{12}\text{D}$
1323	$\text{CO}_2^-$ ( $\delta_s$ )	BHC
1375	$\text{CH}_3$ ( $\delta_s$ )	$\text{C}_{12}\text{D}$
1409	$\text{CO}_2^-$ ( $\nu_s$ )	BHC
1466	$\text{CH}_2$ ( $\delta_s$ )	$\text{C}_{12}\text{D}$
1485	$\text{CH}_3$ ( $\delta_{as}$ )	$\text{C}_{12}\text{D}$
1584	$\text{CO}_2^-$ ( $\nu_{as}$ )	BHC
1597	$\text{CO}_2^-$ ( $\nu_{as}$ )	BHC
1690	$\text{H}_2\text{O}$ ( $\delta_s$ )	water
2852	$\text{CH}_2$ ( $\nu_s$ )	$\text{C}_{12}\text{D}$
2872	$\text{CH}_3$ ( $\nu_s$ )	$\text{C}_{12}\text{D}$
2922	$\text{CH}_2$ ( $\nu_{as}$ )	$\text{C}_{12}\text{D}$
2954	$\text{CH}_3$ ( $\nu_{as}$ )	$\text{C}_{12}\text{D}$
3030	$\text{H}_2\text{O}$ ( $\nu_s$ )	water
3370	$\text{H}_2\text{O}$ ( $\nu_{as}$ )	water

The second group of vibration frequencies of major importance originates from transitions of the  $\text{CO}_2^-$  group (1323, 1409, 1584, 1597, from the BHC tecton). Since the BHC molecule is completely symmetric no absorption bands corresponding to vibrations of the  $\text{C}=\text{C}$  bond is found. The ordering of the BHC molecules can be investigated from the  $\text{CO}_2^-$  vibrations only.

One should expect the presence of carboxylic acid dimers due to strong hydrogen bonding. Carboxylic acid dimers display very broad and intense O–H stretching absorption in

the region of  $3300 - 2500 \text{ cm}^{-1}$ .<sup>[77]</sup> As can be seen from Fig. 3.9 this band is practically absent in the IR spectrum of the complex. Instead the presence of bands corresponding to the carboxylate anion  $\text{CO}_2^-$  is observed. This is an additional prove of the formation of an one-to-one charge ratio complex.

The transition moments of the scissoring (1323) and symmetrical stretching (1409) vibrations of the carboxylate anion are in the plane of the BHC molecules. Similar to UV measurements, a decrease of the p-polarized component of absorption is found for this band. The calculated spectroscopic order parameters for these transitions are:  $S'(1323) = -0.34 \pm 0.02$  and  $S'(1409) = -0.34 \pm 0.02$ . Again determining the director perpendicular to the plane of BHC molecules the order parameter of the normals is calculated to be  $S = 0.5 - S' = 0.84 \pm 0.02$ . These results are in reasonable agreement with estimations of the order parameter from angular-dependent polarized UV spectroscopy measurements. The value of the order parameter calculated from IR spectra is more realistic because, as was mentioned above, the assumption of an isotropic distribution of refractive index does not give quantitative results in the UV range.

The band at  $1584 \text{ cm}^{-1}$  corresponds to the asymmetrical stretching of the  $\text{CO}_2^-$  group. The transition moment can be, on average, at any angle to the plane of the benzene ring. This tilt may add a nonpredictable influence to the changes of absorbance of this band during tilting of the sample. In addition, this band overlaps with another band (1597) for the p-polarized component of absorbance on tilt of the sample, and therefore no estimation of the order parameter from changes of this band were made. The band at  $1597 \text{ cm}^{-1}$  is assigned to the antisymmetric (out-of-phase) mechanically coupled asymmetric stretching vibration of  $\text{CO}_2^-$  group.<sup>[78]</sup> The transition moment of this vibration is perpendicular to the plane of the BHC molecule (that is, the plane of the benzene ring) and is not observed at normal incidence. This peak appears only on the tilt of the sample for the p-polarized component of absorbance. These changes are clearly seen in Fig. 3.9.

Based on all the above observations and results the liquid-crystalline phase of the BHC-( $\text{C}_{12}\text{D}$ )<sub>6</sub> complex with details of the ordering of the different molecular fragments can be presented. At room temperature the complex exhibits a bilayer smectic A liquid-crystalline phase ( $\text{SmA}_2$ ). The layered structure can be described in two ways. One way is more formal and connected to the definition of the phase. It is based on the results of X-ray investigations. From this point of view the first sublayer consists of charged groups (a stratum of BHC anionic tectons sandwiched between two stratum of cationic head-groups of the  $\text{C}_{12}\text{D}$  surfactants) and the second sublayer consists of alkyl tails of the  $\text{C}_{12}\text{D}$  surfactants. Within the

negatively charged stratum the BHC molecules are aligned with their planes of the molecules (planes of benzene rings) parallel to the stratum with an order parameter of  $S = 0.84 \pm 0.02$ . Within the sublayer of the alkyl tails of the  $C_{12}D$  surfactants the alkyl tails are aligned perpendicular to the sublayer with an order parameter of  $S = 0.75 \pm 0.02$ .

The second way to describe the phase is to consider that each 'molecule' of the complex consists of a  $BHC^{6-}$  anion and six  $C_{12}D^+$  cationic surfactants, on average three cationic surfactants can be found on each side of the anion. This aggregate can be considered as a 'mesogen'. These 'molecules' or 'mesogens' are ordered to form a layer in a way that a negatively charged sublayer of BHC molecules sandwiched between two sublayers of the  $C_{12}D$  surfactants, compensating the negative charges. The alkyl tails of adjacent sublayer of the surfactants are completely interdigitated. From this point of view the phase can also be called as simple smectic A liquid-crystalline phase (SmA). However, as the designation of the liquid crystalline phases is usually done from X-ray investigations, the first definition is used through this work.

### 3.4. Ordering within the complex at different temperatures

To understand what is happening in the complex on change of the temperature more detailed investigations are needed. The most used parameter to characterize liquid crystalline state is the order parameter. So, the main question that will be answered in this section is how the order parameter variation on change of the temperature? What is happening with the order parameter on phase transitions?

To obtain information about the temperature dependence of the order within these complexes temperature-dependent IR spectroscopy measurements were performed (see experimental section 2.2.7). The LC sample is assumed to be aligned with the director normal to the substrates. The dichroic ratio for an unpolarized beam was calculated using equation (2.6). Because of broadening of the bands on heating of the sample the integrated absorbance was used instead of peak intensity. In general, the transition dipole moment of a vibration can be at angle  $\beta$  to the symmetry axis of molecule. For two particular cases of the orientation of the transition dipole moments, the order parameter was calculated from the change of dichroic ratio using equations (2.13) or (2.14).

Aligned samples for these measurements were prepared between two ZnSe slides. The samples were tested with transmission null-ellipsometry to show a negative homeotropically oriented optical axis (what ensures the director to be normal to the substrates) with the same parameters as between two glass slides. Spectra in the range 2500-4000  $\text{cm}^{-1}$  were measured on thin sample (thickness of 2.4  $\mu\text{m}$ ). Spectra in the range 650-2500  $\text{cm}^{-1}$  were measured on thicker samples (thickness 7.5  $\mu\text{m}$ , to ensure high enough absorbance for reproducible results). Temperature control of the samples was achieved within  $\pm 0.1^\circ\text{C}$ . The heating and cooling rate was  $0.1^\circ\text{C}/\text{min}$ . Spectra were collected in the temperature range  $-45$  to  $130^\circ\text{C}$  in  $5^\circ\text{C}$  steps. Temperature-dependent changes of the IR spectra (at two temperatures) are presented in Fig. 3.10. One further band, the rocking vibration of the  $\text{CH}_2$  group near  $721 \text{ cm}^{-1}$ , was also used (Table 3.1).

All spectra were smoothed, and baseline corrections made. PEAKFIT software was used to find the peak position, to fit peaks to the sum of the Lorentzian and Gaussian functions, and to calculate the integrated areas under the peaks. The integrated intensities of some peaks were used to calculate the dichroic ratio and corresponding order parameter of the alkyl chains of the surfactants and BHC molecules. In these calculations a problem was encountered in that it was not clear if all the fragments of the complex were in an isotropic state at high temperature (Fig. 3.3, there is a peak in SAXS diffractogram recorded at  $120^\circ\text{C}$ ).



To overcome this problem and to find the integrated absorbance in the isotropic phase the reverse calculations were performed. From angular-dependent polarized IR spectroscopy order parameters at 25°C was obtained (section 3.3.2). These values were used to determine the dichroic ratio from equation (2.13) or (2.14), and then using equation (2.6) the integrated absorbance in the isotropic phase for an appropriate band was obtained. The obtained values were used for further calculations of temperature-dependent order parameters of appropriate fragments.

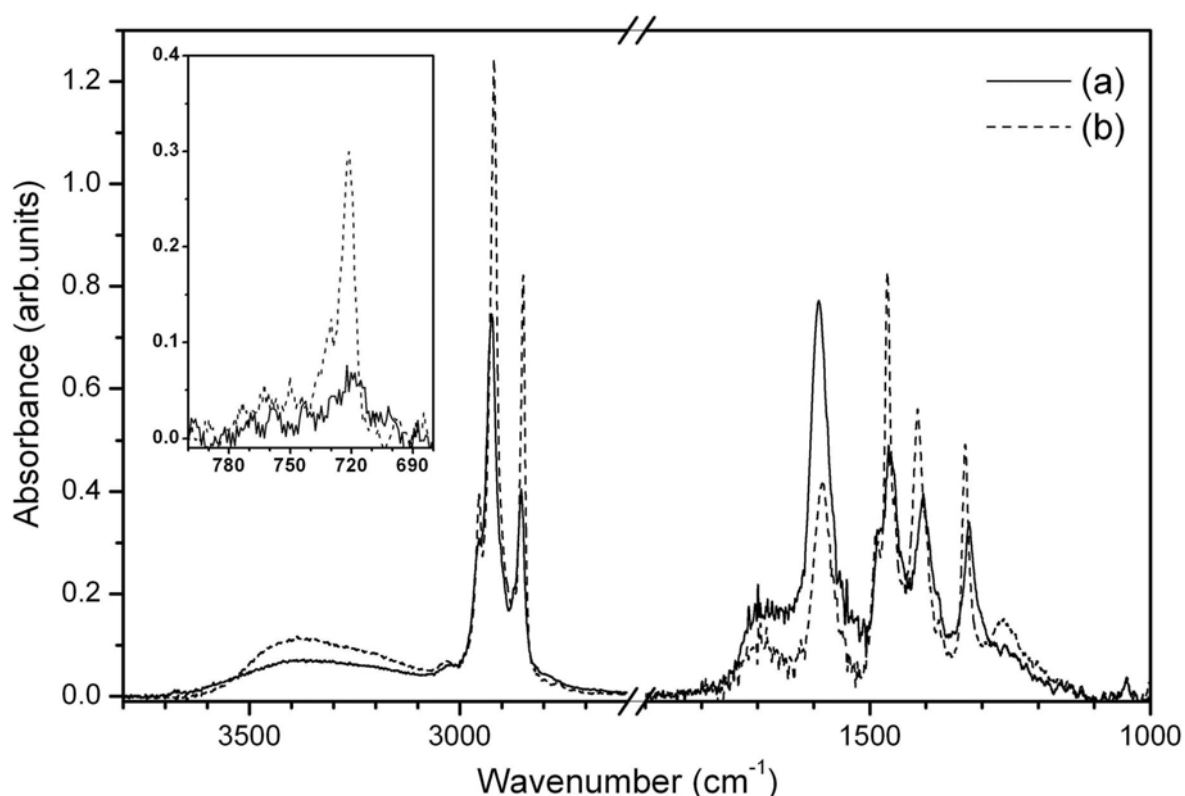


**Fig. 3.10:** Changes in IR absorption spectra of aligned sample of the BHC-(C<sub>12</sub>D)<sub>6</sub> complex at different temperatures: (a) 120°C; (b) -40°C.

The calculated order parameter of alkyl chains from absorbance changes of the asymmetrical and symmetrical stretching vibrations of the CH<sub>2</sub> group is presented in Fig. 3.11a. The alkyl chains are still ordered at high temperatures (above 60°C), as can be seen from the order parameter which reaches a plateau (0.4) and does not show any tendency to decrease with increasing temperature. It means that the complex does not go to isotropic phase at elevated temperature. At least the transition to the isotropic phase was not observed till decomposition temperature (170°C). At low temperatures (below -10°C) the alkyl chains crystallize and one may expect the order parameter in the range of or very close to 1.

However, the order parameter is only about  $0.89 \pm 0.03$ , clearly indicating that crystallization is restricted. These restrictions are probably due to the influence of the ionic interactions in the complex and the restrictions they impose on the organization and packing (as compared to pure covalent materials) of the long alkyl tails.

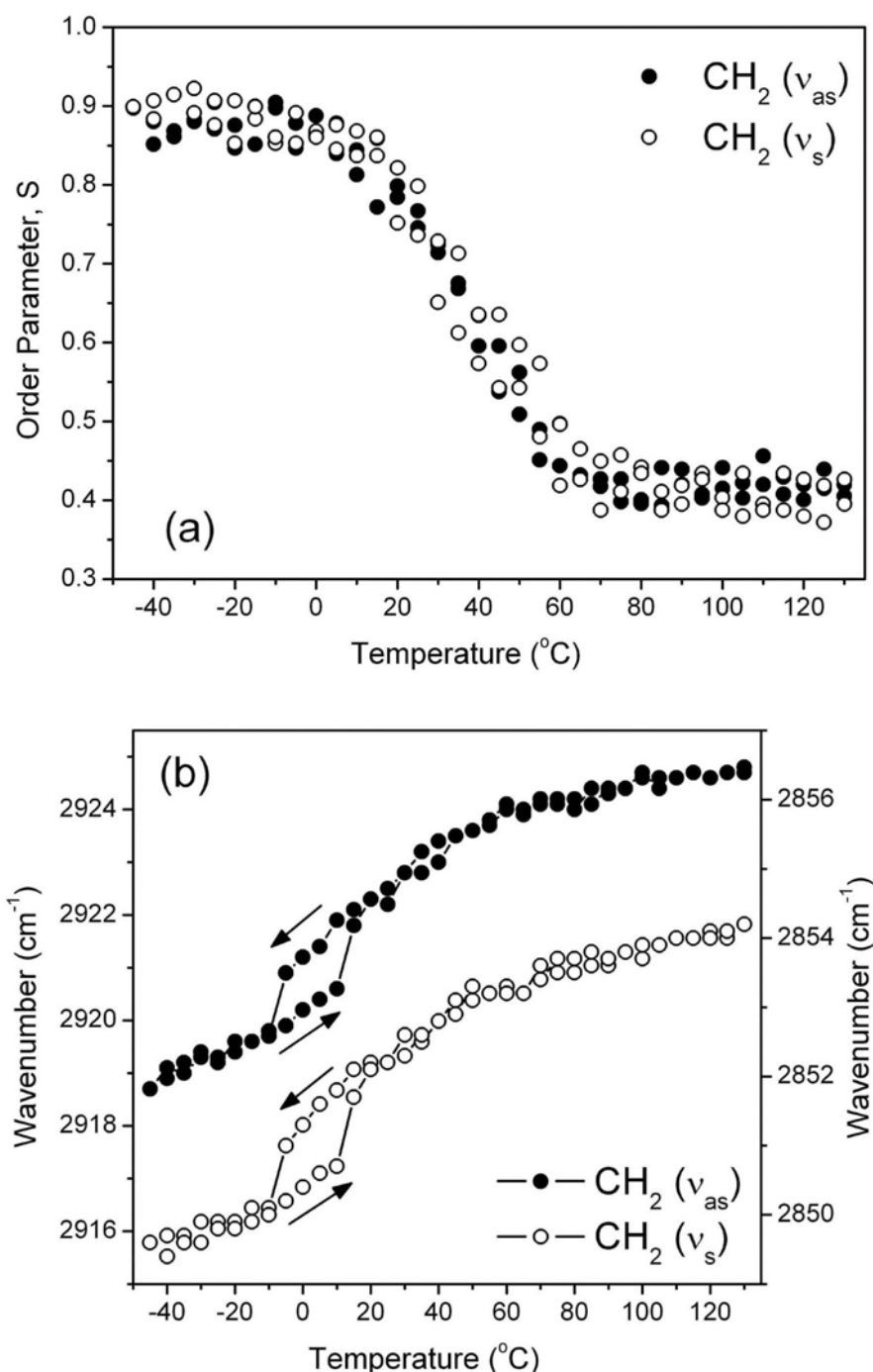


**Fig. 3.11:** (a) Calculated changes of temperature dependent order parameter of alkyl chains of the surfactant from absorbance changes of asymmetrical and symmetrical stretching vibrations of  $\text{CH}_2$  group; (b) and appropriate frequency shift for these vibrations on cooling-heating circle (left axes:  $v_{\text{as}}$ ; right axes:  $v_{\text{s}}$ ).

An additional remarkable feature of these ISA materials is that, with a decrease in temperature, the complex crystallizes from an aligned LC phase into a single crystal domain. No formation of crystalline domains was observed in polarized light microscope on cooling the sample. Practically all known low molecular LCs crystallize in multidomain structure because of thermal fluctuations. In the ISA complex the ionic interactions dominates and suppresses these fluctuations, resulting in very large monodomain structures.

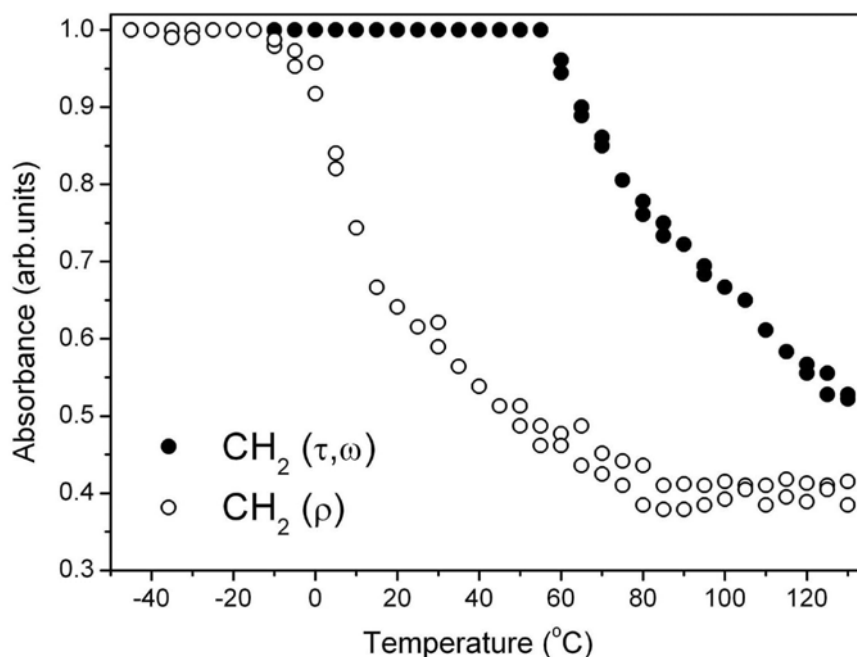


**Fig. 3.12: Temperature changes of normalized integrated absorbance of out-of-plane bending ( $\tau, \omega$ ) and in-plane bending ( $\rho$ ) vibrations of CH<sub>2</sub> group.**

The frequency shifts for the CH<sub>2</sub> asymmetrical and symmetrical stretching vibrations are presented in Fig. 3.11b. An abrupt change in frequency is found in the heating cycle at 10°C, with an hysteresis of 20°C in the cooling cycle. Abrupt changes in frequency and hysteresis was also observed for scissoring vibration of CH<sub>2</sub> group. These changes are attributed to changes in the packing of the alkyl chains with the onset of crystallization processes/events. A similar hysteresis is observed in DCS curves (Fig. 3.2) for transition peaks marked with 2.

The changes in order parameter are strongly correlated to the crystallization (packing) process. This can be seen from temperature changes of the normalized integrated absorbance of the in-plane CH<sub>2</sub> bending (rocking) vibration (Fig. 3.12), which acts as indicator of the crystallization (packing) behavior of the alkyl chains. Here it should be also noted that the

transition marked with 1 in DSC curves (Fig. 3.2) is attributed to crystallization of alkyl chains.

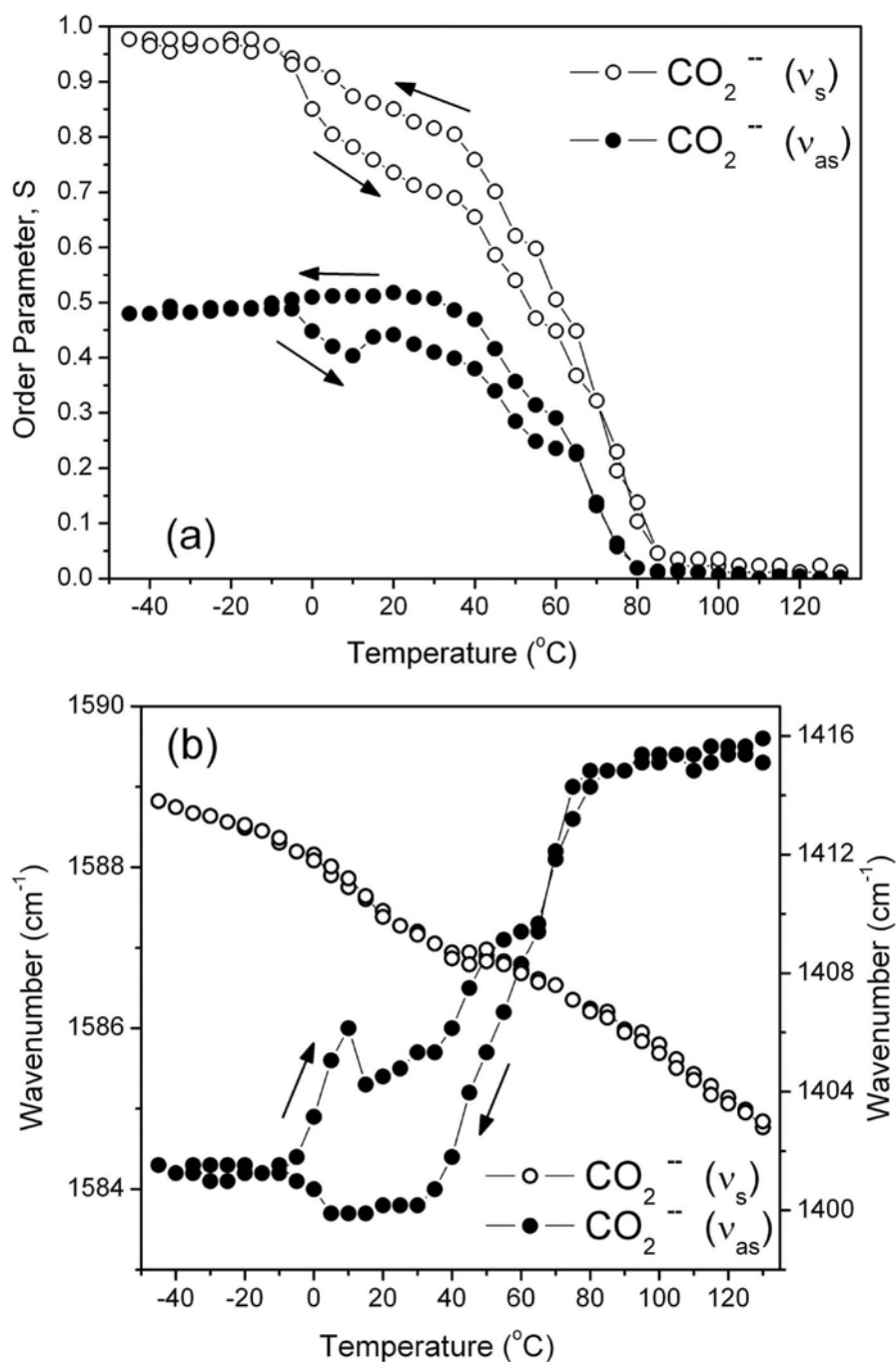


**Fig. 3.13:** (a) Calculated changes of temperature dependent order parameter of alkyl chains of the surfactant from absorbance changes of asymmetrical and symmetrical stretching vibrations of  $\text{CO}_2^-$  group; (b) and appropriate frequency shift for these vibrations on cooling-heating circle (left axes:  $\nu_{as}$ ; right axes:  $\nu_s$ ).

Changes in the integrated absorbance of the out-of-plane  $\text{CH}_2$  bending ( $\tau, \omega$ ) vibration are connected to the ‘bending’ process of alkyl tails (Fig. 3.12). The peaks marked with 3 on

DSC curves (Fig. 3.2) are attributed to the straitening-bending transition of alkyl chains and correspond to the observed change. One should expect the transition to the isotropic phase to be connected with the onset of bending of the alkyl chains. However, the order parameter of the alkyl chains remains constant (0.4), which may indicate that the chains are held in their positions by the ionic interactions found within the complex.

The calculated order parameter of the BHC molecules from absorbance changes of symmetrical and asymmetrical stretching vibrations of  $\text{CO}_2^-$  group is presented in Fig. 3.13a. The order parameter calculated from symmetrical vibration represents the real ordering of the benzene rings because the transition dipole of the symmetrical vibration lies in the plane of the benzene ring (i.e. it forms an angle  $\beta = 90^\circ$  with the normal of the benzene ring plane). As was already mentioned in section 3.3.2, the transition dipole of the asymmetrical vibration may form a certain angle  $\beta$  with the normal of the benzene ring plane. The order parameter of the asymmetrical vibration is calculated from an assumption that this angle  $\beta = 0^\circ$  (Fig. 3.13a). The lower values of the order parameter are caused by this angle. There is a simple correlation between the measured order parameter and the real order parameter in the case of non-zero angle  $\beta$  between the transition dipole and the symmetry axis of the molecule. If the transition dipole of the asymmetrical vibration forms an angle  $\beta$  with the axis of the molecule, the order parameter should be calculated from the formula:<sup>[80(Chap. 2, p. 41)]</sup>

$$S = \frac{S_0}{1 - \frac{3}{2} \cdot \sin^2 \langle \beta \rangle} \quad (3.4)$$

where  $S_0$  is the order parameter calculated with the assumption that  $\beta = 0^\circ$ , and  $S$  is the real order parameter. Therefore having values of the order parameter calculated for  $\beta = 0^\circ$  it is possible to calculate the average angle  $\langle \beta \rangle$  of deviation of the transition dipole of the asymmetrical vibration from the normal of the benzene ring plane. This angle is also the angle between the plane of  $\text{CO}_2^-$  group and the normal of benzene ring plane (Fig. 3.7). Calculations of this angle in the temperature range  $-45$  to  $-10^\circ\text{C}$  give the value  $\langle \beta \rangle = 35 \pm 1^\circ$ , and in the temperature range  $10$  to  $60^\circ\text{C}$ :  $\langle \beta \rangle = 31 \pm 1^\circ$ . Hysteresis is found at intermediate temperatures, as is also observed in DCS curves (Fig. 3.2, peak 2), exists for transition peaks marked with 2. Calculations at elevated temperatures were not possible because of uncertainties caused by values of the order parameter being close to zero.

Hysteresis in the order parameter can be attributed to the influence of crystallization (packing) processes of the alkyl chains, which, in turn changes the position of the cationic groups. The proof that changes in the positions of the cations influence the packing of

benzene rings can be seen from the frequency shift of the symmetrical and asymmetrical stretching vibrations of the  $\text{CO}_2^-$  group shown in Fig. 3.13b. The transition dipole of the symmetrical vibration should not depend on the influence of the cationic layers if it is oriented in the plane of benzene ring. However, the transition dipole of the asymmetrical vibration is out of this plane at an angle  $90^\circ - \langle\beta\rangle$  and is suppressed by two layers of cations. In addition the hysteresis in the order of the benzene rings appear in the same temperature range as where the repacking process of alkyl chains take place (compare Fig. 3.12 and Fig. 3.13). An additional small hysteresis in the frequency of the asymmetrical vibration of the  $\text{CO}_2^-$  group (Fig. 3.13b) in the  $-10$  to  $10^\circ\text{C}$  temperature range, which is connected to the re-crystallization of alkyl chains (peak 2 in Fig. 3.2) should also be indicated. Finally, it should be noted that an increase of the angle  $\langle\beta\rangle$  when the alkyl chains are in a crystalline state, indicating very strong immobilization of the BHC molecules within the layered structure. Increase of the angle  $\langle\beta\rangle$  can be explained by the fact that on crystallization the alkyl tails of the surfactants become straight and suppress BHC molecules. This suppressing is supplemented by the fact that the order parameter in this range is close to 1 (Fig. 3.13a). The ordering of the BHC tectons is strongly influenced by the packing of the alkyl chains, which are in turn strongly influenced by the presences of the (neutralized) charges. All these processes are interconnected.

### 3.5. Other complexes

The formation of complexes with surfactants of different length and number of alkyl tails, that is, similar double-tailed ammonium surfactants ( $C_{10}D$ ,  $C_{14}D$ ,  $C_{16}D$  ( $n = m = 10, 14, 16$  respectively; Table 2.1) and the single-tail surfactant  $C_{16}S$  ( $n = 16, m = 1$ ; Table 2.1) has also been investigated. All these complexes show alignment behavior similar to the investigated BHC- $(C_{12}D)_6$  complex. On heating they show a strong tendency to align uniformly between two glass slides. Null ellipsometry supplemented with thickness and refractive index measurements revealed negative homeotropically oriented axes with  $\Delta n = -0.020 \pm 0.003$  at  $\lambda = 632.8\text{nm}$ . From this result one can predict the existence of similar layered liquid-crystalline phases in all of these complexes. Additional proof that these complexes possess similar phases is the similar optical textures observed under crossed polarizers.

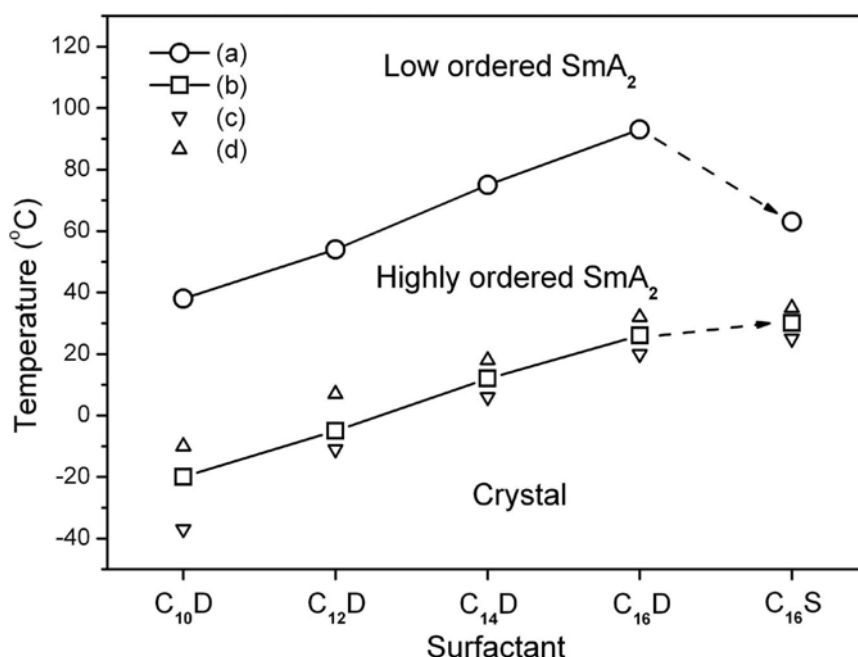


**Fig. 3.14:** Phase transition shifts of the BHC based complexes on change of the length and structure of the surfactants: (a) – corresponds to peak 3 in Fig. 3.2; (b) – corresponds to peak 1 in Fig. 3.2; (c),(d) – correspond to hysteresis of peak 2 in Fig. 3.2 on cooling and heating curves respectively.

Similar transition peaks, which were observed for the BHC- $(C_{12}D)_6$  complex, were also observed for all other complexes in their DSC curves. The shift of the phase-transition

temperatures on change of the length and structure of the surfactants is shown in Fig. 3.14. An increase in the phase-transition temperatures with an increase of the length of alkyl chains is clearly observed. Similar increase in the temperature of phase transitions on increase of the length of the surfactant for pure surfactants was also detected by DSC measurements. From this dependence one can conclude that there is an opportunity, for example, to obtain a single-crystal aligned sample at room temperature just by increase of the length of the alkyl tails of the surfactant.



### 3.6. Conclusions

The influence of ionic interactions on the formation of LC phases in ISA complexes using the simple BHC-(C<sub>12</sub>D)<sub>6</sub> complex as a model system have been investigated. Detailed studies of ordering in the complex, alignment properties and phase transitions using a variety of different techniques were carried out. As was shown all results for the BHC-(C<sub>12</sub>D)<sub>6</sub> complex can be easily extended to the whole series of the complexes with different length and number of alkyl chains of the surfactant.

These complexes exhibit a bilayer smectic SmA<sub>2</sub> liquid-crystalline phase. First sublayer consists of charges (BHC molecules and charged headgroups of the surfactants) and the second sublayer consists of completely interdigitating alkyl tails of the surfactants. Within the first sublayer the BHC molecules are ordered with their planes parallel to the layers. Within the second sublayer, alkyl chains are ordered perpendicular to the layers. This is in stark contrast to the usual phase behavior found for any benzene-based discotic materials, which usually form columnar phases.

The complex aligns spontaneously, with the alignment properties not depending on the nature or treatment of the slides. The aligned complex possesses a negative homeotropically oriented optical axis (at room temperature), with layers aligned parallel to the slide surface.

Temperature-dependent IR spectroscopy measurements on the aligned BHC-(C<sub>12</sub>D)<sub>6</sub> complex revealed that the complex crystallize from the aligned LC phase into a single crystal domain on cooling below -10°C. This is a remarkable feature of the ionic interactions in ISA complexes, where dominating ionic interactions suppress fluctuations appearing during the crystallization process. Practically all known low molecular weight LCs crystallize in multidomain structures because of these fluctuations. The presence of the ionic interactions also suppresses the transition to an isotropic phase. This would therefore also indicate that all other interactions, except the ionic interactions between the tectonic groups and hydrophobic interactions between the alkyl tails, can be largely neglected.

Besides the importance of such simple complexes in the basic investigations of the influence of ionic interactions on the formation of ISA complexes, these complexes may also find industrial applications. The first application of such complexes could be as negative compensation film for improvement of viewing angle of liquid-crystal displays.<sup>[81,82]</sup> Cheap in synthesis, easy in alignment and broad retardation range depending on the film thickness (10 – 600 nm) are remarkable advantages of these materials. Since the SAXS diffractogram of

this material shows a series of well-defined, sharp interferences, films prepared from the complexes could therefore also be envisaged as possible candidate for low-cost X-ray monochromators.

## 4. Liquid crystallinity and alignment of perylenediimide-based ISA complexes

As was shown in the previous chapter the ISA strategy proved to be facile and viable non-classical alternative to the LC materials. Liquid crystalline properties are strongly influenced by ionic interactions in the ISA complexes. The ionic interactions stabilize the complex restricting transition to the isotropic phase and allowing the complex to crystallize from ordered LC phase to a monodomain crystal.

The next step would be to complicate the system by replacement a simple benzene-based tecton by a more complicated one with additional interactions and investigate the phase behavior and alignment of the resulting ISA material. Derivative of perylenediimide with presence of strong  $\pi$ - $\pi$  interactions were used as tectonic units. This choice was done in order to demonstrate the potential applicability of the ISA approach. This is supported by the fact that this technological important dye has found wide use in pigments,<sup>[83]</sup> organic thin film polarizers,<sup>[84,85,86,87,88]</sup> organic semiconductors,<sup>[89]</sup> in thin film transistors,<sup>[90]</sup> lasers,<sup>[91]</sup> solar cells,<sup>[92]</sup> and organic light-emitting diodes.<sup>[93]</sup>

For these investigations of liquid crystalline and alignment properties two ISA complexes were used (1-DHDP and 1-AOT, see Table 2.1). In this chapter the thermotropic as well as novel lyotropic phases of the ISA complex is presented. A variety of techniques are utilized for both alignment and consequent quantification of the optical properties of the aligned material.

The perylenediimide has two covalently attached cations on both sides. Two charged anionic surfactants were used to form a complex with charged perylenediimide. One surfactant (DHDP) is double tail surfactant with 16 carbon atoms in each alkyl tail. It is similar to the C<sub>16</sub>D surfactant. The only difference is that the charge is opposite. One should expect the phase transitions corresponding to crystallization-melting and straitening-bending transitions of alkyl tails DHDP surfactant to be in the same temperature range as for the C<sub>16</sub>D surfactant. So, the DHDP was selected from the simple reason to have comparison with the known results. The second surfactant (AOT) has branched alkyl tails. This surfactant does not show any transitions corresponding to crystallization-melting and straitening-bending behavior. No corresponding peaks were expected to observe in the DSC curves of the corresponding complex. This surfactant was selected to compare influence of non-branched and branched surfactants on liquid crystalline and alignment properties of the resulting complexes.

## 4.1. Thermotropic liquid crystalline phase

### 4.1.1. Phase characterization

Both ISA materials (1-DHDP and 1-AOT) exist in a form of dark-colored powder at room temperature. The materials were subjected to thermal analyses to determine their stability. TGA showed that the materials degrade at 225°C (1-DHDP) and 275°C (1-AOT) respectively. On heating the 1-DHDP material becomes soft starting from 80°C. The 1-AOT material becomes gradually softer on heating and no abrupt changes in viscosity was observed. Polarized light microscopy indicated that neither of the two complexes exhibits a clearing point (transition to isotropic phase) before the onset of degradation.

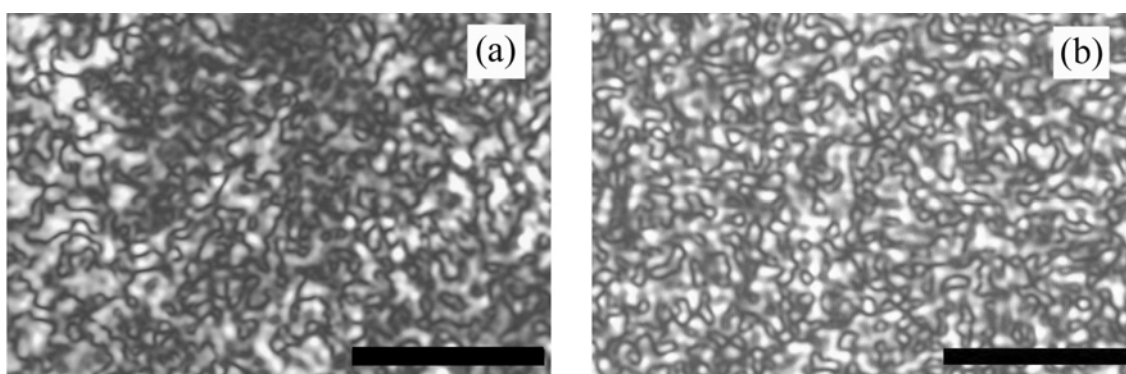


**Fig. 4.1:** Typical textures of (a) 1-DHDP complex and (b) 1-AOT complex as observed in polarized light microscope (crossed polarizers, bar: 10  $\mu\text{m}$ )

Thin films for microscopy investigations were obtained by two methods: either by direct melting of the brown powder materials between glass slides (performed at 200°C, to reduce the viscosity of the material), or by casting from chloroform solution (30 mg/ml). Due to easier handling at room temperature, the latter route was used. Both methods of preparation yielded highly birefringent films exhibiting Schlieren-like textures when investigated by means of temperature-dependent polarized light microscopy. The textures present at high temperatures were preserved throughout the heating-cooling process. No evidence of crystallization, i.e. formation of crystallites, was observed, as is seen in Fig. 4.1 (taken at room temperature after heating to 200°C). Here it should be noted that the size of texture defects is really small (order of micrometer). It was impossible to distinguish a specific structure of the defects by visible light and to make any prediction of the phase in which both complexes exist.

The phase behavior of the complexes was investigated by differential scanning calorimetry (DSC). The DSC curve of 1-DHDP (Fig. 4.2) shows no less than three consecutive transitions. All these peaks are attributed to transitions in the complex connected with crystallization-melting of alkyl tails of the 1-DHDP surfactant. The DSC curve of the 1-AOT complex showed no transitions. This indicates that the complex exists in a LC phase in the temperature range at least from -50 to 200°C. This is in contrast to the 1-DHDP, which showed reversible transitions from a LC to a partially crystalline state.

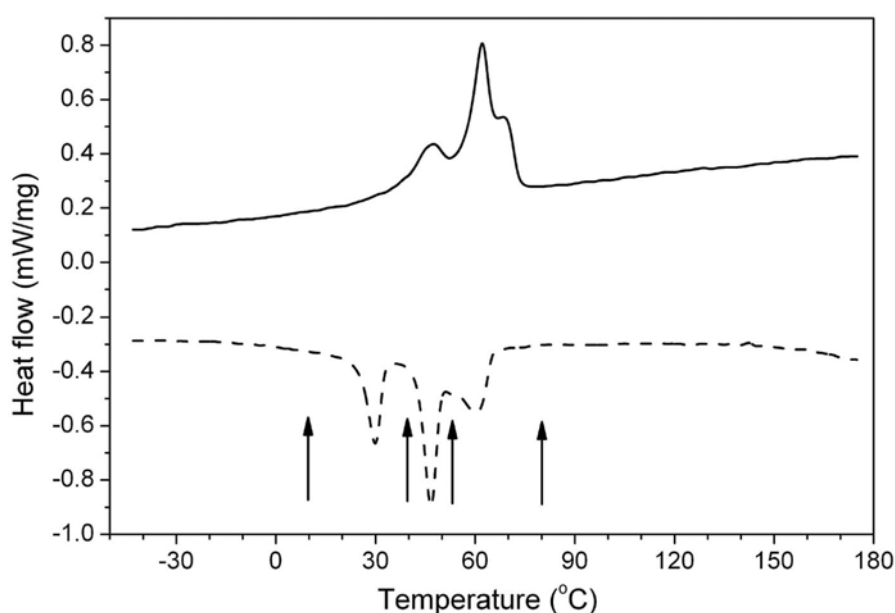


**Fig. 4.2: DSC curves of the 1-DHDP complex: second cooling cycle (dashed curve) and third heating cycle (solid curve).**

Both complexes were investigated by means of temperature dependent X-ray analyses to clarify the supramolecular organization and phase behavior.

In the case of the 1-DHDP complex, which exhibited several phase transitions, X-ray diffractograms were recorded at the following five temperatures in the cooling curve: 200, 80, 53, 40 and 10 °C. In the WAXS diffractograms recorded at 200, 80 and 53 °C no reflections indicative of crystalline packing of the alkyl tails could be found. The measurements at both 40 and 10 °C exhibited only one very strong reflection at a d-spacing of 0.41 nm, indicative of partial crystallinity in the alkyl side chains. Even though this change was also observed in the DSC curve (by the strong transition at 47°C), this was not reflected in the textures observed by polarized light microscopy. On further heating of the sample, WAXS measurements confirmed the reversible transition to a thermotropic liquid-crystalline

phase. The WAXS diffractograms showed the presence of very weak stacking of the perylene diimide tectonic units at d-spacing of approximately  $0.33 \div 0.34$  nm a little varying on change of the temperature.

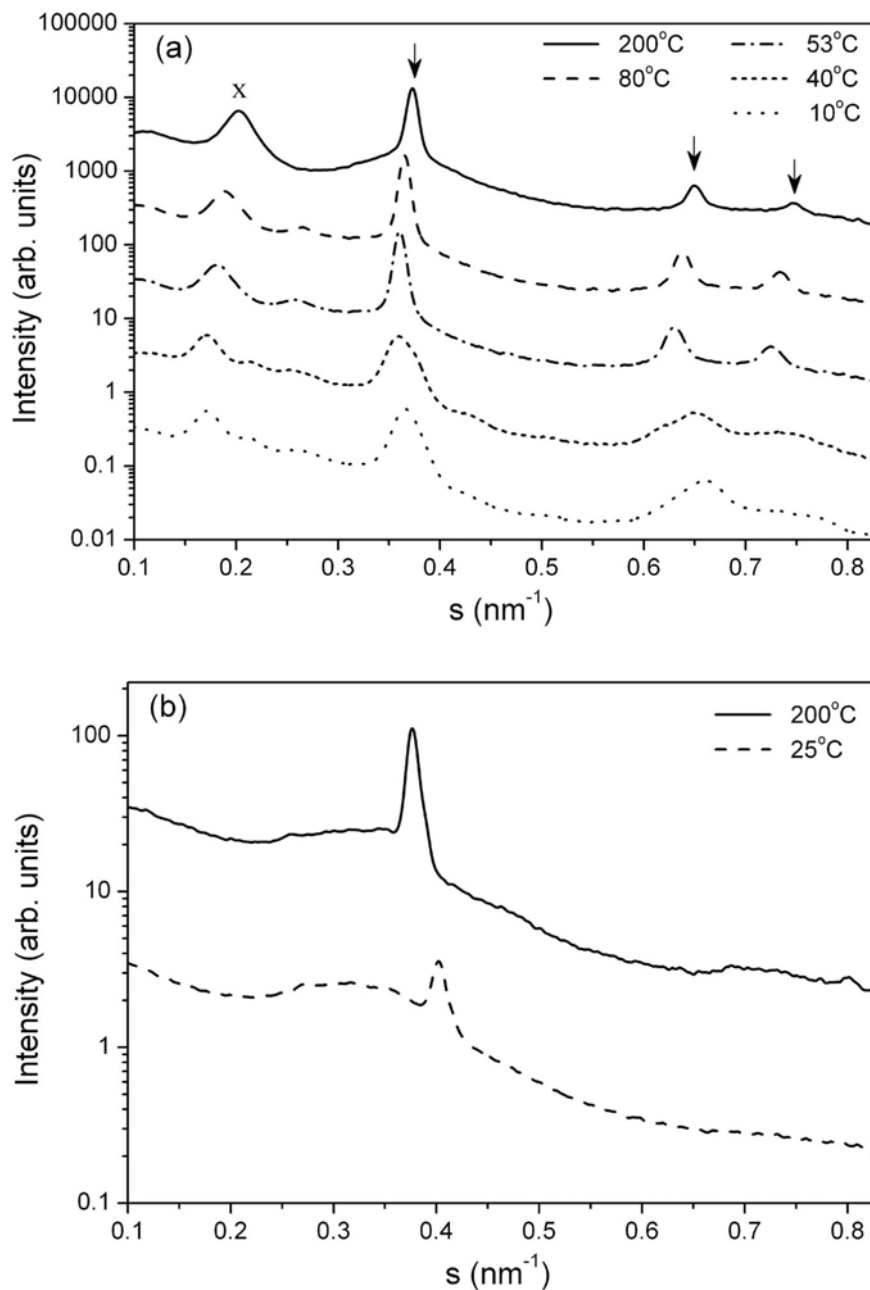


**Fig. 4.3:** SAXS diffractogram for (a) the 1-DHDP complex and (b) the 1-AOT complex at different temperatures recorded during the cooling cycle.

SAXS diffractograms for the 1-DHDP complex showed a high degree of molecular order of the perylene diimide column packing. Fig. 4.3a presents the data from measurements taken at 200, 80, 53, 40 and 10°C. A hexagonal columnar phase with d-spacing of 2.77 nm ( $s$

$= 0.36 \text{ nm}^{-1}$ ) is easily identified (indicated by the arrows in Fig. 4.3a). The reflection at  $s = 0.18 \text{ nm}^{-1}$ , marked with an x, is at exactly twice the repeat distance of the hexagonal columnar phase. At lower temperatures (i.e. at 40 and 10 °C), the hexagonal columnar phase is slightly distorted due to the influence of the observed partial crystallinity of the surfactant alkyl tails.

In summary, the 1-DHDP complex exists in disordered hexagonal columnar liquid crystalline phase ( $\text{Col}_{\text{hd}}$ ). Below the transition to the partially crystalline phase of the surfactant alkyl tails the order of columns is even more disturbed. It is an opposite situation to the BHC-based complexes (Chapter 3) where the crystallization of alkyl tails brings the system to the crystalline state with order parameter close to 1. In the case of the 1-DHDP complex there is no evidence of the perfect ordering in the complex. That is why only because of partial crystallinity of the surfactant alkyl tails the phase below this transition is called partially crystalline. Above this transition the phase is liquid crystalline.

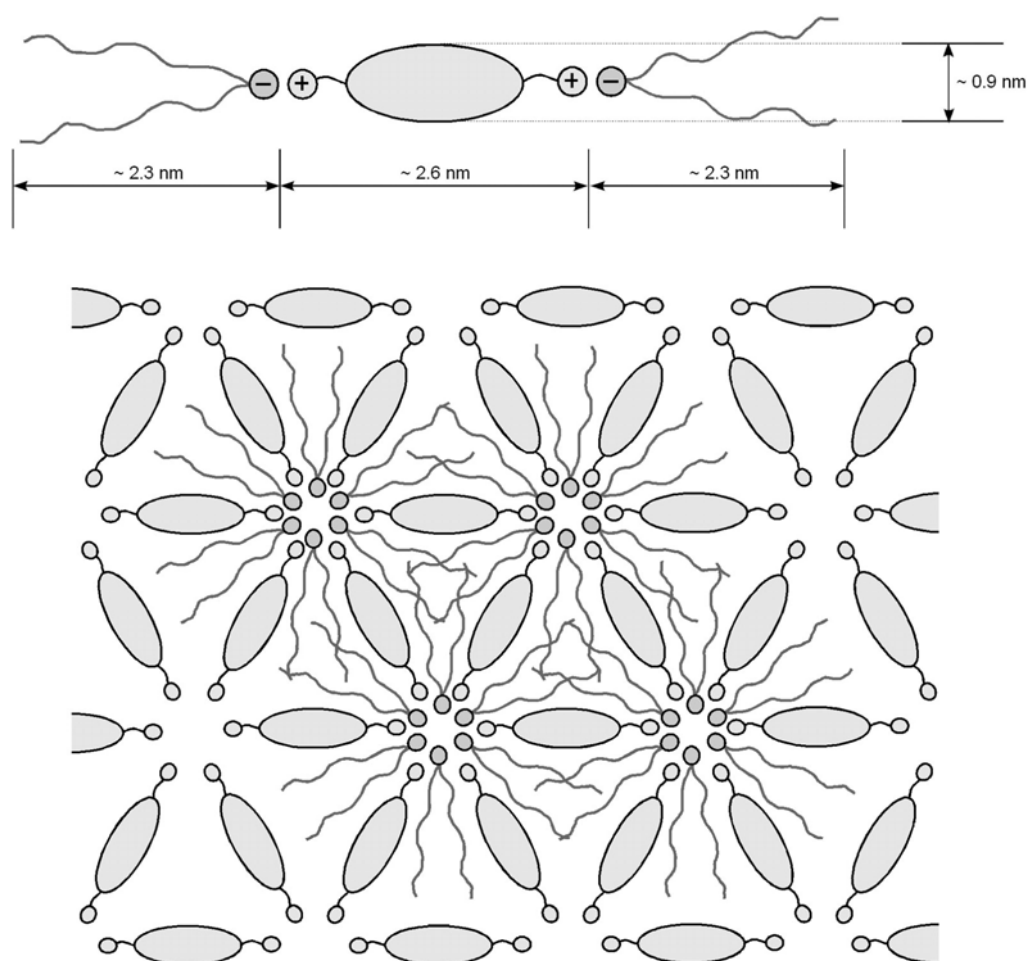


**Fig. 4.4:** Schematic representation of the molecular dimensions and proposed packing of molecules ahead of the hexagonal architecture of the 1-DHDP complex.

In order to propose the model of molecular packing in the hexagonal columnar liquid crystalline phase of the 1-DHDP complex with d-spacing of 2.77 nm calculations of the molecular dimensions of the tectons of the complex using known lengths of the appropriate covalent bonds<sup>[74(Section 9, pp.1-14)]</sup> and van der Waals radii of elements<sup>[75(Chap. 4, p.71)]</sup> were performed. Calculated molecular dimensions are shown in Fig. 4.4. To fit into d-spacing of the hexagonal phase the model of molecular packing was proposed. It is shown in Fig. 4.4 (for clarity not all surfactant tectons are shown). In this model the fact of complete compensation of charges in the complex is considered.

It should be noted that within this model the disturbing of the hexagonal columnar phase on partial crystallization of the alkyl tails of the surfactant can be explained: it is clearly seen that alkyl tails located between adjacent columns will disturb this columns on their crystallization process.

In order to identify the phase present in the 1-AOT complex, X-ray scattering measurements were performed. Temperature-dependent WAXS diffractograms, measured at 200 and 25°C, showed the presence of stacking of the perylenediimide tectonic units with a d-spacing of approximately  $0.33 \div 0.34$  nm. No other sharp reflections were observed in the wide-angle region. The SAXS diffractograms (Fig. 4.3b) recorded at these temperatures indicated that short-range order on the nanometer scale was also preserved throughout the temperature cycle, confirming the liquid-crystalline nature of the material. Because 1-AOT and 1-DHDP complexes are quite similar in the structure than they should possess similar phase packing. From stacking of perylenediimide tectons one can conclude that there is presence of columns in the 1-AOT complex. From SAXS data it is clear that there is no specific packing of columns is present. From these data one can conclude that the 1-AOT complex exists in a nematic columnar phase ( $N_{col}$ ) in the temperature range under investigation ( $-50 \div 250^\circ\text{C}$ ) with d-spacing of  $\sim 2.5$  nm at room temperature which increases on heating of the complex. On increase of the temperature there is small increase in the d-spacing between columns and between perylenediimides in columns was observed.

Stacking of perylenediimide should be reflected in UV-Visible spectra. Results from the UV-Visible spectroscopic investigation of isolated perylenediimide chromophores in solution (ethanol,  $2.3 \times 10^{-7}$  M) and aggregated chromophore for both complexes complexes in thin films are presented in Fig. 4.5. It can be seen that in the case of the isolated chromophores, the UV-Visible spectrum is characterized by four absorption maxima (522, 486, 456 and 428 nm). All maxima correspond to the electronic  $\pi$ - $\pi^*$  transition superimposed



with vibrational transitions.<sup>[94]</sup> In the aggregated thin film state, the spectrum has, as expected, a different shape. Here the originally second maximum (486) is strongly enhanced, the first (522) is suppressed (forming a shoulder) and the others overlapped by the second. This behavior is typical for aggregation<sup>[95]</sup> and was observed in many cases for perylene derivatives.<sup>[64,96,97]</sup> The shoulder around 570 nm is caused by resonance interactions between the transition dipoles in the solid aggregated state.<sup>[64]</sup> The mentioned changes in the spectra are similar to that found for the parallel arrangement of chromophore dipoles (H-aggregates). The results of UV-Visible spectra confirm in addition to X-ray data that the perylenediimide tectons stack into columns.

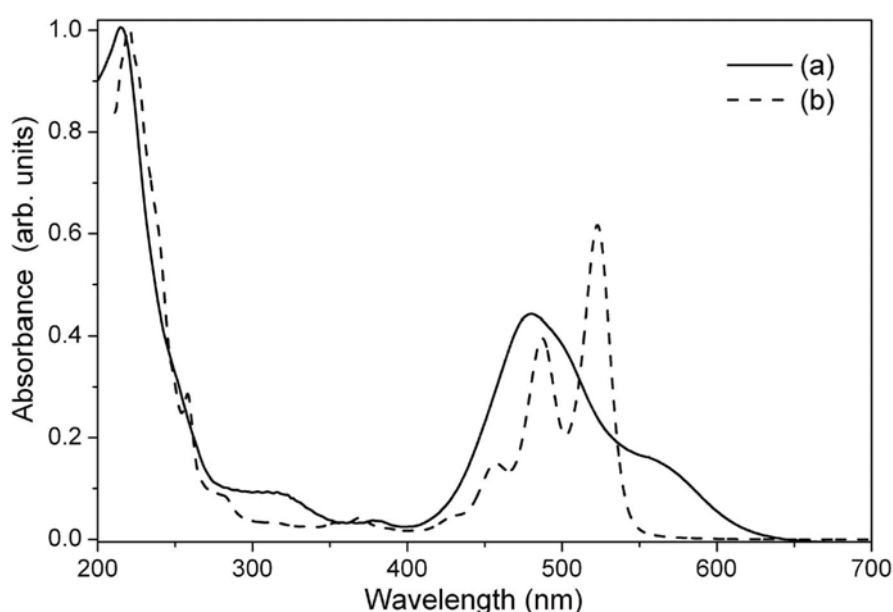


**Fig. 4.5:** UV-Visible spectra of the complexes measured (a) in film and (b) solution (ethanol,  $2.3 \times 10^{-7}$  M). These are the data for the 1-AOT complex. For the 1-DHDP complex the curves are practically the same.

#### 4.1.2. Alignment in the thermotropic phase

In order to investigate the alignment of the complexes in external fields, films of 0.5-2  $\mu\text{m}$  thickness were prepared by spincoating from chloroform solution ( $7.1 \times 10^{-5}$  M) onto clean glass slides. The influence of both a magnetic field (2 Tesla) and an electric field ( $10^7$  V/m) were investigated. To investigate the alignment of the complex by surface interactions, thin films were spincoated on the following: rubbed polyimide films, photo-oriented azobenzene-containing polymer films, surface modified glass (hydrophobic and hydrophilic), charged polymer layers (positive and negative) deposited onto glass slides and friction

transfer oriented PTFE films.

None of the above classical/standard methods used for LC alignment employed proved to be a successful to align the materials. This is probably caused by the combination of the existence of a well-structured phase of the complex and the presence of ionic interactions within the materials. In addition the alignment of highly ordered and complex phases (e.g. smectic, columnar discotic, lyotropic, chromonic)<sup>[29]</sup> has proved to be difficult and is the reason for the successes achieved with the low-ordered classical nematic phases. The success achieved for alignment of smectic phase of BHC-based complexes should be attributed to the nature of these complexes and their simplicity. Additional functional groups bring additional interactions in the ISA complexes that complicates the system and restricts their processability.

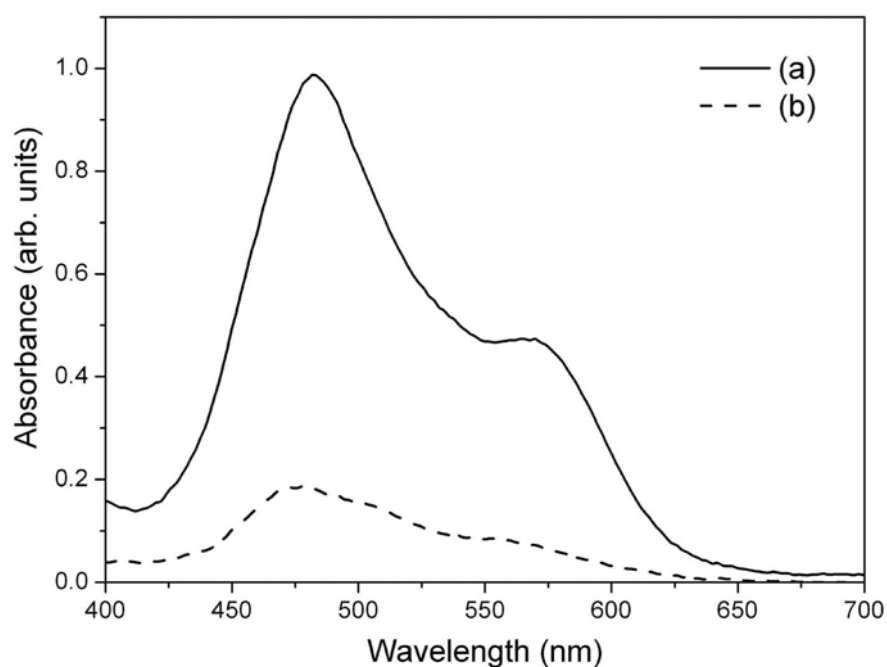


**Fig. 4.6: Normalized polarized visible absorption spectra of film of the complex aligned by shear force: (a) perpendicular and (b) parallel to the shear force.**

The next route for alignment investigated was alignment by application of shear force. This method has already been used to produce aligned films of discotic columnar phases.<sup>[98,99,100]</sup> Since it was also applied to produce aligned films of perylene diimide-based compounds from their lyotropic phase,<sup>[64,86,87,101,102]</sup> indications therefore were that this strategy might prove to be successful. Since the both materials (1-DHDP and 1-AOT) become softer on heating, they were placed on a clean (nontreated) glass slides and heated to 200°C. The

materials were then sheared with a blade by hand (the tilt of the blade in relation to the substrate was approximately  $10^\circ$ ). To control the thickness of the film, powder glass spacers (1, 3 or 5  $\mu\text{m}$ ) were used. This strategy proved to be more successful than the methods mentioned above, and characterization of the orientation within the thin films was performed.

Polarized absorption spectra were measured on the sheared thin films. The results for 1-AOT complex are presented in Fig. 4.6. The similar results were obtained for 1-DHDP complex. The oriented samples show maximum absorbance when the plane of polarized light is perpendicular to the shearing direction. It is therefore suggested that columns of stacked perylenediimide tectonic units are oriented in the direction in which the shear force was applied. Since these measurements only provide in-plane information, it was not possible to predict the dipole orientation in the out-of-plane direction.

The quality of the films prepared using this method was poor, since control of the uniformity of the thin film using mechanical contact is difficult (especially at  $200^\circ\text{C}$ ). Films produced by this method were also investigated by polarized light microscopy. By focusing on different planes inside the film very good alignment of the material was noticed at the interfaces, while some defects still existed in the bulk of the film. The presence of these defects therefore led to a relatively small value for the dichroic ratio. The maximum dichroic ratio obtained for several prepared films was 6.

## 4.2. Lyotropic liquid crystalline phase

Two complexes (1-DHDP and 1-AOT) have been tested for alignment with methods described below. However the successful results were obtained only for the 1-AOT complex. That is why all discussion is focused on the 1-AOT complex.

### 4.2.1. Phase characterization

It was found that the 1-AOT complex forms lyotropic phases in DMSO (as determined by polarized light microscopy and X-ray analysis). The complex also showed lyotropic phase behavior in 1-methyl-2-pyrrolidinone, but initial tests indicated that DMSO is more suitable for processing. The optical texture of the complex in the lyotropic phase was similar to that of the thermotropic one.

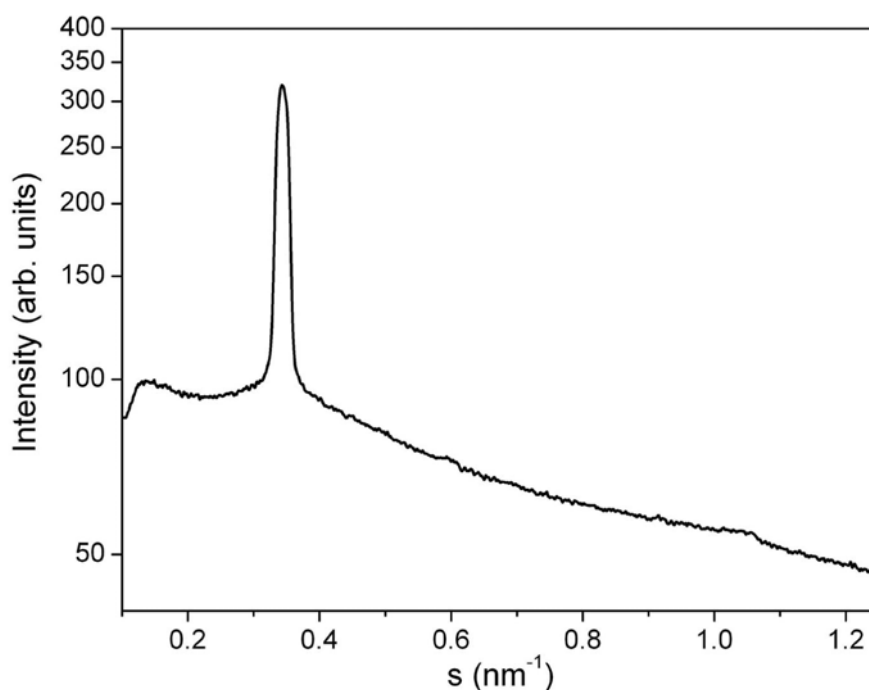


**Fig. 4.7: Recorded SAXS diffractogram for the 1-AOT complex in a lyotropic phase in DMSO (approximately 28 wt. % solution) at room temperature.**

A lyotropic phase (approximately 28 wt. % solution) of the complex in DMSO shows a very broad transition to the isotropic phase at  $\sim 70$ - $90^\circ\text{C}$ . WAXS analysis of the solution at room temperature showed that the perylenediimide units aggregate only very weakly, with very weak reflection recognizable at  $2\theta$ . SAXS analysis of this phase at room temperature showed the presence of a nematic columnar phase ( $N_{\text{col}}$ ) with d-spacing of 2.94 nm (Fig. 4.7).

#### 4.2.2. Alignment in the lyotropic phase

At first the possibility to orient the complex in this lyotropic state by means of external fields and by surface interactions, as was done in the case of the thermotropic phase, were investigated. Once again, aligned films could not be produced by these methods. Furthermore, application of the shearing force technique to the lyotropic phase at room temperature yielded similar results as from the thermotropic phase. Again, alignment was found near the interfaces, with defects existing in the bulk.

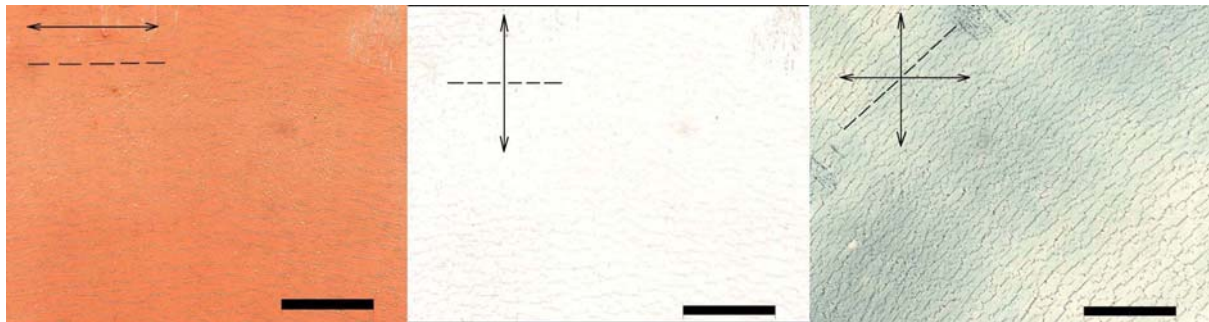


**Fig. 4.8: Pictures of film made by directed domain growth (arrows represent axes of polarizers, dashed line represents the phase-transition front (PTF), bars: 200 $\mu$ m).**

During investigations into the phase behavior and transitions (from the isotropic to the lyotropic liquid-crystalline phase) directed alignment of the material at the phase-transition front (PFT) was observed. It seemed that the material formed or aligned in a single domain following the PFT. In order to investigate this promising route in detail, the following procedure was developed: First, a lyotropic phase of 1-AOT in DMSO was prepared, and chloroform added to this solution (concentration of 1-AOT in the two solvents  $\sim 7.1 \times 10^{-5}$  M). This solution was then cast on a clean glass slide and kept at room temperature under quiescent conditions to ensure slow evaporation of the chloroform. The film (in the lyotropic state) obtained in such a way was then heated to the isotropic phase (100°C). At this temperature the DMSO starts to evaporate slowly, and, due to nonuniform evaporation of the DMSO (faster at the edges of the film), a concentration gradient is formed. The rate of evaporation of DMSO was not controlled but assumed to be determined by the temperature. As a result of this, an isotropic – LC phase-transition front (PTF) is formed. On this front directed domain growth appears. After film formation was complete, the films were dried at 150°C for a day to ensure the evaporation of all residual DMSO. The PTF was not linear and rounded at the corners of the sample. It was possible to find areas of about square centimeter where the PTF was practically linear to make characterization of the alignment.

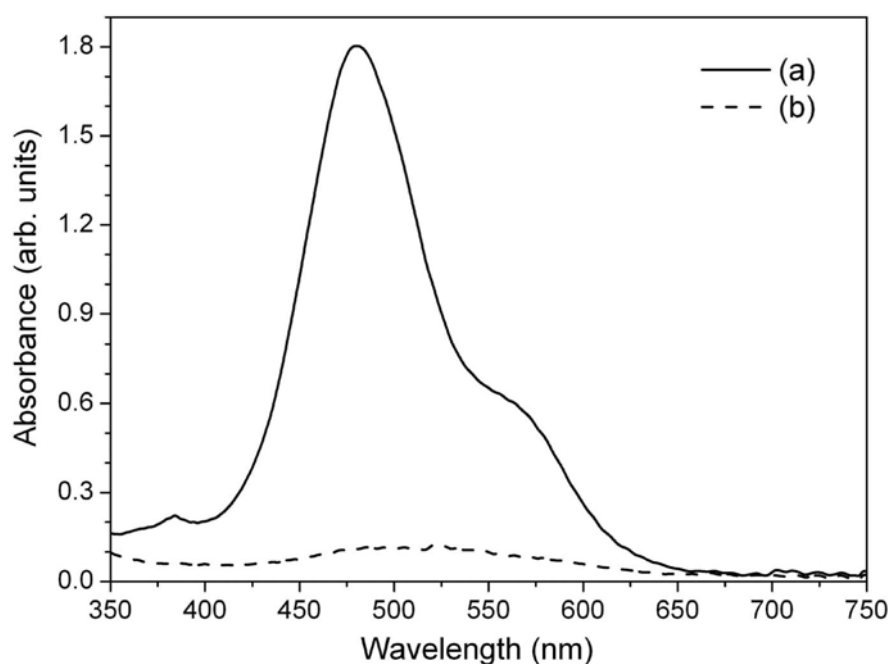


**Fig. 4.9: Polarized visible absorption spectra of film of the complex made by directed crystallization: (a) parallel and (b) perpendicular to the phase-transition front (PTF).**

The anisotropic optical properties of the films were examined by polarized light microscopy. The films were red (blue and green light was absorbed) when the polarization axis of the incident light was parallel to the PTF (Fig. 4.8). In contrast, the films were colourless and transparent when the polarization axis of the incident light was orthogonal to the PTF. Films were highly birefringent when observed under crossed polarizers. The optical anisotropy of these films was quantified by polarized visible spectroscopy. As shown in Fig. 4.9, the films exhibited very high absorbance parallel to the PTF, whereas absorbance perpendicular to the PTF was very low. The dichroic ratio at the maximum of absorbance was found to be 18. This corresponds to a spectroscopic order parameter of 0.85. These results suggest that the perylenediimide-based tectons are oriented on the substrate in such a way that their electronic transition moment dipoles are preferentially aligned parallel to the phase transition front. This therefore suggests that columns of the tectons are aligned perpendicular to this front. Since there is high dichroic ratio of absorbance perpendicular to the columns we can conclude that the dipole transition moment of the perylenediimide moieties is mostly perpendicular to the formed columns.

To characterize the 3D packing of the tectons in the film, transmission null-ellipsometry was performed on the prepared films. The dependence of the change of the

angle of polarization  $\varphi$  (after the quarter wave plate) on the tilt angle  $\alpha$  of the sample for two mutually orthogonal positions of the sample was measured. Using a biaxial structure model, this dependence relationship have been theoretically generated (for details see section 2.2.4). Both the experimentally obtained and the theoretically calculated curves are shown in Fig. 4.10. From this, the in-plane and out-of-plane birefringence of the film was found to be  $(n_x - n_y) d = -66.0$  nm and  $(n_x - n_z) d = -50.0$  nm respectively (where the z-axis is normal to the substrate, the y-axis is parallel to the phase transition front, and the x-axis perpendicular to it, details provided in Fig. 4.11).

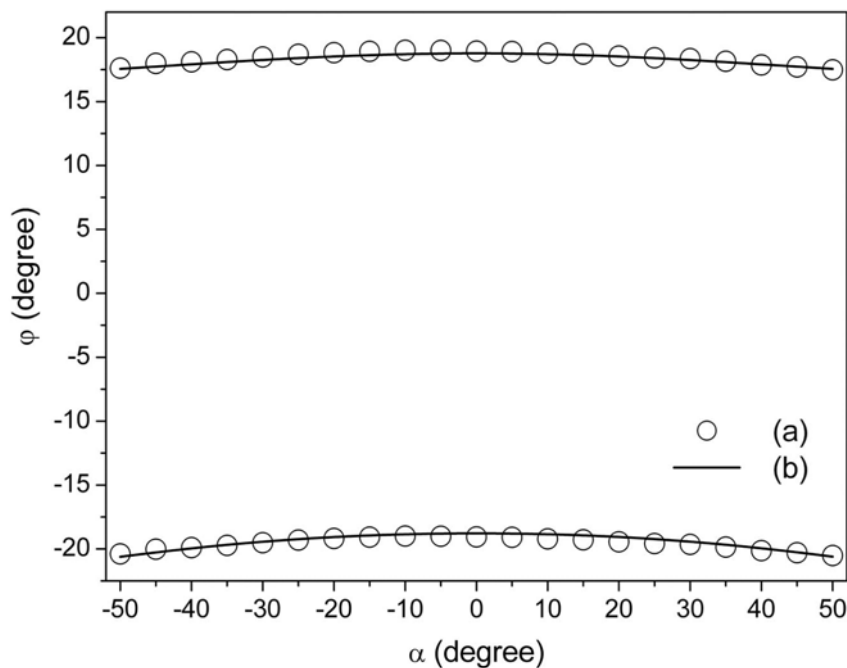


**Fig. 4.10:** Measured (a) and fitted (b) dependence of the change of angle of polarization  $\varphi$  after quarter wave plate on the tilt angle  $\alpha$  of the sample for the film made by directed domain growth. The two curves correspond to two mutually orthogonal positions of the sample.

Separate measurement of the thickness of the prepared films and the average refractive index at  $\lambda = 632.8$  nm of a non-aligned film yielded values of  $d = 400$  nm and  $\langle n \rangle = 1.550$  respectively. Combination of these values with the results obtained from null ellipsometry measurements (see above), allows for the determination of the principal refractive indices of the film, with  $n_x = 1.450$ ,  $n_y = 1.615$ ,  $n_z = 1.575$  at  $\lambda = 632.8$  nm. In these calculations it was assumed that the average refractive index does not change with the alignment of the material because i) no chemical reactions take place, and ii) only

macroscopic alignment of microdomains (which are not aligned in the isotropic non-aligned film) is effected.

Taking the dispersion of the refractive index near an absorption band into account (in our case this is the  $\pi$ - $\pi^*$  transition absorption band of the perylene-3,4,9,10-tetracarboxylic diimide-based tectons), it can be stated that columns are packed in the plane of the film and perpendicular to the PTF in the aligned film. Considering that the dipole moment of the  $\pi$ - $\pi^*$  transition of perylene-3,4,9,10-tetracarboxylic diimide is parallel to its long axis<sup>[85]</sup> and the anisotropic distribution of the refractive indices ( $n_y > n_z \gg n_x$ ), one can say that the long axes of the perylene-3,4,9,10-tetracarboxylic diimide tectons are preferentially distributed within the yz-plane (Fig. 4.11). There is some small preference in orientation in the y-direction that might be a result of the influence of the interfaces.

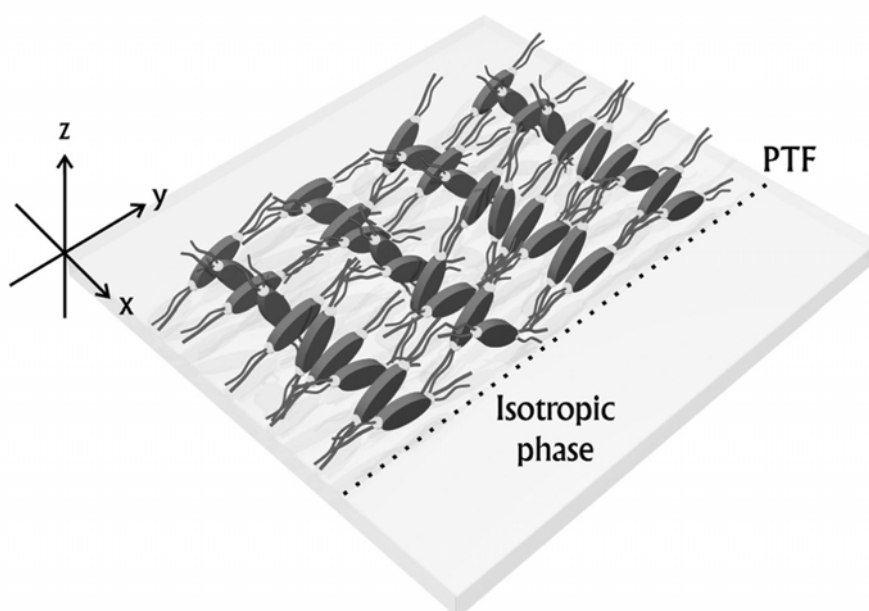


**Fig. 4.11: Schematic representation of the alignment of the material in at the LC – isotropic phase transition front (PTF).**

It is evident from Fig. 4.9 that the film is not uniform. Dark lines, parallel to the PTF, are observed under crossed polarizers, and are the result of topological features created by shrinkage of the material during evaporation of DMSO. The depth of these features reaches 300 nm (as measured by AFM), whereas the total thickness of the film was only 400 nm.

Investigation of the films by polarized light microscopy at high magnification revealed the existence of microdomains, with their optical axes aligned (mostly) parallel to each other. The domains are 2-5  $\mu\text{m}$  in width and 50-200  $\mu\text{m}$  in length with their long axes parallel to the PTF. It is believed that they are obtained under nonuniform evaporation of



DMSO. Existence of such domains is probably the cause for not obtaining higher values for the order parameter. With better control of the preparation conditions (deposition of the film by capillary action at 100°C, ensuring the existence of a temperature gradient to ensure uniform evaporation, quiescent conditions) it was possible to produce more uniform films, however with some loss in anisotropy. Finding the optimal conditions for the production of highly ordered and uniform films is a technical problem.

### 4.3. Conclusions

Liquid crystalline behavior and alignment properties of perylenediimide functionalized ISA complexes have been investigated in detail. Both ISA complexes exist in columnar liquid crystalline phases. Columns are formed by stacking of perylenediimide tectons at d-spacing of approximately  $0.33 \div 0.34$  nm. Planes of perylenediimides are ordered perpendicular to the columns. The 1-DHDP complex (with non-branched surfactant) exists in disordered hexagonal columnar liquid crystalline phase ( $Col_{hd}$ ) with d-spacing of 2.77 nm. Below  $\sim 47^\circ C$  the complex is partially crystalline and the hexagonal order is a little bit disturbed because of partial crystallization of alkyl tails of the surfactant. The 1-AOT complex exists (with branched surfactant) in a nematic columnar phase ( $N_{col}$ ) in the temperature range under investigation ( $-50 \div 250^\circ C$ ) with d-spacing of  $\sim 2.5$  nm at room temperature which increases on heating of the complex. No transition to the isotropic phase was observed for both complexes before the onset of degradation.

The standard methods used for the LC alignment (surface interactions and external fields) were employed to align both complexes and proved to be not successful. This is probably caused by existence of additional interactions between functional perylenediimide tectonic units in addition to the ionic interactions in the ISA complexes. These additional interactions are  $\pi$ - $\pi$  and steric interactions. These interactions make the complex more structured and increase the viscosity of the ISA complex what makes the complexes more difficult to align.

Both complexes were aligned in the thermotropic phase using shear force at elevated temperature ( $200^\circ C$ ). The maximum dichroic ratio obtained for several prepared films was 6. The quality of the films prepared using this method was poor, since control of the uniformity of the thin film using mechanical contact is difficult (especially at  $200^\circ C$ ). Very good alignment of the material was noticed at the interfaces, while some defects still existed in the bulk of the film. The presence of these defects therefore led to a relatively small value for the dichroic ratio.

It was found that the 1-AOT complex forms lyotropic phase in DMSO. The complex in the lyotropic phase (approximately 28 wt. % of solution) exists at room temperature in a nematic columnar phase ( $N_{col}$ ) with d-spacing of 2.94 nm and shows a very broad transition to the isotropic phase at  $\sim 70$ - $90^\circ C$ .

Lyotropic phase of the 1-AOT complex proved to be much more successful to get the alignment of the material. Working from the isotropic phase as starting point, it was possible

to obtain films with dichroic ratios of 18, and corresponding spectroscopic order parameters  $S = 0.85$  from oriented domain formation at a phase transition front (PTF). Polarized Visible spectroscopy and null ellipsometry was used to show the preferred orientation of columns of optical active tectons within thin films to be perpendicular to the PFT with dipole transition moment dipoles of perylenediimide are mostly isotropically distributed perpendicular to the columns. Such alignment results in formation of oblate dichroic film with in-plane non-absorbing axis.

It have been demonstrated that supramolecular materials produced by the ionic self-assembly route are viable candidates for the production of macroscopically ordered functional materials. These results therefore show that the use of this new class of liquid-crystalline materials can lead to development of real applications. An added advantage of these specific materials is the very high thermostability of alignment exhibited. This, combined with the possibility to process these materials from solutions, makes them very attractive and promising candidates for use and application in, for instance, dichroic film polarizers.



## 5. Liquid crystallinity and photo-alignment of azobenzene-based ISA complexes

Induction of optical anisotropy in photosensitive organic materials upon irradiation with polarized light has been known since the beginning of the last century.<sup>[103]</sup> This effect was widely studied in viscous solutions containing azobenzene dyes<sup>[104]</sup> and in azobenzene-containing dye – polymer blends.<sup>[105]</sup> The anisotropy induced in these systems is rather unstable. Stable photo-induced optical anisotropy was observed later on in polymers containing chemically linked azobenzene chromophores.<sup>[106,107,108]</sup> Photo-induced modifications in photosensitive materials are very promising for optical data storage, optical processing and photo-alignment of liquid crystals.<sup>[109,110,111,112]</sup> However, studies of photo-induction of optical anisotropy were mainly focused on polymeric materials because of their good film-forming properties and stability of induced optical anisotropy in a glassy or liquid-crystalline (LC) state of the polymer. Induction of optical anisotropy in low molecular weight materials with reasonable film-forming properties has been found for several systems.<sup>[113,114,115,116]</sup> These materials exist in a glassy state at room temperature and exhibit restricted crystallization due to steric hindrances.

From the variety of methods tested for alignment of the ISA complexes described in previous chapters, there is one method that was not tested. It is photo-alignment in the bulk. To realize this technique, a photosensitive unit capable of photoreaction, such as photo-isomerizations, photo-cycloadditions or photo-induced rearrangements, should be incorporated or embedded into the chemical structure of an ISA complex. The most promising candidate for this purpose is the azobenzene-containing moiety,<sup>[117]</sup> which is capable of photo-isomerization. The simplest way to embed this functional group into an ISA complex is to use a charged azobenzene-containing dye.

In order to realize the photo-alignment the commercially available azobenzene dye Ethyl Orange – EO was selected. The EO dye was selected as the tectonic unit for the following reasons: maximum axial symmetry of the molecule and minimum number of charges for a better understanding of possible molecular ordering in the resulting complexes. The dye was complexed (section 2.1) with double-tailed ammonium surfactants. Two commercially available surfactants with different alkyl tails lengths were used: C<sub>12</sub>D and C<sub>16</sub>D. The surfactants were selected for ease of comparison with other complexes, which have been already investigated in detail (Chapter 3). The chemical structures of the resulting EO-C<sub>12</sub>D and EO-C<sub>16</sub>D complexes are shown in Table 2.1.

### 5.1. Phase characterization

Both complexes show mosaic textures when observed in a polarized light microscope when cast from chloroform solutions onto a glass slide (see texture of EO-C<sub>12</sub>D in Fig. 5.1 as a typical example). The mosaic texture is typical for highly ordered smectic phases.<sup>[69,112]</sup> Schlieren-like textures were observed in thin areas of the obtained films and in spin-coated films, with the distance between defects approximately one micrometer. However, the observed Schlieren texture might be the same mosaic one which is hard to observe because of finite resolution of the microscope, and the fact that, in thin films, the texture of mosaic domains can have the appearance of Schlieren textures because of their small size. Domains of the EO-C<sub>16</sub>D complex were always smaller than that of the EO-C<sub>12</sub>D complex. The observed textures indicate that the complexes exist in LC phases at room temperature. However, it is not possible to unambiguously identify the LC phase of the complex by only using polarized light microscopy. Only a cautious prediction can be made that the complexes possibly possess a highly ordered layered structures.

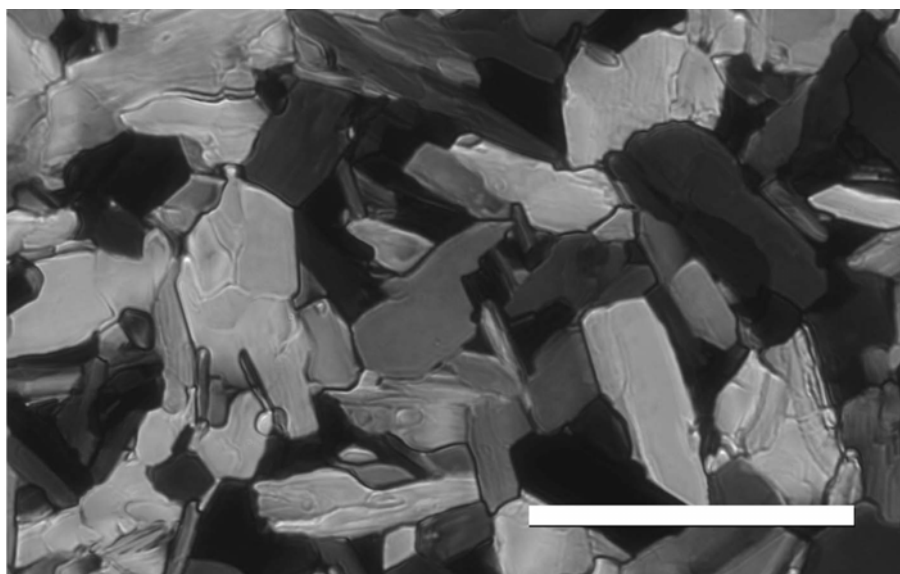


**Fig. 5.1:** The mosaic texture of the EO-C<sub>12</sub>D complex at 20 °C as observed in polarized light microscope (crossed polarizers, bar: 25 μm).

The phase behavior of the complexes was also investigated by differential scanning calorimetry (DSC) and temperature-dependent X-ray analysis. The DSC investigations showed several transition peaks (Fig. 5.2). Peaks marked with 1 and 1' are assigned to the melting (heating curves) or crystallization (cooling curves) of the surfactant alkyl chains.

Peaks at these temperatures were observed for pure surfactants and for the complexes containing the same surfactants (cf. Section 3.1). Peaks marked with 2 are connected to a “stretched-bent shape” transition of the surfactant alkyl tails (these peaks should be in the range of 50 .. 90 °C). Absence of peak connected to the “stretched-bent shape” transition of the surfactant in the DSC curve for the EO-C<sub>16</sub>D complex indicates that these changes of the surfactant does not influence the structure of the complex. For the EO-C<sub>12</sub>D complex there is a clear hysteresis of peak 2: on heating there is some structural changes connected with this transition; on cooling there is supercooling and the same structural changes take place just before the onset of crystallization of the alkyl chains of the surfactant below 20 °C. The transition peaks marked with 3 and 3' are assigned to dramatic changes in the aggregation of the EO tectonic units, what effects order in the complex, as was observed with temperature-dependent X-ray and UV-Visible spectroscopy (see below). This transition is connected to a change of packing of these units that is specific for the formed complexes (since it was not observed for the pure Ethyl Orange dye). In addition, it is noteworthy that neither of the two materials shows a transition to the isotropic phase on heating before onset of degradation above 200 °C (as shown by TGA) and during all investigations the complexes were not heated above 180°C to prevent onset of the degradation process.

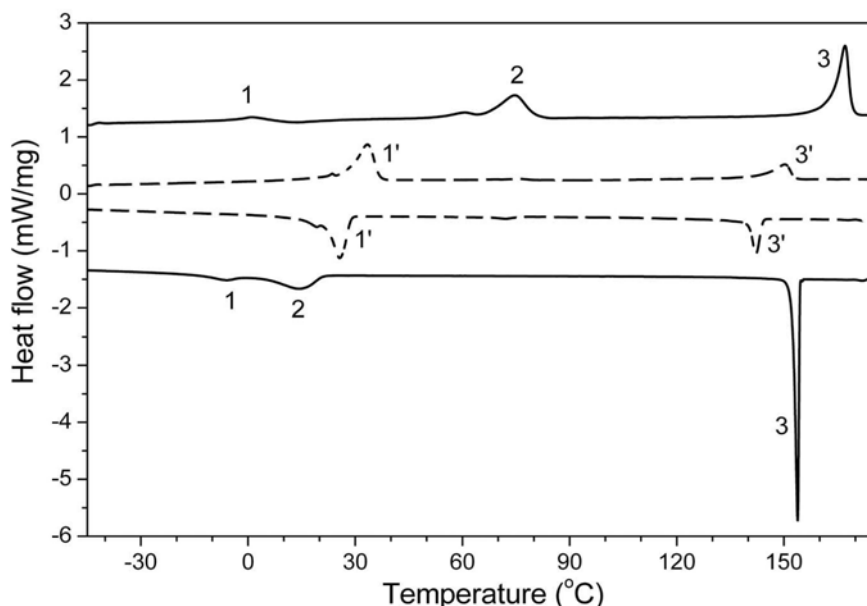


**Fig. 5.2:** DSC curves of the EO-C<sub>12</sub>D (solid curves) and EO-C<sub>16</sub>D (dashed curves) complexes; 1, 1', 2, 3, 3' – indicate transition peaks.

In-situ temperature-dependent X-ray scattering measurements were performed in order to identify the phases present in the materials. Two diffuse peaks at 170 °C

corresponding to repeat distances of 2.23 and 0.45 nm for the EO-C<sub>12</sub>D complex and 2.63 and 0.45 nm for the EO-C<sub>16</sub>D complex were observed (see Fig. 5.3 for the case of the EO-C<sub>12</sub>D complex). While the transition above peak 3 or 3' should correspond to the transformation of the regular phase (see below) into a weakly ordered morphology it can be assumed that above this transition the EO-C<sub>12</sub>D complex exists in low-ordered Smectic A liquid-crystalline phases and the EO-C<sub>16</sub>D complex exists in nematic columnar phase. Although at these temperatures, the materials become liquid-like they still possess internal order remaining in LC phase before onset of degradation.

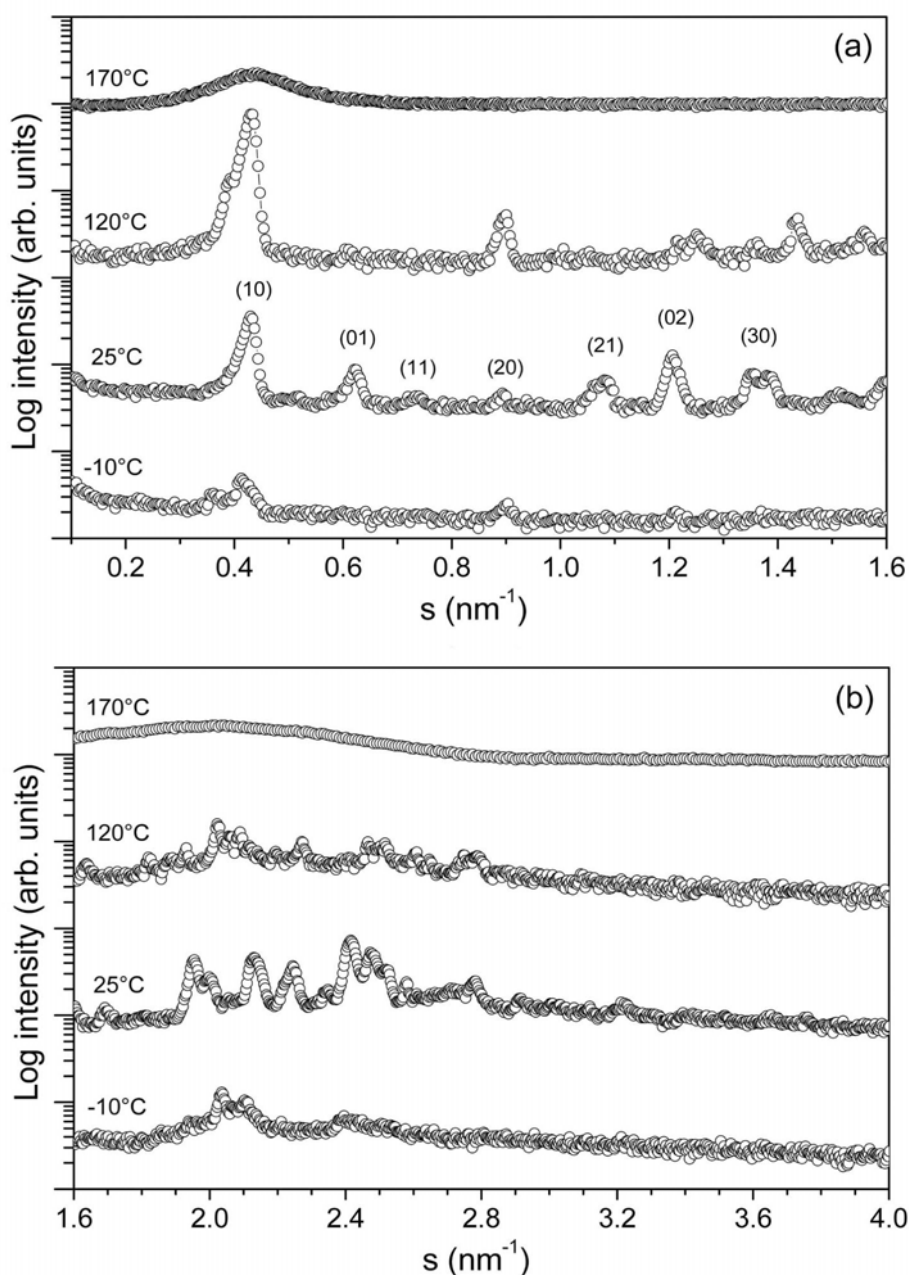


**Fig. 5.3:** (a) Small-angle and (b) Wide-angle X-ray scattering diffractograms of the EO-C<sub>12</sub>D complex recorded at -10 °C, 25 °C , 120 °C and at 170 °C on heating.



The data for the EO-C<sub>12</sub>D complex (Fig. 5.3) at 25 °C show a sequence of well-defined reflections in the small-angle scattering region, which could be indexed as a 2D rectangular phase with the dimensions  $a = 1.64$  nm and  $b = 2.28$  nm, i.e. a rectangular columnar (Col<sub>r</sub>) LC phase. The wide-angle X-ray scattering (WAXS) region indicates the presence of crystalline packing within the complex. This is assigned to packing of highly aggregated azobenzene tectonic units. Intensity of these peaks are in correlation with the aggregation of the EO tectons: the highest aggregation is observed in the Col<sub>r</sub> LC phase. At temperatures above ca. 65°C the SAXS data significantly change into a series of equidistant peaks corresponding to repeat distance  $d_0 = 2.25$  nm assigned to a lamellar bilayer LC phase (Smectic A, SmA<sub>2</sub>). The first sublayer of this phase consists of charges and the second one of alkyl tails and azobenzene units mixed together. From the WAXS data in this temperature range, it is seen that aggregation behavior (packing) of azobenzene units is disturbed. The transition between columnar and smectic LC phases corresponds to transition peak 2 in the DSC curve. The transition between these LC phases is common for lyotropic phases of surfactants, however, such transitions have not been observed for thermotropic LCs. The reason for transition between columnar to layered phases is a change of phase volume of alkyl tails of the C<sub>12</sub>D surfactant because of “stretched-bent shape” transition. Similar to DSC, the in-situ X-ray scattering experiments reveal a significant hysteresis during the cooling. The relaxation of the supercooled complex at room temperature from smectic to columnar phase is on the order of ca. 60 min and in accordance with other experiments (see below).

Taking into account the lengths of the surfactant C<sub>12</sub>D and the EO unit (Fig. 5.4) reasonable models of molecular packing in columnar and smectic phases are suggested, in which side-length  $b$  (or layer repeat distance  $d_0$ ) is commensurable with size of the C<sub>12</sub>D unit and the shorter side  $a$  with size of the EO unit. Here it should be noted that proposed molecular packing is also supported by the results of the characterization of the photo-alignment of the complex.

In contrast to the EO-C<sub>12</sub>D complex the EO-C<sub>16</sub>D complex does not show transition between layered and columnar phase and exists in square columnar liquid crystalline phase with average intercolumnar distance of about 2.40 nm slightly varying with the temperature in the temperature range between peaks 1' and 3'. The reason for that is the bigger phase volume of the surfactant alkyl chains which does not allow more compact packing. Columns are formed with charges and filled around with surfactant tails and azobenzene units.

On cooling below transition 1 or 1' the molecular packing in both complexes is

strongly disturbed. It is connected to immobilization of alkyl tails into all-trans configuration, which on crystallization disturb the columnar structure. This phase can not be considered as a crystalline phase because of lack of the order, but rather classified as a glassy state.

Further prove of presence of these phases are given in the following sections by non-direct methods in which experiments can be explained only by presence of these phases.

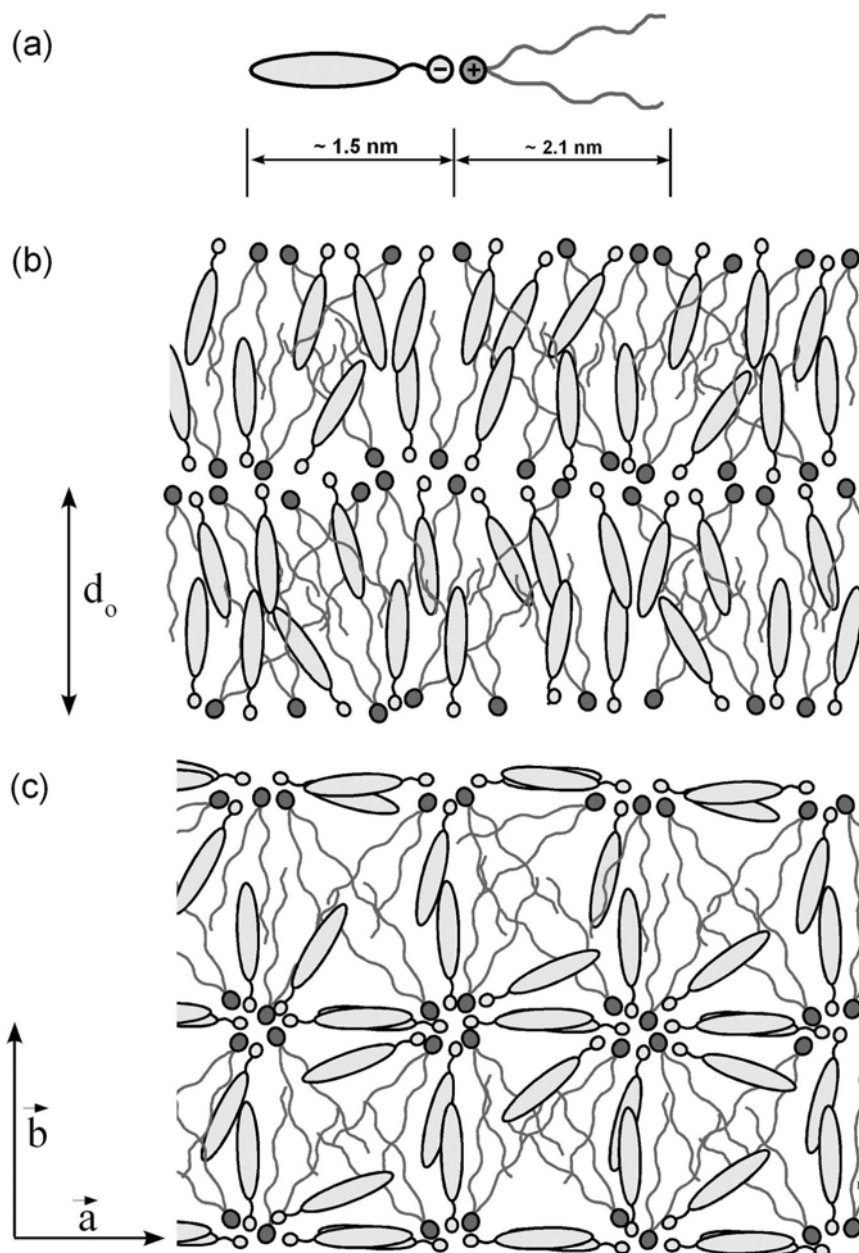


**Fig. 5.4:** Schematic representation of (a) molecular dimensions; (b) molecular packing of bilayer Smectic A ( $SmA_2$ ); and (c) molecular packing of rectangular columnar ( $Col_r$ ) LC phases of the EO- $C_{12}D$  complex.

## 5.2. Aggregation and film-forming properties

Comparison of the UV-Visible spectra of the pure EO dye in solution (water,  $\sim 10^{-7}$  M), the complexes in solution (ethanol,  $\sim 10^{-7}$  M), and in thin films are presented in Fig. 5.5. The UV-Visible spectra of the materials are characterized by maxima of the absorbances of EO (solution), and the EO-C<sub>12</sub>D and EO-C<sub>16</sub>D complexes (solution and film) at 475, 425 and 405 nm respectively, which correspond to the strong  $\pi$ - $\pi^*$  transition of the E isomer of the azobenzene moiety. The dramatic blue shift of the maximum of the azobenzene chromophores of the complexes in ethanol, when compared with pure dye in water, might be a result of solvatochromic effect in solution or can be an indication of the existence of aggregates, even at such low concentrations because of a strongly cooperative complex formation and aggregation process.<sup>[49]</sup> These two effects can not be distinguished because it was not possible to find the same solvent for both materials. However, there is clear blue shift of the maximum in the spectra of the complex in films when compared with solution. These observations are typical for the parallel arrangement of chromophore dipoles forming H-aggregates.<sup>[118]</sup> The aggregation behavior is strongly influenced by packing considerations, phase transitions, and film preparation conditions as showed by temperature-dependent UV-Visible spectral investigations.

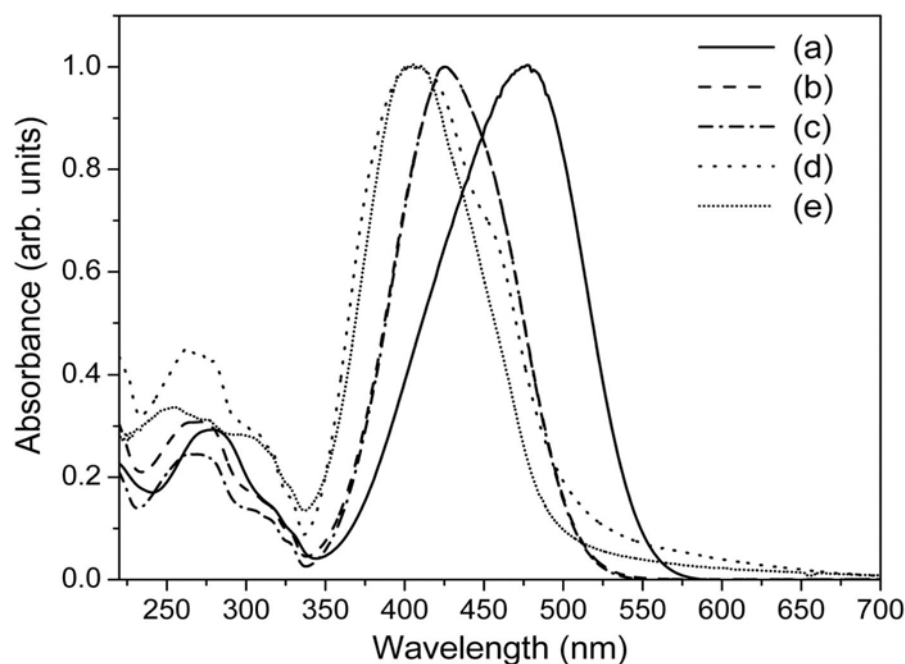


**Fig. 5.5:** Normalized UV-Visible spectra of: (a) Ethyl Orange in water ( $\sim 10^{-7}$  M); (b) EO-C<sub>12</sub>D in ethanol ( $\sim 10^{-7}$  M); (c) EO-C<sub>16</sub>D in ethanol ( $\sim 10^{-7}$  M); (d) EO+C<sub>12</sub>D in film of approximately 200 nm; (e) EO+C<sub>16</sub>D in film of approximately 200 nm.

Therefore, because the aggregation processes strongly influence photochemical reactions in the film, detailed investigations of the film-forming and aggregation properties of the complex were performed before starting investigations into the photo-induction of optical anisotropy. The correlation between aggregation and film-forming properties is more pronounced for the EO-C<sub>12</sub>D complex. Therefore, all experiments were performed mostly with the EO-C<sub>12</sub>D complex. The changes in aggregation for the EO-C<sub>16</sub>D complex will be shown at the end as a comparison.

The films of the EO-C<sub>12</sub>D complex were deposited by spin-coating (1000 rpm) on fused silica glass slides from chloroform solutions of the complex (5 – 100 g/l) at 25 °C. Films deposited from solutions with concentrations higher than 25 g/l showed pronounced scattering. The films deposited from the solutions of concentrations of 25 g/l and lower exhibited high optical quality. For all further investigations solutions of 25 g/l were used. The films deposited from this solution had thicknesses in the range of 100 to 200 nm. As determined with transmission null ellipsometry and angular-dependent polarized UV-Visible spectroscopy, the dipole transition moment of azobenzene dyes (EO) are oriented with a small preference in the plane of the film. The determined order parameter  $S = -0.05 \pm 0.03$  results in a difference of the principal refractive indexes of  $\Delta n = n_e - n_o = -0.05 \pm 0.03$  (at  $\lambda = 632.8$  nm). An increase of the thickness of the film, i.e. deposition from solutions of higher concentrations, leads to optically isotropic films at thickness of about 1000 nm. Films with thicknesses less than 100 nm show a strong tendency for homeotropic orientation of the dipole transition moments of the azobenzene dyes, e.g. yielding a positive homeotropically-oriented optical axis. This might be a result of influence of the interfaces at small thicknesses. It is worth to note here that all experimental results presented below are qualitatively the same for films of different thickness. For this reason, the data for films deposited from the solution of concentration of 25 g/l are presented.

As aggregation processes are directly reflected in UV-Visible spectra of the material, temperature dependent UV-Visible spectral measurements on films of the complex were recorded. Changes of the spectra of the complex on heating-cooling of the material are shown in Fig. 5.6a. The films of the complex were not heated above 150 °C because heating to the temperatures above transition marked with 3 in Fig. 5.2 destroys the film by dewetting (but does not destroy the material). Changes in the spectra above 150 °C were measured in a thin layer of the complex between two fused silica slides. The absorbance of this thin layer was high because it was not possible to produce films of thickness less than a micrometer (presence of dust in the air during preparation). However, it was clearly detected that there is

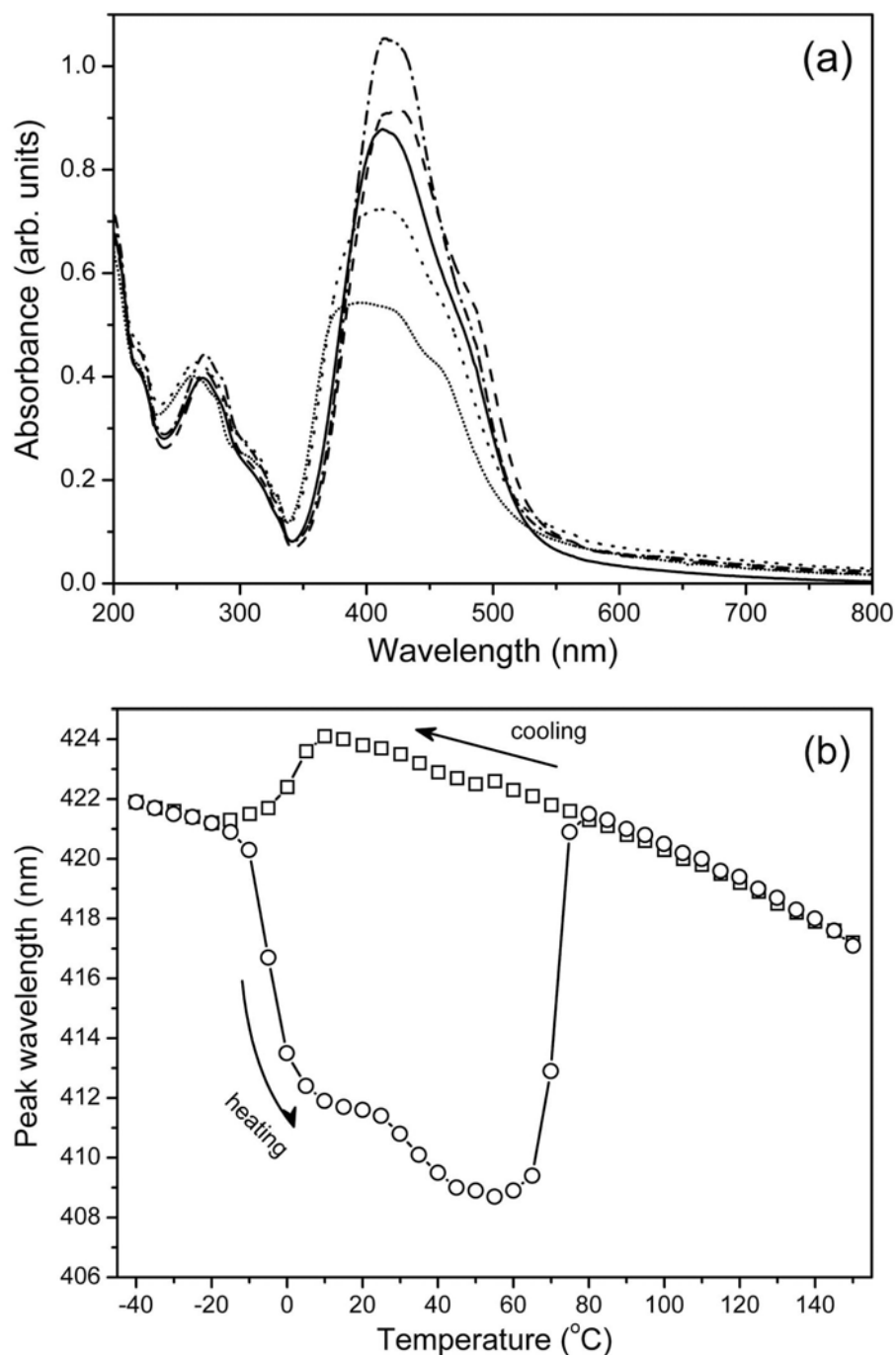


**Fig. 5.6:** (a) Changes of the spectra of the EO-C<sub>12</sub>D complex on heating-cooling circle: (solid line) 150 °C; (dash line) 25 °C on cooling; (dash dot line) -20 °C; (dot line) 25 °C on heating; (short dot line) 25 °C on the next day after relaxation. (b) Shift of the absorbance peak wavelength of the  $\pi$ - $\pi^*$  transition of the EO tectonic unit in the EO-C<sub>12</sub>D complex on change of the temperature.

a strong and abrupt red shift of about  $8 \pm 2$  nm of the peak of absorbance to the long wavelength region at elevated temperatures. This indicates that above the transition marked with 3 in Fig. 5.2 disruption of the aggregation of the azobenzene tectonic units takes place.

From the spectra obtained in the consequent cooling and heating cycles (Fig. 5.6) it can be seen that the azobenzene units are strongly aggregated in the rectangular columnar liquid crystalline state (between peaks 1 and 2 in Fig. 5.2). The aggregation is enhanced if the film is left to relax at room temperature. From Fig. 5.6b it is clearly seen that there is a hysteresis on the cooling and heating cycle. These changes correlate with the found hysteresis of peaks marked with 2 on DSC curves in Fig. 5.2.

Before providing an explanation of the temperature-dependent aggregation behavior, relaxation behavior in the spectra should be noted. After heating of the film to 150 °C (i.e., to the SmA<sub>2</sub> LC phase) and subsequent cooling of the sample to 25 °C, relaxation of the complex to the aggregated state (the Col<sub>r</sub> LC phase) is observed (see Fig. 5.6). This state is the same one as after film preparation. This relaxation is connected to the supercooling of the material, which was also observed by X-ray measurements (i.e., that on cooling from the SmA<sub>2</sub> LC phase to room temperature the transition to Col<sub>r</sub> LC phase appears gradually). The complex stays in the SmA<sub>2</sub> LC phase for at least one hour at room temperature, and the transition to the Col<sub>r</sub> LC phase then appears gradually over several hours.

To explain the correlations between phase transitions and aggregation in the complex, it is worth to remind some properties of the complex with the same surfactant, which was investigated in details (Chapter 3). For that complex it was found that at temperature around -5 °C there is crystallization-melting transition of alkyl chains of the surfactant appears. At the temperature around 65 °C there is “stretched-bent shape” transition of alkyl chains of the surfactant. In that complex the influence of the other tecton on these phase transitions was neglectful. In present case cooperativity of all tectons in the EO-C<sub>12</sub>D complex should be considered. Having this information in mind it is already possible to give reasonable explanation of the correlation between phase transitions and aggregation in the complex, and even explain the reasons of transition between columnar and smectic phases.

At elevated temperatures (above transition 3 in Fig. 5.2) the complex exists in a low-ordered Smectic A (SmA) liquid-crystalline phase. In this phase, the azobenzene tectonic units practically do not aggregate, as indicated by the position of the absorbance maximum of the  $\pi$ - $\pi^*$  transition near 425 nm, which is similar to that found for diluted solution of the complex (see Fig. 5.5). On cooling below transition 3 in Fig. 5.2, the aggregation of the azobenzene units (EO) and transition to highly ordered SmA<sub>2</sub> LC phase is observed, and because of interaction between EO units, the interlayer distance becomes fixed (this is clearly detected by SAXS). However, aggregation of the EO units in this phase is not very strong because attraction of EO tectons is compensated by repulsion of the surfactant alkyl tails.

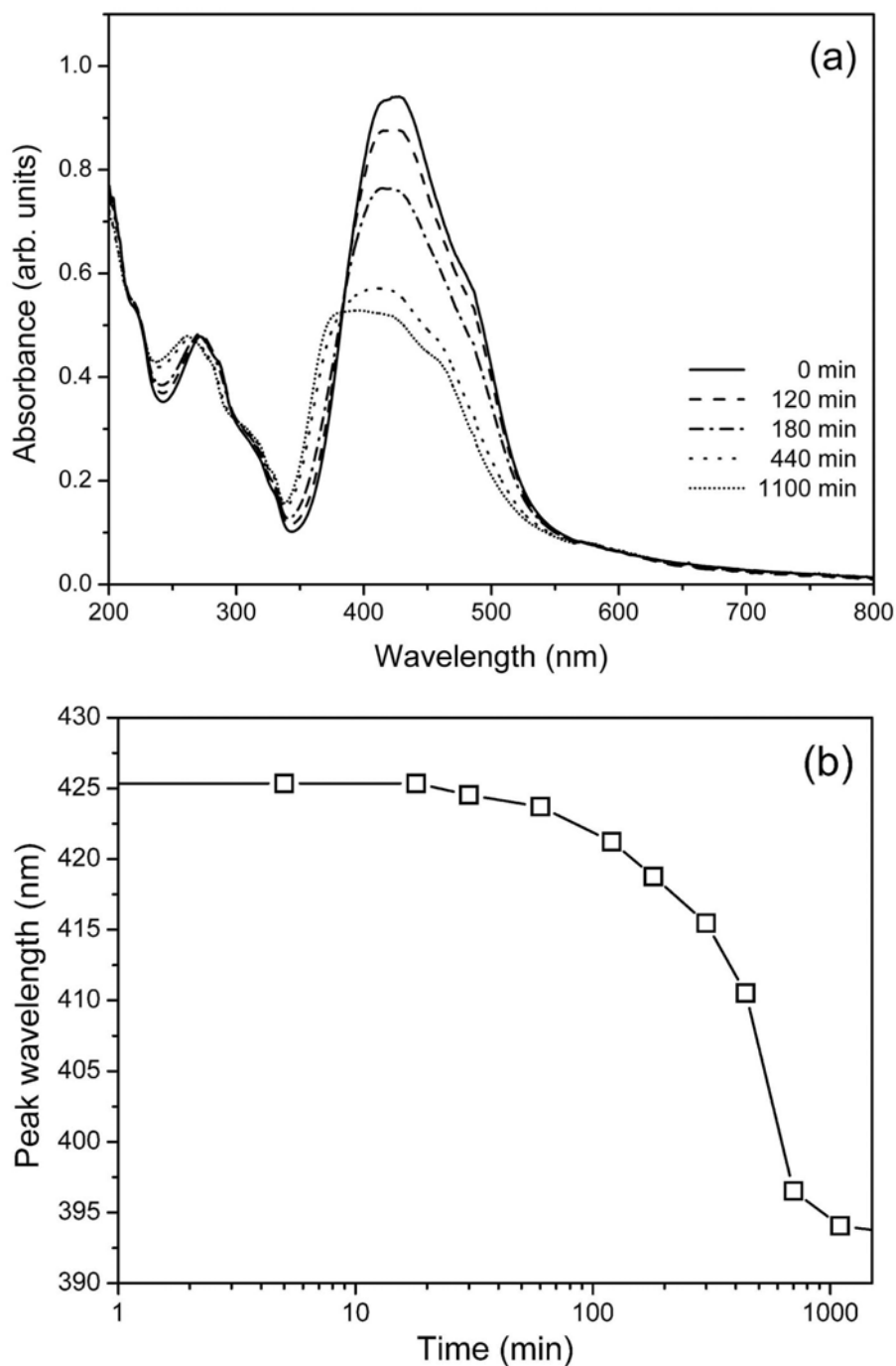


**Fig. 5.7: Relaxation of the spectra of the EO-C<sub>12</sub>D complex after heating to 150 °C and subsequent cooling to 25 °C; (a) relaxation of the UV-Visible spectra and (b) shift of the peak wavelength on relaxation.**

This is supported by the fact that the interlayer distance correlates very well with the length of the surfactant (see Fig. 5.4). There is also very small dependence of aggregation in this phase on the temperature: at higher temperature there is higher aggregation (see Fig. 5.6b, temperature range 70 – 150 °C). This is explained by the fact that at higher temperatures alkyl tails are softer and their impact on aggregation of EO tectons is smaller.

On further cooling to the temperature below transition marked with 2 in Fig. 5.2 the alkyl tails straighten out and become less mobile. The hysteresis will not be considered in this discussion and it is assumed that this transition appears around 65 °C. Because of this straightening the phase volume of alkyl tails increases, and they can not fit between azobenzene units. It should be noted that in addition to this process, charges can not be distributed uniformly throughout the material because of phase separation of charged and non-charged fragments. Ionic interactions are much stronger than van der Waals and steric interactions, and to minimize energy within the material charges should form either layers, columns or spheres, with non-charged fragments filling free space between these structures. From this reason if there is no space for non-charged units between layers the transition from layered to columnar phase should appear. In our particular case because of increase of phase volume of alkyl tails, the transition to columnar phase appears. However, because length of azobenzene units is smaller than that of the alkyl tails the azobenzene units fill space between columns first. Within layers, columns are formed, and the space between columns is filled by azobenzene units. The X-ray measurements revealed that in this case a columnar rectangular phase is formed. One repeat distance is mostly the same as for the layered structure and corresponds to the surfactant length. The second repeat distance is in good agreement with calculated length of the EO tectonic unit (see Fig. 5.4). In this phase, there are good conditions for aggregation of azobenzene units.

Now let's return to the case of hysteresis. On cooling although there is an increase of phase volume of alkyl tails, but the interaction between azobenzene units is very strong. In addition, layers of charges should be divided to form columns which requires additional energy. These interactions hold the material in layers and supercooling appears. However, this is metastable state, and finally if to hold the material in the temperature range of the columnar phase (it was done at 25 °C in our case), this transition appears because of fluctuations (see Fig. 5.7). Another way to induce the transition to the columnar phase is to cool the complex further to the crystallization temperature of the alkyl tails. In this case, there is further increase of phase volume of alkyl tails which gives rise start to this transition. In this case, the transition appears (see Fig. 5.2b and Fig. 5.6b), but the columnar phase is strongly disordered because of lack of flexibility of the alkyl tails. On heating from the disordered columnar phase, there is melting of alkyl tails of the surfactant (transition marked with 1 in Fig. 5.2b). The alkyl tails become flexible, and this allows better order in the system and the transition from a disordered (disturbed) columnar to a highly ordered Col<sub>r</sub> LC phase is observed. In this case, there is no restriction for the aggregation of EO tectonic units which



is clearly reflected in the temperature-dependent spectral measurements on heating (see Fig. 5.6b). On further heating to the bending temperature of the alkyl tails, there is decrease of phase volume of alkyl tails and transition to highly ordered  $\text{SmA}_2$  LC phase can be observed. As was detected from temperature dependent X-ray measurements, the transition from  $\text{SmA}_2$  to  $\text{Col}_r$  and back is not complete. There is always some part of material exists in  $\text{SmA}_2$  phase in the temperature range of  $\text{Col}_r$  phase and vice versa. However, holding the complex for long time (maximum a day) at 150 °C brings the complex to  $\text{SmA}_2$  phase and holding the complex at room temperature at least for a day brings the complex to the  $\text{Col}_r$  phase.

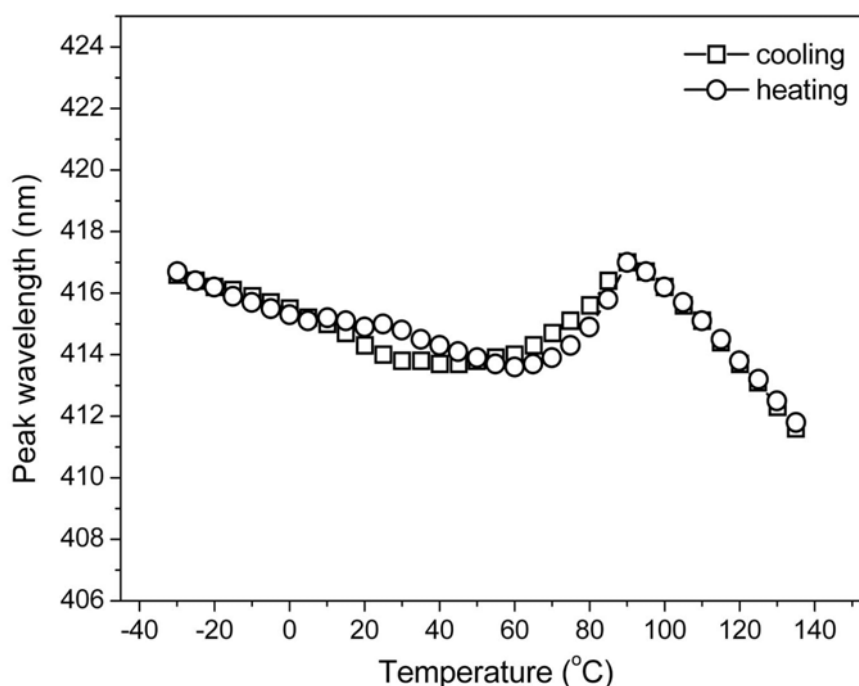


**Fig. 5.8: Shift of the absorbance peak wavelength of the  $\pi$ - $\pi^*$  transition of the EO tectonic unit in the EO-C<sub>16</sub>D complex on change of the temperature.**

In contrast to the EO-C<sub>12</sub>D complex there is no hysteresis of the absorbance peak wavelength for the EO-C<sub>16</sub>D complex (cf. Fig. 5.8 and Fig. 5.6b). However, there are clear changes connected to the “stretched-bend shape” transition of the alkyl tails. These changes are not reflected in the DCS curve indicating that this small change in aggregation does not reflect the structural order in the complex. Heating of the EO-C<sub>16</sub>D complex above 150 °C leads also to breaking of aggregation similar to the EO-C<sub>12</sub>D complex.

During film preparation process of the EO-C<sub>12</sub>D complex, it was noticed that when solution of the complex was cooled to 20 °C or lower, films with very high optical quality were obtained. This was independent of the solution concentration and spin-coating

conditions employed. After first annealing at 150 °C, all films show small light scattering. This metastable state of the film could appear because the surfactant alkyl tails are in all-trans configuration (crystalline in the film) state during spin-coating process (additional cooling of the solution on evaporation of the solvent on spin-coating also has influence on this process). So, on deposition of the films, the tails in all-trans configuration restrict the aggregation of EO tectons that somehow influences optical properties of the films. As was determined experimentally the films in this state (prepared from cooled solution and not annealed) are temporarily stable and give reproducible results which are not dependent on film thickness and deposition conditions. Films deposited from solution at 25 °C or higher (and films prepared from cooled solution and annealed) also gave reproducible results, but they are quantitatively (but not qualitatively) dependent on the film thickness. So, for all further investigations films deposited from the cooled solutions without annealing were used.

In the case of the EO-C<sub>16</sub>D complex spin-coated films always had good optical quality. There were no difference if the solution was cooled or not. This is explained by the fact that at room temperature the alkyl chains of the surfactant in the EO-C<sub>16</sub>D complex are already in an all-trans configuration state which restricts formation of large domains during the film preparation process as was observed from optical textures of the complex.

Since all processes in the the EO-C<sub>12</sub>D complex are more pronounced in comparison to the EO-C<sub>16</sub>D complex, all further investigations were again prepared on the former one. Data for the the EO-C<sub>16</sub>D complex are discussed as a comparison.

### 5.3. Photo-alignment properties

It is worthy to note that for the first time, the idea of using of azobenzene photosensitive units in ISA complexes for induction of optical anisotropy has been realized for the EO-C<sub>12</sub>D complex. Application of this idea to other azobenzene-containing complexes was also successful. It is also noteworthy that until this investigation, no one has ever prepared low molecular photosensitive materials on the base of ISA strategy despite their simplicity.

The first observation of the induction of optical anisotropy were really surprising. No one could expect that in highly ordered and aggregated systems, effective photo-orientation processes are possible. However, induction of optical anisotropy in spin-coated film of the EO-C<sub>12</sub>D complex under irradiation with polarized light of an Ar<sup>+</sup> laser was very effective (Fig. 5.9). Maximum dichroic ratio obtained was 50, and it is still not a saturation as can be seen from the insert graph. Efficiency of the induction process was varying from film to film. In this section processes of photo-alignment in the EO-C<sub>12</sub>D complex are discussed in details.

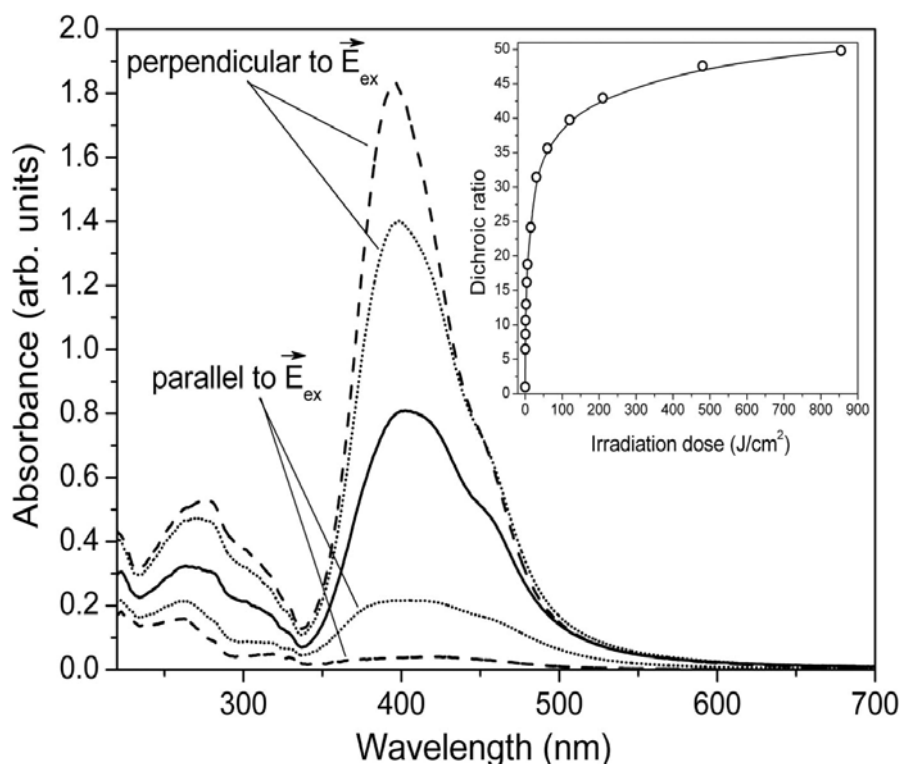


**Fig. 5.9:** Changes of polarized absorbance spectra in film of the EO+C<sub>12</sub>D complex under irradiation with linearly polarized light  $E_{ex}$  of an Ar<sup>+</sup> laser ( $\lambda_{ex} = 488 \text{ nm}$ ,  $P = 50 \text{ mW cm}^{-2}$ ): solid line – initial spectrum, dotted line – after irradiation dose of  $0.25 \text{ J cm}^{-2}$ , dashed line – after irradiation dose of  $850 \text{ J cm}^{-2}$ ; Insert: Kinetics of induced dichroic ratio in film of the complex calculated at  $\lambda_{test} = 400 \text{ nm}$ .

Thin films of the EO-C<sub>12</sub>D complex were prepared from cooled (15 °C) solutions by spin-coating method. It was noted in the previous section that after deposition, the films exist in some kind of metastable state. However, from phase characterization at room temperature, the complex should exist in Col<sub>r</sub> liquid crystalline phase. This means that if during film preparation the alkyl tails, which are in all-trans configuration (crystalline in the film) state, influence somehow the order of the complex in the film than after some time, there should be relaxation to the state with minimum energy (i.e. to the Col<sub>r</sub> liquid crystalline phase). However, neither in the UV-Visible spectra nor in optical textures, there were no changes since film preparation even after several weeks. This means that film preparation from a cooled solution influences the optical properties of the films, but not the phase of the complex. Comparison of optical textures of films prepared from cooled solution and the same films annealed at 150 °C for 1 hour (or films prepared from heated solution) showed that the former films have very small domains and in latter ones domains are much larger in size (compare textures in the insert of Fig. 5.10a). It was also noticed that thicker annealed films have larger domains. This therefore indicates that deposition from cooled solutions restricts only aggregation processes and the size of domains, but not the LC phase of the complex. Comparison of UV-Visible spectra of annealed films of different thickness showed that thicker films are in more aggregated state (compare spectra marked with 1 in Fig. 5.10a). In addition, thick annealed films (with large domains) scatter light, which might also have an influence on the induction of optical anisotropy.

In order to investigate influence of domain size on the processes involved in the induction of optical anisotropy, two identical films (prepared under the same conditions with the same thicknesses) were prepared. One film was annealed at 150 °C for 1 hour. Both films were irradiated with linearly polarized light of an Ar<sup>+</sup> laser of the same intensity. Changes of the spectra for both nonannealed and annealed films after irradiation with an exposure dose of 100 J cm<sup>-2</sup> are shown in Fig. 5.10a. Optical textures of these films before irradiation are shown in the insert of Fig. 5.10a. The kinetics of the changes of the dichroic ratio versus exposure dose for both films are shown in Fig. 5.10b. It is clearly seen that the efficiency of induction of the anisotropy is strongly dependent on domain size; the smaller the domain size the higher the induced anisotropy. It should be noted that there is no saturation even after an exposure dose of 100 J cm<sup>-2</sup>. Very long irradiation and/or irradiation with higher intensity lead to steady increase of anisotropy. After very long and intense exposure (> 1 kJ cm<sup>-2</sup>), it is possible to reach dichroic ratio of more than 35 for the annealed film as well. For nonannealed films, irradiation with an exposure dose of approximately 1 kJ cm<sup>-2</sup> leads to a

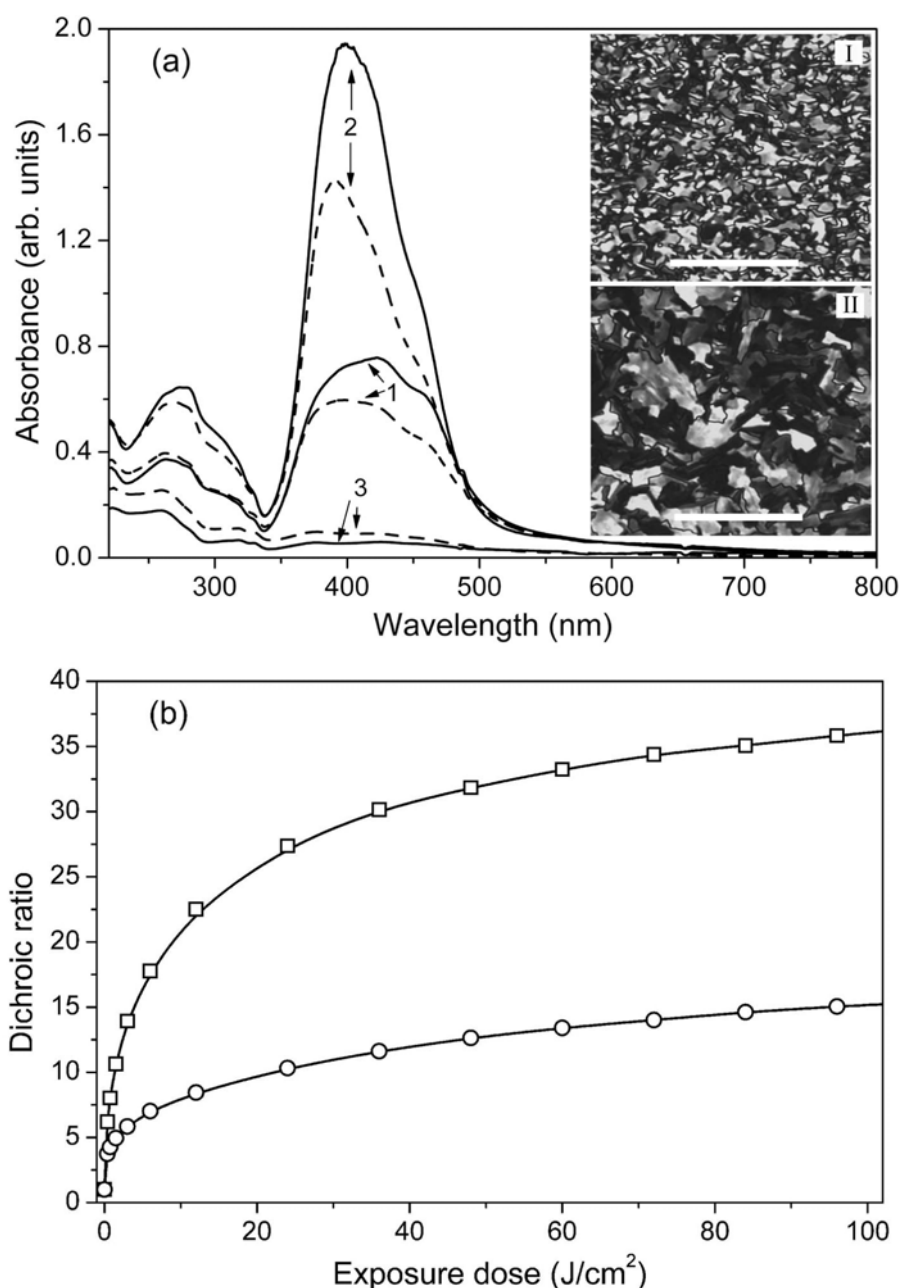


**Fig. 5.10:** (a) Changes of the polarized spectra of (solid line) non-annealed and (dash line) annealed films of the EO-C<sub>12</sub>D complex under irradiation with linearly polarized light of an Ar<sup>+</sup> laser ( $\lambda = 488$  nm), (1) initial spectra, polarized spectra (2) perpendicular and (3) parallel to the polarization of the exciting light after irradiation with exposure dose of 100 J cm<sup>-2</sup>; Insert: optical texture of (I) non-annealed and (II) annealed films before irradiation (crossed polarizers, bar: 25  $\mu$ m). (b) Kinetics of the changes of dichroic ratio calculated at 400 nm as a function of exposure dose for (□) non-annealed and (○) annealed film of the EO-C<sub>12</sub>D complex.

dichroic ratio of 50, with no saturation evident. A decrease of light scattering with increased exposure dose was observed. Since it was not clear how the size of domains influences the efficiency of induction of anisotropy, some additional experiments were performed to address this issue.

Before looking for an explanation of the influence of domain size on the induction of anisotropy, a specific feature of the induction of anisotropy which was observed in all cases should be noted. If a film of the complex (annealed or nonannealed) is irradiated with small irradiation doses, a very pronounced jump in the anisotropy just at the beginning of the irradiation process (after an exposure dose of approximately  $0.1 \text{ J cm}^{-2}$ ) is observed (Fig. 5.11a). This anisotropy is temporarily stable after irradiation is stopped. Further irradiation leads to a very slow but gradual increase of the dichroic ratio. This behavior is very clearly seen from Fig. 5.11b and insert. In this figure changes of spectra and kinetics of changes of absorbance at 400 nm under irradiation are shown. The biggest change of the dichroic ratio of 7 for non-annealed films with a very small domain size was observed at the beginning of the irradiation. The smallest change of dichroic ratio of 2 was observed for annealed films with very large domains. From this experiment, the conclusion can also be drawn that the domain size has direct influence on the processes of induction of optical anisotropy.

In order to follow the changes within domains on irradiation, the following experiment was carried out. A film of the EO-C<sub>12</sub>D complex was annealed in order to get domains large enough to observe and clearly distinguish in a polarized light microscope. In order to ensure that the same area was investigated on later stages, some marks (scratches) were made on the film. The film was then irradiated with small irradiation steps and images of the same area were recorded in the polarized light microscope. The results of this experiment are present in Fig. 5.12. The following observations can be made: from comparison of the pictures at small irradiation doses reorientation of small domains and enlargement of large domains is observed. On further irradiation, a division of large domains into smaller parts is observed. From this experiment, the conclusion can be made that reorientation of the azobenzene (EO) units is not local, like in polymers, but a cooperative process which leads to the reorientation of domains. Small domains reorient under irradiation to align the dipole moments of the photosensitive units perpendicular to the polarization direction of the exciting light. Very large domains cannot undergo such reorientation, and they simply divide into smaller parts. Finally, the domains which are already aligned combine, which leads to an increase of the size of these domains. Finally, all domains align in such a way that all azobenzene units become mostly perpendicularly aligned to the exciting light polarization. This means that columns of charges (and stacks of azobenzene units between these columns) in the complex align parallel to the polarization of the exciting light. The smaller size of domains the more effective photo-reorientation process. The size of domains plays a main role in the reorientation process. The first big increase in the anisotropy

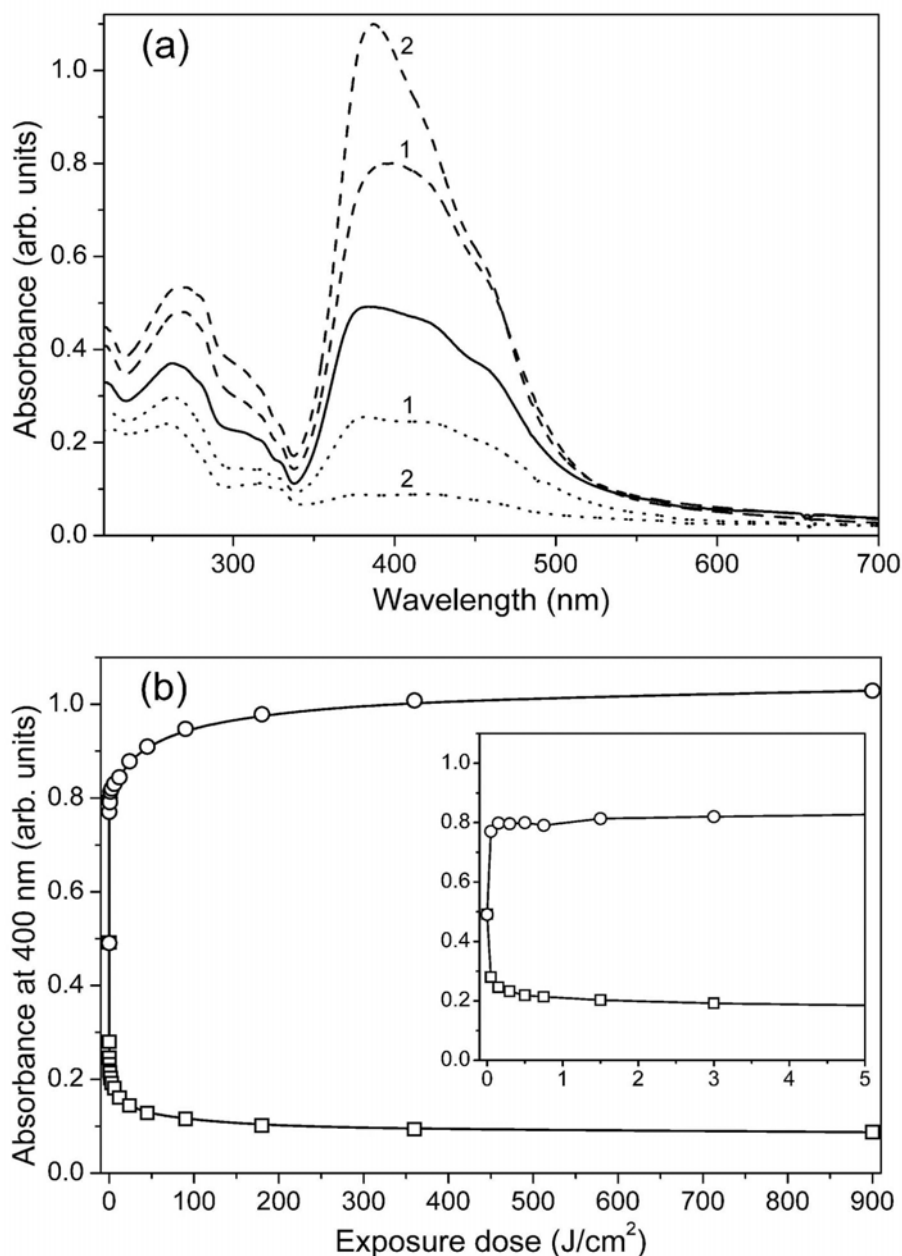


**Fig. 5.11: (a) Changes of the polarized spectra of annealed film of the EO-C<sub>12</sub>D complex under irradiation with linearly polarized light of an Ar<sup>+</sup> laser ( $\lambda = 488$  nm): (solid line) initial spectrum and spectra (dot line) parallel and (dash line) perpendicular to the polarization of the exciting light after exposure dose of (1) 0.15 J cm<sup>-2</sup> and (2) 900 J cm<sup>-2</sup>. (b) Kinetics of the changes of absorbance at 400 nm of annealed film of the EO-C<sub>12</sub>D complex (□) parallel and (○) perpendicular to the polarization of the exciting light as a function of exposure dose.**

(Fig. 5.11) is therefore caused by the reorientation of domains of small size. Further reorientation of domains of large size needs larger exposure doses for their division and further reorientation, which would explain the last slow part of orientation process as can be seen from Fig. 5.11.

Observation of domain reorientation under irradiation with polarized light does not

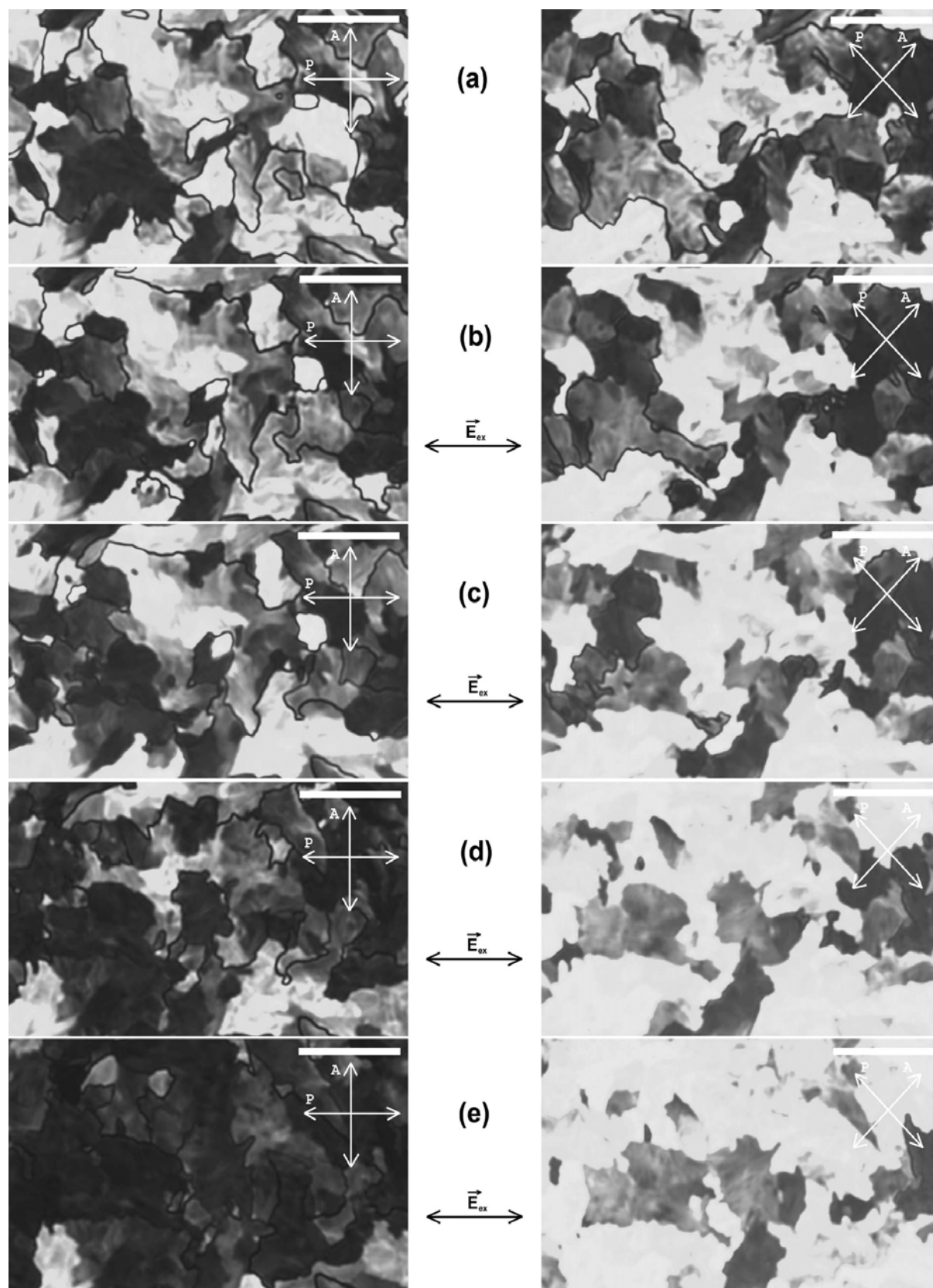


**Fig. 5.12:** Changes of optical textures in the same area of annealed film of the EO-C<sub>12</sub>D complex under irradiation with linearly polarized light of Ar<sup>+</sup> laser ( $\lambda = 488$  nm): (a) initial texture, and textures after exposure dose of (b) 0.15 J cm<sup>-2</sup>; (c) 3 J cm<sup>-2</sup>; (d) 90 J cm<sup>-2</sup>; (e) 900 J cm<sup>-2</sup> (crossed polarizers, bar: 10  $\mu$ m). P and A indicate directions of transmission axes of polarizer and analyzer,  $E_{ex}$  indicates the polarization direction of the exciting light.



give information about the real molecular process within domains when they reorient. These processes include: (a) mechanical rotation of domains under irradiation with polarized light or (b) process such as a transition of domains into a highly disordered state under irradiation, followed by a transition back to a highly ordered state where the probability of domain excitation is lower (i.e., case where azobenzene units are perpendicular to the light polarization). The possible process of domain reorientation by transition within domains in some kind of disordered state can be excluded because of the following reasons. First of all, it is worthy to note that (i) no transition to the isotropic state of the complex is observed before degradation of the material; (ii) films of the complex can be destroyed by dewetting on heating to the low ordered SmA phase; (iii) the photo-alignment kinetics were not dependent on the light intensity. Even at very high light intensities the films were not destroyed because of the possible transition to low ordered SmA phase (local heating under light absorbance). No change in absorbance spectrum (red shift of the absorbance maximum) related with the break of aggregation of azobenzene units, which caused by the transition to highly ordered SmA phase, was observed under irradiation with different intensities. All these factors indicate that the complex in film under irradiation remains in a columnar phase. The reason for the stability of columnar phase under irradiation is connected to the properties of the complexes. In Chapter 3 it was shown that ionic interactions hold the complex in an ordered state even if all fragments should be in an isotropic phase. It means that even if irradiation destroys aggregation of the azobenzene units and tries to transfer all of them into isotropic phase, the columns of charges still hold them. To reorient the domain all columns should be therefore reoriented together. It means that the only way to reorient the system is to mechanically rotate the whole domain. From all this discussion of and comparison of results it is possible to conclude that reorientation of the domains is connected to their mechanical rotation and this is a cooperative process. Small domains need small torque to their reorientation. For bigger domains the threshold is too high to prepare such rotation, and they simply divide into smaller ones and then rotate.

Reorientation (rotation) of domains as a whole is a cooperative process. Cooperativity in general is connected to behavior of a system as a whole and usually characterized by threshold (critical concentration, external field, force, momentum, energy and others). Pure cooperative processes would be for example Freedericksz transition in liquid crystal cell (critical field). The threshold for domain reorientation is that critical torque (created by pumping of the domain with light) needed to rotate the domain. The presence of this critical torque was observed in all kinetics: for films prepared in the same conditions the initial jump

in the anisotropy (see insert in Fig. 5.11) was dependent on light intensity. From comparison of kinetics of dichroic ratio versus exposure dose for different light intensity it was noticed that the higher the light intensity was, the bigger the first jump of anisotropy was. If one is to assume some kind of domain size distribution (starting practically from zero, having a maximum, and ending with maximum domain size) then the higher intensity will cause more domains to reorient under initial light pulse. This is a clear indication of threshold existence and cooperativity of the photo-alignment of the complex. The origin of this cooperativity can therefore be found in the induced order in the LC phase owing the presence of the ionic interactions in the complex.

The photo-alignment of the complex is a cooperative process. This type of the behavior is in contrast to polymers where the photo-alignment is a local process. However, in the literature the term 'cooperativity' is usually used instead of correlation and even instead of phase transition (no references are given because of aesthetic reasons of authors who used the term cooperativity). In photosensitive polymers, temporal stability of the photo-alignment can be realized if the photosensitive units are attached to polymer matrix. There is a correlation between matrix and photosensitive units. This correlation extends to several molecular dimensions, the correlation length. The alignment processes in this case are clearly local (one might say locally cooperative but it stays local) and happen in a glassy state of the polymer (practically all investigated polymers are in a glassy state). If, for example, the correlation length within a LC domain is bigger than domain size, then the reorientation processes will be cooperative within the domain. Cooperativity in photosensitive polymers might be observed if one takes an aligned LC polymer in a LC state and try to reorient it. A threshold in intensity should exist, but it is not clear if above this threshold the system will reorient as a whole, or if there is simple transition to the isotropic state under photochemical reaction and back transition to the aligned LC state with alignment which needs higher threshold intensity. A further example where the term cooperativity is also used can be found: If a photo-sensitive polymer is irradiated in the glassy state to introduce low degree of anisotropy and then heated to LC state, there is an amplification of order after annealing in the LC state. However, this process is simply a phase transition with centers for transition. A similar process appears if a LC is cooled from the isotropic phase to a LC phase in a cell with aligning layers (in this case the centers are at the interface with aligning layers).

Irradiation of films of the EO-C<sub>12</sub>D complex leads to alignment of columns parallel to the polarization of the exciting light (the long axes of the photosensitive azobenzene units are perpendicular to the columns). These columns are parallel to the substrate because the electric

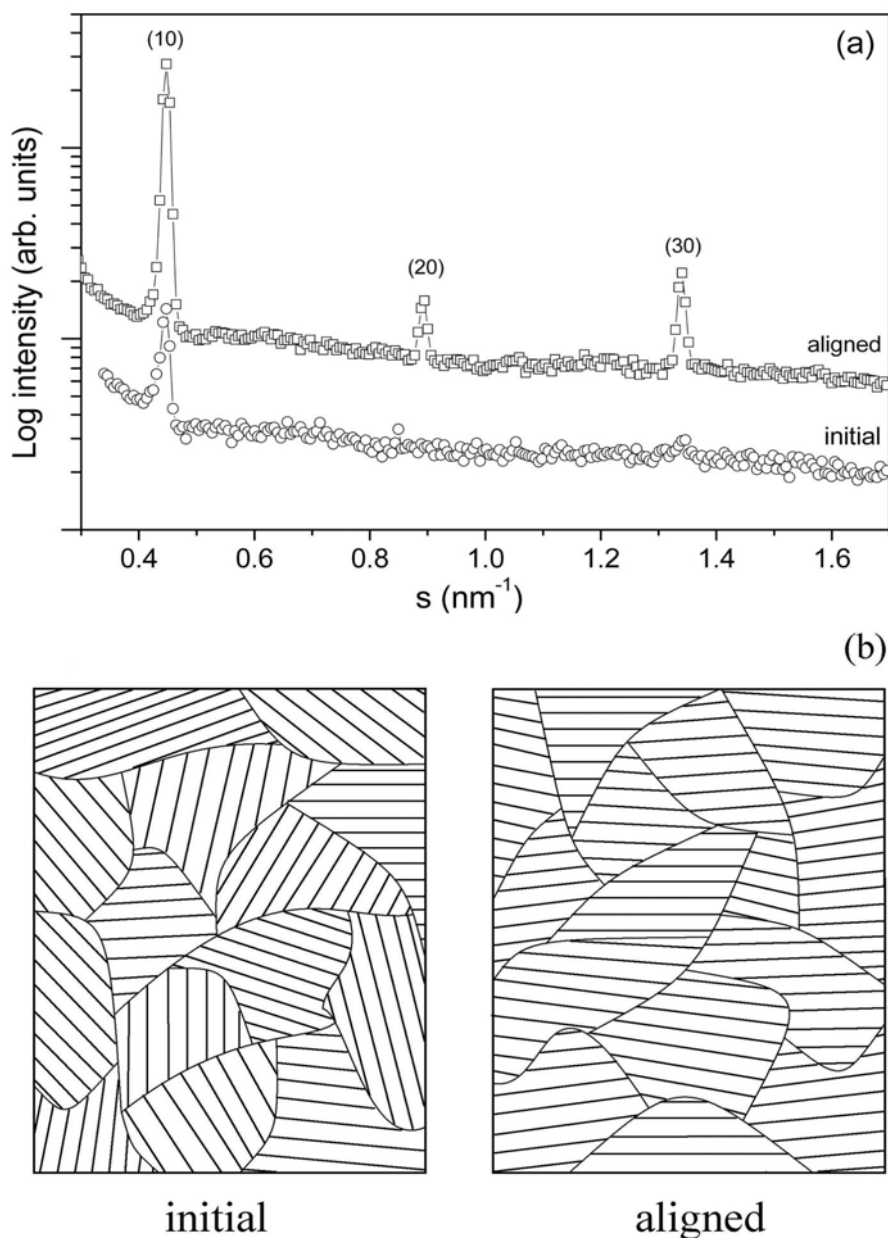


**Fig. 5.13: (a) Small-angle x-ray reflectivity measured on initial and aligned film sample of the complex at room temperature; (b) Schematic representation of order of columns within domains for initial and aligned sample.**

field vector of the exciting light is parallel to the substrate. The liquid-crystalline phase of the complex is rectangular columnar with dimensions of 2.28 and 1.64 nm. In order to elucidate the orientation of the rectangular structure relative to the substrate, SAXS measurements were performed on samples before and after irradiation (Fig. 5.13a). While the irradiated (aligned) sample shows a sequence of equidistant ( $h0$ ) reflections with  $d = 2.28$  nm, the non-irradiated (initial) one only shows the first interference maximum. First, these results prove that indeed the columns are parallel to the substrate in both cases. Second, the damping of the higher order reflections for the non-irradiated material suggests that the liquid-crystalline

domains are isotropically distributed in the plane of the film. Irradiation leads to an alignment and consequently to an enforcement of the (h0) peaks (see Fig. 5.13b). In both cases planes of columns which correspond to repeat distance  $b$  (Fig. 5.4c) are parallel to the substrate.

A specific effect connected to molecular order in the complex that has never been observed in photosensitive polymers should also be noted. If one looks at the changes in the UV-Visible spectra after irradiation (Fig. 5.10a and Fig. 5.11a), it is seen that in addition to the alignment of dipole moments of the azobenzene photosensitive units alignment of dipole moments of the benzene rings which are part of the EO photosensitive units (peak of absorbance around 270 nm,  $\pi-\pi^*$  transition) is also observed. The dipole transition moment of this transition is parallel to the plane of benzene ring. In azobenzene containing polymers, for example, benzene rings are isotropically distributed, even in the aligned state. In the case of the EO-C<sub>12</sub>D ISA complex, planes of benzene rings are aligned perpendicular to the polarization direction of the exciting light.

From all the information obtained about the order and the photo-alignment of the complex, one can conclude that the complex aligns under irradiation with polarized light with columns parallel to the polarization of the light. The azobenzene (EO) tectonic units are perpendicular to the columns and are aggregated in stacks between columns of charges in a way that planes of benzene rings are perpendicular to the stacks.

Finally, an answer to the question about distribution of azobenzene units around columns of charges should be given. From X-ray data, it is proposed that in the SmA<sub>2</sub> LC phase of the complex azobenzene units of the EO tectons are mixed in a layer with alkyl tails of the surfactant. In the Col<sub>r</sub> LC phase the azobenzene units are separated of the layers and form aggregated stacks between columns. However, it is not clear if distribution of azobenzene units around columns of charges is really isotropic. The following results should shed some light on this question. In the case of an isotropic distribution of azobenzene units around columns and unidirectional alignment of the columns in the plane of the film the absorbance in the plane perpendicular to the columns will be the same in all directions. However, in the case of an anisotropic distribution, this effect will not be easy to measure by polarized tilted UV-Visible spectroscopy because anisotropic distribution of refractive index has a strong impact on beam propagation on tilting the sample. In this case measurements of spatial refractive index distribution far from the absorbance band of the azobenzene units will be the best choice to answer the question about distribution of azobenzene units because there is direct correlation of refraction index dispersion with absorbance. For this purpose, a nonannealed film prepared from cooled solution was irradiated with an exposure dose of

about  $1 \text{ kJ cm}^{-2}$  in order to get maximum alignment in the film. This film was characterized with null ellipsometry supplemented with thickness measurements. Modeling of the experimental curves gives the following results:  $n_x - n_y = 0.30 \pm 0.02$ ,  $n_x - n_z = 0.10 \pm 0.02$ ,  $n_z - n_y = 0.20 \pm 0.02$ ,  $n_z - (n_x + n_y)/2 = -0.05 \pm 0.02$ , where  $xy$  – is the plane of the film and  $y$  is parallel to polarization direction of the exciting light. In this configuration  $xz$  – is the plane of distribution of the azobenzene units. This experiment clearly shows that  $n_x > n_z > n_y$  and azobenzene units are preferably distributed in the plane of the film, i.e. in Col<sub>r</sub> LC phase they are separated from layers (which are parallel to the substrate) to form stacks between columns. This is in perfect agreement with proposed model of molecular order in the complex. It should be noted that the out-of-plane anisotropy was not changed under irradiation process:  $n_e - n_o$  (before irradiation) =  $n_z - (n_x + n_y)/2$  (after irradiation) =  $-0.05 \pm 0.02$ . This, in addition, supplements the previous conclusion that under irradiation columns reorient in the plane of the film, and there are no changes in the out-of-plane direction.

All results described above are connected to the EO-C<sub>12</sub>D complex. Similar effects of the induction of the optical anisotropy were also observed for the EO-C<sub>16</sub>D complex. However, in the case of the EO-C<sub>16</sub>D complex the size of the domains in spin-coated films are smaller, because at room temperature the complex is in the glassy state which restricts formation of large domains. The kinetics of the induction of the anisotropy were similar to that of the EO-C<sub>12</sub>D complex. The only difference that maximum dichroic ratio obtained in this case was 20. It is explained by the fact that the complex exists in the disturbed columnar glassy state and in this state the maximum macroscopic ordering is restricted by internal order in the complex. There is also a jump of the anisotropy at the beginning of the irradiation process indicating that the alignment of the complex is also connected to the reorientation of domains. Null ellipsometry characterization of the initial film gives the following results:  $n_e - n_o = 0.14 \pm 0.02$ . This indicates homeotropically oriented optical axis. Characterization of aligned film gives:  $n_x - n_y = n_z - n_y = 0.30 \pm 0.02$ ,  $n_x - n_z = 0.00 \pm 0.02$ ,  $n_z - (n_x + n_y)/2 = 0.14 \pm 0.02$ , where  $xy$  – is the plane of the film and  $y$  is parallel to polarization direction of the exciting light. It is seen that in the aligned film there is an in-plane oblate structure. These results can be again explained by reorientation of columns of the EO-C<sub>16</sub>D complex in the plane of the film. In the initial film, the domains are isotropically distributed with the columns of charges parallel to the plane of the film (similar to the EO-C<sub>12</sub>D complex). Azobenzene (EO) tectonic units are perpendicular to the columns which results in a small absorbance (refractive index) parallel to the columns. This on average gives

positive homeotropic optical axis. On irradiation there is unidirectional alignment of the columns in the plane of the film. In the aligned state all columns are parallel. Existence of negative in-plane uniaxial structure indicates that azobenzene tectonic units are uniformly distributed perpendicular to the columns. These results are in agreement with proposed model of molecular order based on the X-ray analysis.

Finally, photo-reorientation of the induced optical structures in the complexes have been successfully achieved. Well-defined optical patterns were obtained when a second irradiation was prepared through a standard photo mask (Fig. 5.14a,b). Very effective induction of optical phase gratings in films of the azobenzene-containing complexes was also observed. A diffraction efficiency of approximately 7% was obtained on 100 nm thick films of the EO+C<sub>16</sub>D complex after irradiation with two circularly polarized interfering beams of an Ar<sup>+</sup> laser. The resulting optical pattern is shown in Fig. 5.14c. However, no formation of surface relief gratings was observed for the investigated complexes. These effects are under investigation and are the subject of forthcoming work.

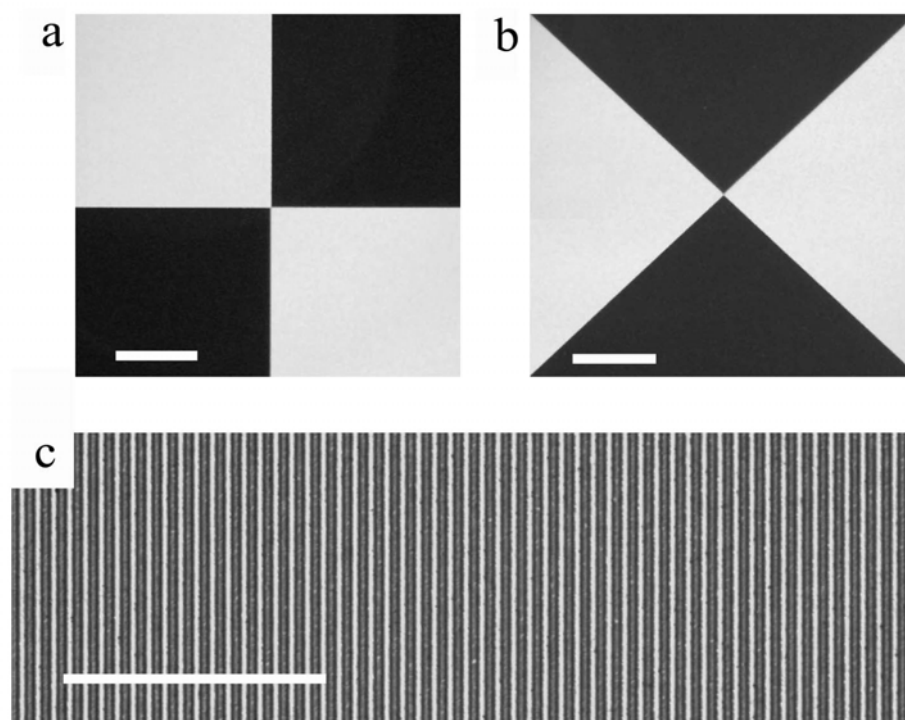


**Fig. 5.14:** (a), (b) Photos of film of the EO+C<sub>16</sub>D complex when the second irradiation was prepared through the mask with polarized light of an Ar<sup>+</sup> laser ( $\lambda_{\text{ex}} = 488 \text{ nm}$ ,  $P = 50 \text{ mW cm}^{-2}$ ) at angle  $45^\circ$  to the first one; crossed polarizers parallel to the sides of the pictures; bar:  $100 \mu\text{m}$ ; (c) Picture of pattern in the film of the EO+C<sub>16</sub>D complex after irradiation with two circularly polarized interfering beams of Ar<sup>+</sup> laser ( $\lambda_{\text{ex}} = 488 \text{ nm}$ , Exposure dose =  $1 \text{ kJ cm}^{-2}$ , bar:  $25 \mu\text{m}$ ).

## 5.4. Conclusions

The phase behavior and photo-alignment of the EO+C<sub>12</sub>D and EO-C<sub>16</sub>D ISA complexes have been investigated in detail. Above 160 °C, the EO+C<sub>12</sub>D complex exists in a low-ordered Smectic A (SmA) LC phase. On cooling the complex exhibits a transition to a highly ordered bilayer Smectic A (SmA<sub>2</sub>) LC phase, and then to a highly ordered rectangular columnar (Col<sub>r</sub>) LC phase near 65 °C. Below -5 °C, the order in the complex is disturbed due to immobilization of alkyl tails of the surfactant into all-trans configuration, which causes a transition to a glassy state. The transition from SmA<sub>2</sub> to Col<sub>r</sub> LC phase shows a marked hysteresis on cooling: supercooling was observed and this transition appears almost simultaneously with the onset of crystallization of the surfactant tails. The transitions from SmA<sub>2</sub> to Col<sub>r</sub> and back are caused by change of phase volume of alkyl tails of the surfactant on their “stretched-bent shape” transition. The EO-C<sub>16</sub>D complex exists in square columnar LC phase in the temperature range from 30 to 145 °C. Below 30 °C, the order in the complex is disturbed, and there is a transition to a less ordered glassy state. Above 145 °C, there is a transition to a nematic columnar phase. Assignment of phase behavior of the complexes is summarized in Table 5.1.

*Table 5.1: Assignment of phases of the EO-C<sub>12</sub>D and EO-C<sub>16</sub>D complexes between transition peaks marked with numbers in Fig. 5.2.*

EO-C <sub>12</sub> D	disturbed rectangular columnar (glassy) phase	1	rectangular columnar LC phase (a = 2.28 nm, b = 1.64 nm)	2	highly ordered Smectic A phase (d <sub>0</sub> = 2.25 nm)	3	low-ordered Smectic A phase (d <sub>0</sub> = 2.23 nm)
EO-C <sub>16</sub> D	disturbed square columnar (glassy) phase	1'	square columnar LC phase (a = b = 2.40 nm)			3'	nematic columnar phase (d <sub>0</sub> = 2.63 nm)

Optical properties of films of the EO-C<sub>12</sub>D complex depend on preparation conditions and thermal treatment. Films deposited from cooled (20 °C and lower) chloroform solution exhibit very good optical quality while films deposited from chloroform solutions at 25 °C or higher (or films annealed at 150 °C) scatter light. Light scattering is connected to size of domains. In the case of films deposited from cooled solution, the formation of large domains are restricted because of all-trans configuration state of alkyl tails of the surfactant. In contrast, the EO-C<sub>16</sub>D complex forms films with good optical quality independently if the

solution was cooled or not. This behavior is connected to the all-trans configuration state of the surfactant alkyl tails at room temperature which restricts formation of large domains.

Very effective photo-alignment of both complexes under irradiation with polarized light was observed. Dichroic ratios of 50 for the EO-C<sub>12</sub>D complex and of 20 for the EO-C<sub>16</sub>D complex have been obtained. Maximum value of the anisotropy is restricted by internal order in the complexes. The photo-alignment of the complexes depends strongly on the size of the domains. In the case of small domains, the photo-alignment is the most effective. Photo-reorientation in the complex is not local like in azobenzene-containing polymers, but is a cooperative process and connected to mechanical rotation of domains. Domains in the initial film are aligned in such a way that columns of the complex are parallel to the substrate with isotropic orientational distribution parallel to the film plane. During irradiation, there is an in-plane reorientation of domains (columns).

Potential application of the complexes for optical data storage have been demonstrated. These examples clearly demonstrate that photosensitive low molecular film-forming ISA complexes are viable alternatives to photosensitive polymers. The ISA complexes have several advantages in comparison with polymers: (I) low production cost from cheap starting materials; (II) they allow induction of higher values of anisotropy; (III) the induced anisotropy is thermally stable (thermal treatment at 130 °C of the investigated complexes does not destroy induced anisotropy); (IV) usually ISA complexes are soluble in environmentally-friendly solvents like ethanol.



## 6. Summary and conclusions

The ultimate goal of this work was to look for the formation of liquid crystalline phases in low molecular materials by application of Ionic Self-Assembly strategy, to test these materials for macroscopic alignment, and to look for correlations between phases of ISA complexes and their alignment properties. In this work, for the first time, existence of new type of liquid crystal was demonstrated. Its name is an ionic self-assembly liquid crystal (ISA LC). In the search of methods for alignment of the ISA LCs, for the first time, photo-alignment of photosensitive ISA complexes was demonstrated. The investigated complexes have good film-forming properties that makes them capable of competition with polymers.

In Chapter 3 the formation of ISA complexes has been investigated using simple molecules (benzene-based complexes). Detailed investigations of ordering of different groups in the complex have been prepared. It was found that ionic interactions within complexes play the main role in the order of the complexes. The presence of these interactions restricts transition to isotropic phase (no transition to isotropic phase was observed for all complexes which have been investigated). In addition, these interactions hold the system (network-like) allowing crystallization into a single domain from aligned LC state. Alignment of these simple ISA complexes was spontaneous on a glass substrate. Existence of negative homeotropically-oriented optical axis makes these complexes attractive for application as compensation films for LCDs.

In Chapter 4 liquid crystallinity and alignment properties of functionalized (perylene-dimide-based) ISA complexes were investigated. Both investigated complexes exist in columnar LC phases. In these complexes the presence of  $\pi$ - $\pi$  interactions between functional tectons complicates alignment properties. None from the classical methods (surface interactions or external fields) of LC alignment have been proved to be successful. Satisfactory macroscopic alignment was achieved by shear-force method. However, the best results of macroscopic alignment have been obtained by zone-casting method (crystallization at the phase-transition front from isotropic phase into lyotropic columnar phase). In the aligned films, the columns of the complex align perpendicular to the phase-transition front. The obtained anisotropy ( $DR = 18$ ) is thermally stable what makes these complexes attractive for application as dichroic polarizers.

In Chapter 5 photosensitive (azobenzene-based) ISA complexes have been investigated. The investigated complexes show formation of columnar LC phases. These thermotropic phases are formed by prolonged molecules which is in contrast to classical

columnar phases which are formed by disk-like molecules. Columns are formed by charges filled between with alkyl chains of the surfactant and azobenzene units mixed together. Formation of columnar phases by prolonged molecules is known only for lyotropic phases of surfactants. It was demonstrated that photo-alignment of such complexes was very effective ( $DR = 50$  has been obtained). It was shown that photo-reorientation in the photosensitive ISA complexes is cooperative process connected to mechanical rotation of domains. In contrast to photosensitive polymers, where photo-reorientation is local, in the complexes photo-alignment is connected with reorientation of domains. The size of domains has direct influence on efficiency of the photo-reorientation process. In the case of small domains, the photo-alignment is the most effective. In the initial films of the investigated complexes columns within domains align parallel to the substrate. Under irradiation with linearly polarized light, domains reorient in the plane of the film leading to macroscopic alignment of columns parallel to the light polarization and the joining of small domains into large ones. To show potential applicability of the photosensitive ISA complexes, reorientation of the macroscopically-aligned structure and induction of the volume phase grating was demonstrated.

Finally, the following distinguishable properties of the ISA liquid crystalline complexes should be noted:

- ☑ the complexes do not solve in water but readily solve in organic solvents like ethanol, chloroform or DMSO;
- ☑ the complexes have good film-forming properties when cast or spin-coated from organic solvent;
- ☑ presence of ionic interactions stabilizes the complexes restricting transition to isotropic phase and allowing crystallization into a single domain from aligned LC state;
- ☑ no transition to the thermotropic isotropic phase was observed for all investigated materials;
- ☑ alignment of the complexes depends on their structure and secondary interactions between tectonic units;
- ☑ cooperative behavior of the complexes was also observed in photo-reorientation of the photosensitive ISA ones.

### The 4x4 matrix method

A numerical technique to calculate transmission and reflection by anisotropic stratified planar structures with obliquely or normally incident light – a 4x4 matrix method was discovered by Billard<sup>[119]</sup> in an unpublished thesis and later rediscovered and published by Teitler and Hennis<sup>[120]</sup>. This method was later applied to liquid crystal systems by Berreman and Scheffer.<sup>[121,122]</sup> General approach of this method is discussed in <sup>[60,Chap. 4.7]</sup>. Here this method is discussed with assumption that all mediums are nonmagnetic and have no optical-rotation activities.

Maxwell's equations in a medium with no free charges and for harmonic wave are written as:

$$\nabla \times \vec{E} = -i k_0 \vec{H} \quad (\text{A.1a})$$

$$\nabla \times \vec{H} = i k_0 \epsilon_{ij} \vec{E} \quad (\text{A.1b})$$

where  $\vec{E}$  and  $\vec{H}$  are the electric and magnetic field respectively.  $\epsilon_{ij} = \epsilon_{ij}(z)$  is the dielectric tensor which varies only in the thickness direction (z-direction) of the investigated layer.

Let's consider the coordinate system shown in Fig. A.1. In our particular problem light is incident in the xz-plane and we can write  $k_x = k_0 N_0 \sin \alpha_0$ ,  $k_y = 0$  where  $N_0$  is the external refractive index,  $\alpha_0$  is the angle of incidence and  $k_0 = \omega/c$  is the wave vector in free space. From the symmetry of the problem there is no variation in the y-direction of any field component, so that

$$\frac{\partial}{\partial y} = 0 \quad (\text{A.2})$$

For the tangential fields to match across the boundaries all the waves that are exited by the incident plane wave must have the same spatial dependence in the x-direction as the incident wave. Therefore all fields should vary as  $e^{-ik_x x}$ , hence

$$\frac{\partial}{\partial x} = -i k_x \quad (\text{A.3})$$

Plugging in equations (A.2) and (A.3) into equations (A.1) we get:

$$\begin{pmatrix} 0 & -\frac{\partial}{\partial z} & 0 \\ \frac{\partial}{\partial z} & 0 & i k_x \\ 0 & -i k_x & 0 \end{pmatrix} \begin{pmatrix} E_x \\ E_y \\ E_z \end{pmatrix} = -i k_0 \begin{pmatrix} H_x \\ H_y \\ H_z \end{pmatrix} \quad (\text{A.4a})$$

## Appendix

$$\begin{pmatrix} 0 & -\frac{\partial}{\partial z} & 0 \\ \frac{\partial}{\partial z} & 0 & i k_x \\ 0 & -i k_x & 0 \end{pmatrix} \begin{pmatrix} H_x \\ H_y \\ H_z \end{pmatrix} = i k_0 \begin{pmatrix} \varepsilon_{xx} & \varepsilon_{xy} & \varepsilon_{xz} \\ \varepsilon_{yx} & \varepsilon_{yy} & \varepsilon_{yz} \\ \varepsilon_{zx} & \varepsilon_{zy} & \varepsilon_{zz} \end{pmatrix} \begin{pmatrix} E_x \\ E_y \\ E_z \end{pmatrix} \quad (A.4b)$$

These last two equations can be expanded into two linear homogeneous algebraic equations and four linear homogeneous first-order differential equations. The two linear homogeneous algebraic equations can be solved for the field components  $E_z$  and  $H_z$  along the z-axis in terms of the other four field components along x- and y- axes:

$$H_z = m E_y, \quad E_z = -\frac{m H_y + \varepsilon_{zx} E_x + \varepsilon_{zy} E_y}{\varepsilon_{zz}} \quad (A.5)$$

where

$$m = \frac{k_x}{k_0} = N_0 \sin \alpha_0 \quad (A.6)$$

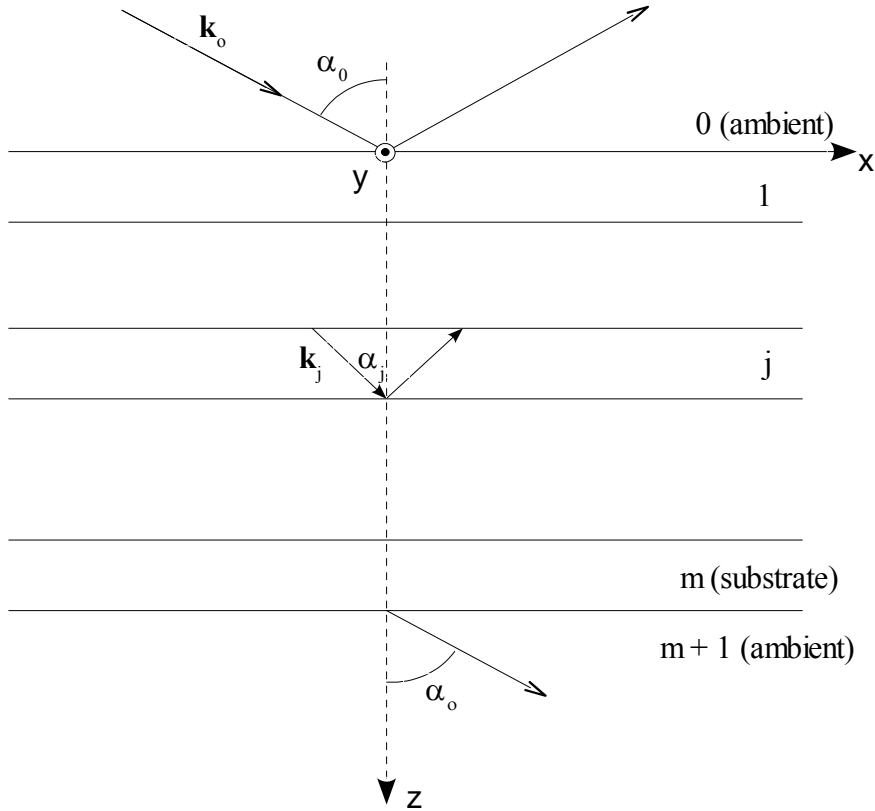


**Fig. A.1: Reflection and transmission of the plane wave by a multilayer structure.**

The values  $E_z$  and  $H_z$  thus obtained are subsequently substituted into the remaining four differential equations to produce four linear homogeneous first-order differential equations in the four field variables  $E_x$ ,  $E_y$ ,  $H_x$ , and  $H_y$ . These can be cast in 4x4 matrix form as follows

$$\frac{\partial}{\partial z} \begin{pmatrix} E_x \\ H_y \\ E_y \\ -H_x \end{pmatrix} = -ik_0 \begin{pmatrix} -m \frac{\epsilon_{xz}}{\epsilon_{zz}} & 1 - \frac{m^2}{\epsilon_{zz}} & -m \frac{\epsilon_{yz}}{\epsilon_{zz}} & 0 \\ \epsilon_{xx} - \frac{\epsilon_{xz}^2}{\epsilon_{zz}} & -m \frac{\epsilon_{xz}}{\epsilon_{zz}} & \epsilon_{xy} - \frac{\epsilon_{xz}\epsilon_{yz}}{\epsilon_{zz}} & 0 \\ 0 & 0 & 0 & 1 \\ \epsilon_{yx} - \frac{\epsilon_{xz}\epsilon_{yz}}{\epsilon_{zz}} & -m \frac{\epsilon_{yz}}{\epsilon_{zz}} & \epsilon_{yy} - \frac{\epsilon_{yz}^2}{\epsilon_{zz}} - m^2 & 0 \end{pmatrix} \begin{pmatrix} E_x \\ H_y \\ E_y \\ -H_x \end{pmatrix} \quad (A.7)$$

In compact form one can write the equation (A.7) as:

$$\frac{\partial \psi(z)}{\partial z} = -ik_0 \Delta(z) \psi(z) \quad (A.8)$$

where

$$\psi(z) = \begin{pmatrix} E_x \\ H_y \\ E_y \\ -H_x \end{pmatrix}, \quad \Delta(z) = \begin{pmatrix} -m \frac{\epsilon_{xz}}{\epsilon_{zz}} & 1 - \frac{m^2}{\epsilon_{zz}} & -m \frac{\epsilon_{yz}}{\epsilon_{zz}} & 0 \\ \epsilon_{xx} - \frac{\epsilon_{xz}^2}{\epsilon_{zz}} & -m \frac{\epsilon_{xz}}{\epsilon_{zz}} & \epsilon_{xy} - \frac{\epsilon_{xz}\epsilon_{yz}}{\epsilon_{zz}} & 0 \\ 0 & 0 & 0 & 1 \\ \epsilon_{yx} - \frac{\epsilon_{xz}\epsilon_{yz}}{\epsilon_{zz}} & -m \frac{\epsilon_{yz}}{\epsilon_{zz}} & \epsilon_{yy} - \frac{\epsilon_{yz}^2}{\epsilon_{zz}} - m^2 & 0 \end{pmatrix} \quad (A.9)$$

In the general case of a stratified anisotropic structure,  $\Delta(z)$  is some arbitrary function of  $z$  and the wave equation (A.8) does not, in general, have an analytical solution. In the special case when  $\Delta$  is constant independent of  $z$  (over some continuous interval of  $z$ ), equation (A.8) is directly integrable to yield

$$\psi(z+d) = L(d) \psi(z) \quad (A.10)$$

where

$$L(d) = e^{-ik_0 d \Delta} \quad (A.11)$$

where  $d$  is the thickness of the layer. In an inhomogeneous anisotropic medium, where  $\Delta(z)$  matrix is a continuous function of  $z$ , equation (A.10) can be applied if the medium is divided into layers which are sufficiently thin to make  $\Delta$  independent of  $z$  within each layer. The resultant matrix can be obtained by multiplication of matrices when  $d = h_1 + h_2 + h_3 + \dots + h_{n-1} + h_n$ :

$$L(d) = L(h_n, h_{n-1}) \dots L(h_3, h_2) L(h_2, h_1) L(h_1, 0) \quad (A.12)$$

In order to compute  $L(d)$  the matrix  $\Delta$  should be diagonalized. In order to diagonalize  $\Delta$  the eigenvalues and eigenvectors need to be computed from the eigenvalue equation:

$$\Delta \cdot \Psi = q \Psi \quad (A.13)$$

## Appendix

---

whose eigenvalues  $q_l$  are the roots of the quadratic polynomial equation

$$\det[\Delta - qI] = 0 \quad (\text{A.14})$$

where  $I$  is the identity matrix.

Insertion of each eigenvalue  $q_l$ ,  $l = 1, 2, 3, 4$ . into equation (A.13) leads to four homogeneous linear equations that can be solved for the elements of the corresponding eigenvectors  $\Psi_{kl}$  (where  $k = 1, 2, 3, 4$ ).  $\Psi_{kl}$  can be considered as a the 4x4 matrix which is constructed from the four eigenvectors as columns.

In particular case of biaxial tilted structure (shown in Fig. A.2) which is sufficient to describe practically all real structures in thin layers the dielectric tensor  $\varepsilon_{ij}$  in a chosen coordinate system can be expressed in terms of principal dielectric constants ( $\varepsilon_a, \varepsilon_b, \varepsilon_c$ ) and angles  $\phi, \theta$  shown in Fig. A.2 as follows:

$$\varepsilon_{xx} = \varepsilon_a \cos^2 \phi + (\varepsilon_b \cos^2 \theta + \varepsilon_c \sin^2 \theta) \sin^2 \phi \quad (\text{A.15a})$$

$$\varepsilon_{yy} = \varepsilon_a \sin^2 \phi + (\varepsilon_b \cos^2 \theta + \varepsilon_c \sin^2 \theta) \cos^2 \phi \quad (\text{A.15b})$$

$$\varepsilon_{zz} = \varepsilon_b \sin^2 \theta + \varepsilon_c \cos^2 \theta \quad (\text{A.15c})$$

$$\varepsilon_{xy} = \varepsilon_{yx} = (\varepsilon_a - \varepsilon_b \cos^2 \theta - \varepsilon_c \sin^2 \theta) \sin \phi \cos \phi \quad (\text{A.15d})$$

$$\varepsilon_{xz} = \varepsilon_{zx} = (\varepsilon_c - \varepsilon_b) \sin \phi \sin \theta \cos \theta \quad (\text{A.15e})$$

$$\varepsilon_{yz} = \varepsilon_{zy} = (\varepsilon_b - \varepsilon_c) \cos \phi \sin \theta \cos \theta \quad (\text{A.15f})$$

Substituting  $\varepsilon_{ij}$  from equations (A.15) into equation (A.9) the matrix  $\Delta$  can be obtained in terms of  $\varepsilon_a, \varepsilon_b, \varepsilon_c$  and angles  $\phi, \theta$ . Analytical solution for eigenvalues and eigenvectors for matrix  $\Delta$  can be found only in simple cases like uniaxial layer (liquid crystal<sup>[123]</sup>) and tilted biaxial layer (with  $\phi = \pi/2$  <sup>[124]</sup>). However, with presence of digital computer there is no need in such analytical expression of eigenvalues and eigenvectors. From a given  $N_0, \alpha_0, \varepsilon_a, \varepsilon_b, \varepsilon_c, \phi$  and  $\theta$  one can calculate  $\varepsilon_{ij}$  and  $m$  using equations (A.6) and (A.15) and then the  $\Delta$  matrix using equation (A.9). Eigenvalues and eigenvectors of  $\Delta$  can be then calculated numerically using equations (A.14) and (A.13) respectively.

In a particular case of null ellipsometry, where the sample was considered to have tilted biaxial structure and was aligned in a way that its principal axis corresponding to  $\varepsilon_a$  was horizontal or vertical, the angle  $\phi$  was fixed to two orthogonal positions and was equal to 0 and  $\pi/2$  respectively.

The eigenvectors represent the ordinary and extraordinary waves in the homogeneous biaxial layer. In order to obtain layer matrix  $L(d)$  in terms of eigenvectors and eigenvalues let's consider several simple matrix manipulations. From the eigenvalue equation (A.13) one

can write:

$$\Delta \cdot \Psi_{kl} = \Psi_{kl} \begin{pmatrix} q_1 & 0 & 0 & 0 \\ 0 & q_2 & 0 & 0 \\ 0 & 0 & q_3 & 0 \\ 0 & 0 & 0 & q_4 \end{pmatrix} \quad (A.16)$$

Using equation (A.11) one can write:

$$L(d) \cdot \Psi_{kl} = e^{n \cdot \Delta} \cdot \Psi_{kl} \quad (A.17)$$

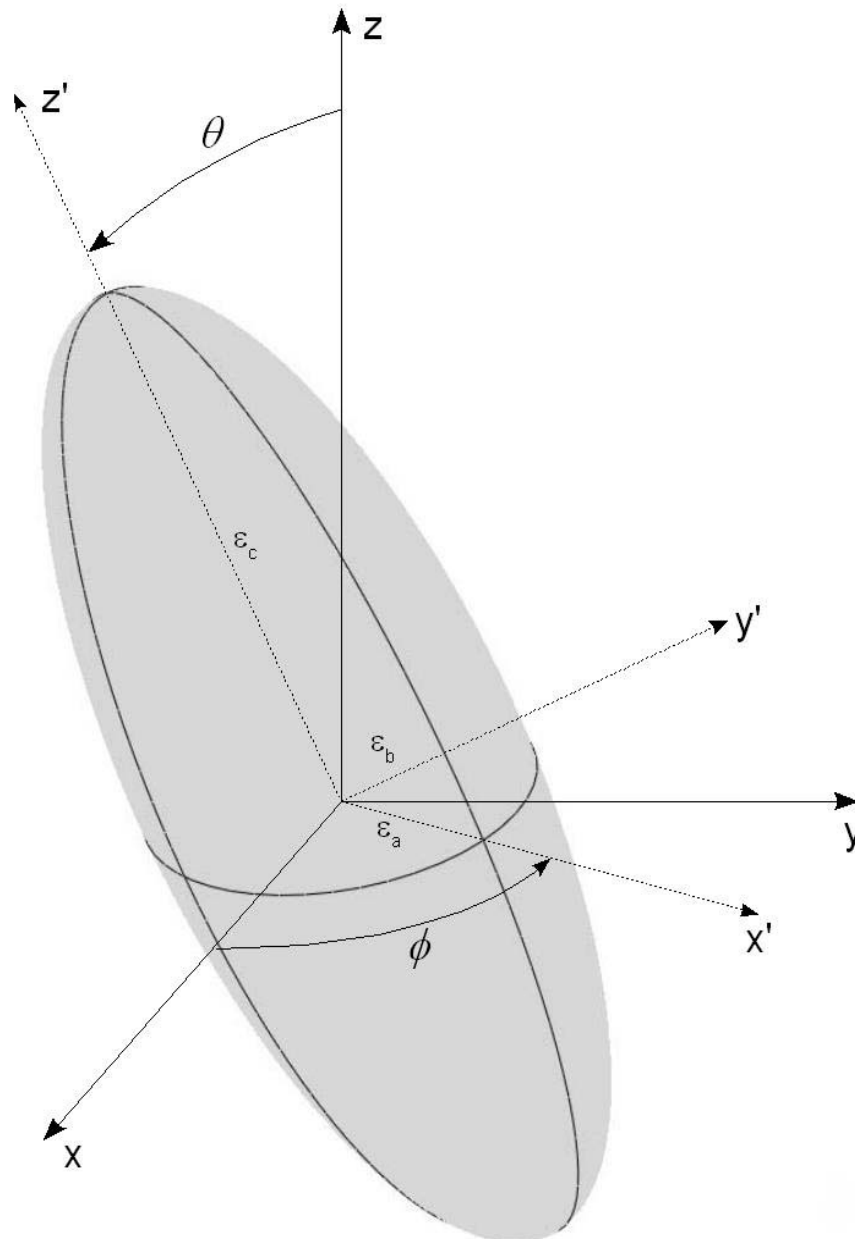


**Fig. A.2: Definition of angles for optical dielectric tensor (based on Euler angles).**

## Appendix

where  $\eta = -ik_0 d$  and the  $\Delta$  matrix is given by equation (A.9). Expanding the exponential in a series form one can get:

$$L(d) \cdot \Psi_{kl} = e^{\eta \Delta} \cdot \Psi_{kl} = \left(1 + \eta \frac{\Delta}{1!} + \eta^2 \frac{\Delta \Delta}{2!} + \dots\right) \Psi_{kl} = \left(\Psi_{kl} + \eta \frac{\Delta}{1!} \Psi_{kl} + \eta^2 \frac{\Delta \Delta}{2!} \Psi_{kl} + \dots\right) = \quad (A.18)$$

$$= \left(\Psi_{kl} + \frac{\eta}{1!} \Psi_{kl} \begin{pmatrix} q_1 & 0 & 0 & 0 \\ 0 & q_2 & 0 & 0 \\ 0 & 0 & q_3 & 0 \\ 0 & 0 & 0 & q_4 \end{pmatrix} + \frac{\eta^2}{2!} \Psi_{kl} \begin{pmatrix} q_1 & 0 & 0 & 0 \\ 0 & q_2 & 0 & 0 \\ 0 & 0 & q_3 & 0 \\ 0 & 0 & 0 & q_4 \end{pmatrix} \begin{pmatrix} q_1 & 0 & 0 & 0 \\ 0 & q_2 & 0 & 0 \\ 0 & 0 & q_3 & 0 \\ 0 & 0 & 0 & q_4 \end{pmatrix} + \dots\right) = \quad (A.19)$$

$$= \Psi_{kl} \left( I + \frac{\eta}{1!} \begin{pmatrix} q_1 & 0 & 0 & 0 \\ 0 & q_2 & 0 & 0 \\ 0 & 0 & q_3 & 0 \\ 0 & 0 & 0 & q_4 \end{pmatrix} + \frac{\eta^2}{2!} \begin{pmatrix} q_1 & 0 & 0 & 0 \\ 0 & q_2 & 0 & 0 \\ 0 & 0 & q_3 & 0 \\ 0 & 0 & 0 & q_4 \end{pmatrix} \begin{pmatrix} q_1 & 0 & 0 & 0 \\ 0 & q_2 & 0 & 0 \\ 0 & 0 & q_3 & 0 \\ 0 & 0 & 0 & q_4 \end{pmatrix} + \dots \right). \quad (A.20)$$

Manipulating the components of the matrices one ends up with:

$$L(d) \cdot \Psi_{kl} = \Psi_{kl} \begin{pmatrix} e^{\eta q_1} & 0 & 0 & 0 \\ 0 & e^{\eta q_2} & 0 & 0 \\ 0 & 0 & e^{\eta q_3} & 0 \\ 0 & 0 & 0 & e^{\eta q_4} \end{pmatrix} \quad (A.21)$$

$$\Rightarrow L(d) \cdot \Psi_{kl} \cdot \Psi_{kl}^{-1} = \Psi_{kl} \begin{pmatrix} e^{\eta q_1} & 0 & 0 & 0 \\ 0 & e^{\eta q_2} & 0 & 0 \\ 0 & 0 & e^{\eta q_3} & 0 \\ 0 & 0 & 0 & e^{\eta q_4} \end{pmatrix} \cdot \Psi_{kl}^{-1} \quad (A.22)$$

$$\Rightarrow L(d) = \Psi_{kl} \begin{pmatrix} e^{\eta q_1} & 0 & 0 & 0 \\ 0 & e^{\eta q_2} & 0 & 0 \\ 0 & 0 & e^{\eta q_3} & 0 \\ 0 & 0 & 0 & e^{\eta q_4} \end{pmatrix} \cdot \Psi_{kl}^{-1} \quad (A.22)$$

The expression of the layer matrix  $L(d)$  can be can be rewritten in the form:

$$L(d) = \Psi_{kl} K(d) \Psi_{kl}^{-1} \quad (A.23)$$

where  $K(d)$  is a diagonal matrix with elements determined by the eigenvalues  $q_l$

$$K_{ll}(d) = e^{-ik_0 d q_l}, \quad l = 1, 2, 3, 4. \quad (A.24)$$

Propagation matrix  $L(d)$  of the whole system including substrate can be calculated by simple matrix multiplication using equation (A.12). Once the propagation matrix is known the reflection and transmission coefficients can be calculated by the following procedure.

Let's consider the components  $(E_{ip}, E_{is})$ ,  $(E_{rp}, E_{rs})$  and  $(E_{tp}, E_{ts})$  of the electric field vectors of the incident, reflected, and the transmitted waves, respectively, parallel (p) and perpendicular (s) to the plane of incidence. In a nonmagnetic optically isotropic medium,



## Appendix

the magnetic field components are simply related to their associated orthogonal electric field components through the index of refraction  $N$ :

$$H_p / E_s = H_s / E_p = N \quad (\text{A.25})$$

Thus, using equations (A.9) and (A.25), the three generalized field vectors  $\psi_i$ ,  $\psi_r$ , and  $\psi_t$  of the incident, reflected, and transmitted waves, respectively, can be calculated from the p and s electric field components alone, without explicit reference to the magnetic field components:

$$\psi_i(0^-) = \begin{pmatrix} E_{ip} \cos \alpha_0 \\ N_0 E_{ip} \\ E_{is} \\ N_0 E_{is} \cos \alpha_0 \end{pmatrix}, \quad \psi_r(0^-) = \begin{pmatrix} -E_{rp} \cos \alpha_0 \\ N_0 E_{rp} \\ E_{rs} \\ -N_0 E_{rs} \cos \alpha_0 \end{pmatrix}, \quad \psi_t(d^+) = \begin{pmatrix} E_{tp} \cos \alpha_0 \\ N_0 E_{tp} \\ E_{ts} \\ N_0 E_{ts} \cos \alpha_0 \end{pmatrix}. \quad (\text{A.26})$$

The condition of matching the generalized fields vector  $\psi$  across the  $z=0$  interface can be put in the form:

$$\psi(0^+) = \psi_i(0^-) + \psi_r(0^-) \quad (\text{A.27})$$

The total field at the output of the sample is due to a single transmitted plane wave, and matching the generalized fields vector  $\psi$  across the  $z=d$  interface leads to:

$$\psi(d^-) = \psi_t(d^+) \quad (\text{A.28})$$

The internal fields inside the layer at  $z=0$  and  $z=d$  are subsequently interrelated by the layer matrix  $L(d) = l_{ij}$  according to equation (A-10). The resulting equation reads:

$$\begin{pmatrix} E_{ip} \cos \alpha_0 \\ N_0 E_{ip} \\ E_{is} \\ N_0 E_{is} \cos \alpha_0 \end{pmatrix} = \begin{pmatrix} l_{11} & l_{12} & l_{13} & l_{14} \\ l_{21} & l_{22} & l_{23} & l_{24} \\ l_{31} & l_{32} & l_{33} & l_{34} \\ l_{41} & l_{42} & l_{43} & l_{44} \end{pmatrix} \begin{pmatrix} (E_{ip} - E_{rp}) \cos \alpha_0 \\ N_0 (E_{ip} + E_{rp}) \\ (E_{is} + E_{rs}) \\ N_0 (E_{is} - E_{rs}) \cos \alpha_0 \end{pmatrix}. \quad (\text{A.29})$$

Equation (A.29) can further be resolved to give relations between reflected (or transmitted) components and incident components in the form:

$$\begin{pmatrix} E_{rp} \\ E_{rs} \end{pmatrix} = \begin{pmatrix} R_{pp} & R_{ps} \\ R_{sp} & R_{ss} \end{pmatrix} \begin{pmatrix} E_{ip} \\ E_{is} \end{pmatrix}; \quad \begin{pmatrix} E_{tp} \\ E_{ts} \end{pmatrix} = \begin{pmatrix} T_{pp} & T_{ps} \\ T_{sp} & T_{ss} \end{pmatrix} \begin{pmatrix} E_{ip} \\ E_{is} \end{pmatrix}. \quad (\text{A.30})$$

The complex-amplitude reflection and transmission matrices can be calculated as follows:

$$R_{pp} = (a_{ip} b_{rs} - a_{rs} b_{ip})(a_{rs} b_{rp} - a_{rp} b_{rs})^{-1}; \quad (\text{A.31a})$$

$$R_{ps} = (a_{is} b_{rs} - a_{rs} b_{is})(a_{rs} b_{rp} - a_{rp} b_{rs})^{-1}; \quad (\text{A.31b})$$

$$R_{sp} = (a_{rp} b_{ip} - a_{ip} b_{rp})(a_{rs} b_{rp} - a_{rp} b_{rs})^{-1}; \quad (\text{A.31c})$$

$$R_{ss} = (a_{rp} b_{is} - a_{is} b_{rp})(a_{rs} b_{rp} - a_{rp} b_{rs})^{-1}; \quad (\text{A.31d})$$

## Appendix

$$T_{pp}=[l_{21} \cos \alpha_0 + l_{22} N_0 + R_{pp}(-l_{21} \cos \alpha_0 + l_{22} N_0) + R_{sp}(l_{23} - l_{24} N_0 \cos \alpha_0)]/N_0 ; \quad (A.31e)$$

$$T_{ps}=[l_{23} + l_{24} N_0 \cos \alpha_0 + R_{ps}(-l_{21} \cos \alpha_0 + l_{22} N_0) + R_{ss}(l_{23} - l_{24} N_0 \cos \alpha_0)]/N_0 ; \quad (A.31f)$$

$$T_{sp}=l_{31} \cos \alpha_0 + l_{32} N_0 + R_{pp}(-l_{31} \cos \alpha_0 + l_{32} N_0) + R_{sp}(l_{33} - l_{34} N_0 \cos \alpha_0) ; \quad (A.31g)$$

$$T_{ss}=l_{33} + l_{34} N_0 \cos \alpha_0 + R_{ps}(-l_{31} \cos \alpha_0 + l_{32} N_0) + R_{ss}(l_{33} - l_{34} N_0 \cos \alpha_0) ; \quad (A.31h)$$

where

$$\begin{aligned} a_{ip} &= \frac{+}{-} \cos \alpha_0 (l_{11} N_0 - l_{21} \cos \alpha_0) + N_0 (l_{12} N_0 - l_{22} \cos \alpha_0) ; \\ a_{rp} & \end{aligned} \quad (A.32a)$$

$$\begin{aligned} a_{is} &= \frac{+}{-} N_0 \cos \alpha_0 (l_{14} N_0 - l_{24} \cos \alpha_0) + N_0 (l_{13} N_0 - l_{23} \cos \alpha_0) ; \\ a_{rs} & \end{aligned} \quad (A.32b)$$

$$\begin{aligned} b_{ip} &= \frac{+}{-} \cos \alpha_0 (l_{31} N_0 \cos \alpha_0 - l_{41}) + N_0 (l_{32} N_0 \cos \alpha_0 - l_{42}) ; \\ b_{rp} & \end{aligned} \quad (A.32c)$$

$$\begin{aligned} b_{is} &= \frac{+}{-} N_0 \cos \alpha_0 (l_{34} N_0 \cos \alpha_0 - l_{44}) + N_0 (l_{33} N_0 \cos \alpha_0 - l_{43}) ; \\ b_{rs} & \end{aligned} \quad (A.32d)$$

In the null ellipsometry measurement the dependence of  $\varphi$  on the tilt angle  $\alpha = \alpha_0$  of the sample for two mutually orthogonal positions of one was measured (see section 2.2.4). In order to fit this dependence the transmission matrix  $T$  of the sample should be recalculated into the angle  $\varphi$  of the analyzer which corresponds to minimum light leakage. This angle corresponds to the azimuth of the elliptically polarized light after the compensator with respect to the coordinate system  $x_{-45^\circ}, y_{-45^\circ}$  rotated at the angle  $-45^\circ$  with respect to the reference coordinate system. The Cartesian components of the electric field with respect to this coordinate system are calculated as follows:

$$\begin{pmatrix} E_{x_{-45^\circ}} \\ E_{y_{-45^\circ}} \end{pmatrix} = \begin{pmatrix} 1 & 0 \\ 0 & e^{i\frac{\pi}{2}} \end{pmatrix} \begin{pmatrix} \cos(-45^\circ) & \sin(-45^\circ) \\ -\sin(-45^\circ) & \cos(-45^\circ) \end{pmatrix} \begin{pmatrix} T_{pp} & T_{ps} \\ T_{sp} & T_{ss} \end{pmatrix} \begin{pmatrix} \cos(45^\circ) & \sin(45^\circ) \\ -\sin(45^\circ) & \cos(45^\circ) \end{pmatrix} \begin{pmatrix} 1 \\ 0 \end{pmatrix}. \quad (A.33)$$

It can be simplified to give:

$$E_{x_{-45^\circ}} = (T_{pp} + T_{ss} - T_{sp} - T_{ps})/2 \quad (A.34a)$$

$$E_{y_{-45^\circ}} = i(T_{pp} - T_{ss} + T_{sp} - T_{ps})/2 \quad (A.34b)$$

The azimuth angle is the angle  $\varphi$  measured by the analyzer can be then calculated as follows:

$$\varphi = \frac{1}{2} \tan^{-1} \left( \frac{2 \Re(\chi)}{1 - |\chi|^2} \right), \quad \text{where } \chi = \frac{E_{y_{-45^\circ}}}{E_{x_{-45^\circ}}}. \quad (A.35)$$

---

## Abbreviations and notations

$A_{min}$	Minimum absorbance
$A_{max}$	Maximum absorbance
$A_{\parallel}$	Absorbance parallel to the director of LC
$A_{\perp}$	Absorbance perpendicular to the director of LC
$A_p$	Absorbance of p-polarized light
$A_s$	Absorbance of s-polarized light
$\alpha, \alpha_0$	Angle of incidence
Col <sub>hd</sub>	Disordered Hexagonal Columnar
Col <sub>ho</sub>	Ordered Hexagonal Columnar
Col <sub>rd</sub>	Disordered Rectangular Columnar
Col <sub>ro</sub>	Ordered Rectangular Columnar
Col <sub>t</sub>	Tilted Columnar
$d$	Film thickness
$D$	Dichroism
$\delta_{as}$	Asymmetrical bending or scissoring IR vibration
$\delta_s$	Symmetrical bending or scissoring IR vibration
$DR$	Dichroic ratio
DSC	Differential Scanning Calorimetry
$\varepsilon_{ij}$	Dielectric tensor
$\varepsilon_a, \varepsilon_b, \varepsilon_c$	Principal dielectric constants
$\vec{E}$	Electric field vector
$\vec{H}$	Magnetic field vector
$I_F$	Integrated absorbance of the band in LC phase
$I_I$	Integrated absorbance of the band in isotropic phase
IR	Infrared
ISA	Ionic Self-Assembly
$\varphi$	Angle of analyzer (in null ellipsometry)
$k_0$	Wave vector in free space
$\lambda$	Wavelength
LC	Liquid Crystal
LCD	Liquid Crystalline Display

---

$\vec{n}$	Director of LC
$n_x, n_y, n_z$	Principal refractive indexes
$\nu_{as}$	Asymmetrical stretching IR vibration
$\nu_s$	Symmetrical stretching IR vibration
$N_{col}$	Nematic Columnar
$N_D$	Nematic Discotic
$\vec{p}_i$	Transition dipole moment vector
PLM	Polarized Light Microscopy
$\rho$	In-plane rocking IR vibration
$R_i$	Dichroic ratio for unpolarized light
$s$	Scattering vector
$S$	Order parameter
SAXS	Small-Angle X-ray Scattering
SmA	Smectic A
SmB	Smectic B
SmC	Smectic C
SmE	Smectic E
SmF	Smectic F
SmH	Smectic H
SmI	Smectic I
$\tau$	Out-of-plane twisting IR vibration
$\omega$	Out-of-plane wagging IR vibration
WAXS	Wide-Angle X-ray Scattering

---

## List of publications

### Related to the work:

- 1) Y. Zakrevskyy, J. Stumpe, C. F. J. Faul.  
A Supramolecular Approach to Optically Anisotropic Materials: Photosensitive Ionic Self-Assembly Complexes.  
*Adv. Mater.*, **18**, 2133 (2006)
- 2) Y. Zakrevskyy, J. Stumpe, B. Smarsly, C. F. J. Faul.  
Photo-induction of optical anisotropy in azobenzene containing ionic self-assembly liquid-crystalline material.  
*Phys. Rev. E*, submitted (2006).
- 3) Y. Zakrevskyy, B. Smarsly, J. Stumpe, C. F. J. Faul.  
Highly ordered monodomain ionic self-assembly liquid-crystalline materials.  
*Phys. Rev. E*, **71**, 021701 (2005).
- 4) Y. Zakrevskyy, C. F.J. Faul, J. Stumpe.  
Film forming photosensitive materials for the light induced generation of optical anisotropy.  
*EP 05009865.6* (2005)
- 5) Y. Zakrevskyy, C. F.J. Faul, Y. Guan, J. Stumpe.  
Alignment of a Perylene-Based Ionic Self-Assembly Complex in Thermotropic and Lyotropic Liquid-Crystalline Phases.  
*Adv. Func. Mater.*, **14**, 835 (2004).
- 6) Y. Guan, Y. Zakrevskyy, J. Stumpe, M. Antonietti, C. F. J. Faul.  
Perylenediimide-surfactant complexes: Thermotropic Liquid-Crystalline Materials via Ionic Self-Assembly.  
*Chem Comm.*, 894 (2003).

### Other publications:

- 7) S. Nešpůrek, Y. Zakrevskyy, J. Stumpe, B. Sapich, A. Kadashchuk.  
Alignment of liquid crystals on poly[methyl(phenyl)silylene] films treated with polarized UV light.  
*Macromolecules*, **39(2)**, 690 (2006).
- 8) S. Nešpůrek, G. Wang, D. Rais, J. Rakušan, M. Karáskova, J. Stumpe, Y. Zakrevskyy.  
Polarized Phthalocyanine Electroluminescence Diodes Prepared on Polysilane Films Treated with Polarized light.  
*Mol.Cryst.Liq.Cryst.*, in print (2006).
- 9) D. Rais, Y. Zakrevskyy, J. Stumpe, S. Nešpůrek, Z. Sedláková.  
Photoorientation of azobenzene side groups in a liquid crystalline polybutadiene based polymer.  
*Opt. Mater.*, in print (2006).
- 10) D. Rais, S. Nešpůrek, Y. Zakrevskyy, J. Stumpe, Z. Sedláková, M. Studenovský.

- 
- Photo-orientation in azobenzene containing polybutadiene based polymer.  
*J. Optoelect. Adv. Mat.*, **7(3)**, 34 (2005).
- 11) O. Yaroshchuk, Yu. Zakrevskyy, S. Kumar, J. Kelly, L.-C. Chien, and J. Lindau.  
Three-dimensional orientational order in the bulk and on the surface of polymer films and its effect on liquid-crystal alignment.  
*Phys. Rev. E*, **69**, 011702 (2004).
  - 12) O. Yaroshchuk, M. Dupont, Y. Zakrevskyy, T. Bidna, J. Lindau.  
Molecular structure of azopolymers and photoinduced 3D orientational order. 1. Azobenzene polyesters.  
*J. Phys. Chem. B*, **108**, 4647 (2004).
  - 13) E. Schab-Balcerzak, D. Sek, B. Jarzabek, Y. Zakrevskyy, J. Stumpe.  
New soluble polyimides containing the hydroxylic group. II: Polymers substituted with Disperse Red 1.  
*High Performance Polymers*, **16**, 585 (2004).
  - 14) O. Yaroshchuk, A. Kiselev, Y. Zakrevskyy, T. Bidna, J. Kelly, L. C. Chien, J. Lindau.  
Photoinduced three-dimensional orientational order in side chain liquid crystalline polymers.  
*Phys. Rev. E*, **68**, 011803 (2003).
  - 15) O. Yaroshchuk, Y. Zakrevskyy, R. Kravchuk, A. Dobrovolsky, A. Pavlov.  
Liquid crystal alignment on the polymer substrates irradiated by plasma beam.  
*Proc. SPIE*, **4418**, 49 (2001).
  - 16) Y. Zakrevskyy, O. Yaroshchuk, J. Kelly, L.-C. Chien, J. Lindau.  
3D orientational order in the photoaligning polymer films and its correlation with LC alignment.  
*Mol. Cryst. Liq. Cryst.*, **375**, 769 (2002).
  - 17) S. Zakrevska, Y. Zakrevskyy, A. Nych, O. Yaroshchuk, U. Maschke.  
Electro-optics of LC-Aerosil-Photopolymer composites.  
*Mol. Cryst. Liq. Cryst.*, **375**, 467 (2002).
  - 18) O. Yaroshchuk, A. Kiselev, Y. Zakrevskyy, J. Stumpe, J. Lindau.  
Spatial reorientation of azobenzene side groups of a liquid crystalline polymer induced by linearly polarized light.  
*Eur. Phys. J. E*, **6(1)**, 57 (2001).
  - 19) V. Syromyatnikov, L. Vretik, O. Yaroshchuk, Y. Zakrevskyy, T. M. Kim, J. H. Jo, J. Y. Kim, S. H. Kim.  
Naphthalene containing polymers as new photoaligning materials for LCs.  
*Mol. Cryst. Liq. Cryst.*, **368**, 4311 (2001).
  - 20) Y. Zakrevskyy, O. Yaroshchuk, J. Stumpe, J. Lindau, T. Sergan, J. Kelly.  
3D orientational order in a homologous series of LC polyesters with azobenzene side groups and different lengths of the alkylene spacer in the main chain.  
*Mol. Cryst. Liq. Cryst.*, **365**, 1371 (2001).

- 
- 21) O. Yaroshchuk, Y. Zakrevskyy, A. Tereshchenko, I. Shanski.  
3D orientational structures in azopolymers studied by UV absorption method.  
*Mol. Cryst. Liq. Cryst.*, **361**, 187 (2001).
  - 22) O. Yaroshchuk, D. M. G. Agra, Y. Zakrevskyy, L.-C. Chien, J. Lindau, S. Kumar.  
Anisotropic surface morphology of azopolymer films generated by polarized UV light irradiation.  
*Liq. Cryst.*, **28(5)**, 703 (2001).
  - 23) A. Kiselev, O. Yaroshchuk, Y. Zakrevskyy, A. Tereshchenko.  
On biaxiality of photoinduced structures in azopolymer films.  
*Cond. Matter Phys.*, **4(1)**, 67 (2001).
  - 24) O. Yaroshchuk, A. Kiselev, J. Lindau, V. Reshetnyak, A. Tereshchenko, Y. Zakrevskyy.  
Effect of bulk orientational ordering on nematic-LC polymer interface.  
*Ukr. fiz. zhurn.*, **46(4)**, 449 (2001).

Conference contributions related to the work:

- 1) Y. Zakrevskyy, C. F.J. Faul, Y. Guan, J. Stumpe.  
New Liquid-Crystalline Materials Through Ionic Self-Assembly: Phase Characterization and Alignment Properties.  
“32. Arbeitstagung Flüssigkristalle”, March 24-26, 2004, Halle, Germany.
- 2) Y. Zakrevskyy, C. F.J. Faul, J. Stumpe.  
Liquid crystallinity and alignment of a perylene-based ionic self-assembled complex.  
“20th International Liquid Crystal Conference”, July 4-9, 2004, Ljubljana, Slovenia.
- 3) Y. Zakrevskyy, J. Stumpe, B. Smarsly, C. F. J. Faul.  
Liquid crystallinity and alignment of a perylene-based ionic self-assembled complex.  
“8th European Conference on Liquid Crystals”, February 27 – March 4, 2005, Sesto, Italy.

## References

---

- [1] *Smectic Liquid Crystals. Textures and Structures*. G. W. Gray and J. W. G. Goodby (Leonard Hill, Glasgow, 1984).
- [2] *Handbook of Liquid Crystals*, edited by D. Demus, J. Goodby, G. W. Gray, H.-W. Spiess, and V. Vill (Wiley-VCH, Weinheim, 1998).
- [3] R. J. Bushby and O. R. Lozman, *Curr. Opin. Colloid Interface Sci.* **7**, 343 (2002).
- [4] *Liquid Crystals. Applications and Uses*, edited by B. Bahadur (World Scientific, Singapore, 1990).
- [5] D. Demus and A. Hauser, in *Selected Topics in Liquid Crystal Research*, edited by H.-D. Koswig (Akademie-Verlag, Berlin, 1990), p.19.
- [6] *The Physics of Liquid Crystals*, P. G. de Gennes and J. Prost (Oxford University Press, New York, 1995).
- [7] W. Sipula, M. Kastler, D. Wasserfallen, T. Pakula, and K. Muellen, *J. Am. Chem. Soc.* **126**, 8074 (2004).
- [8] M. Gharbia, A. Gharbi, H. T. Nguyen, and J. Malthete, *Curr. Opin. Colloid Interface Sci.* **7**, 312 (2002).
- [9] C. T. Imrie and P. A. Henderson, *Curr. Opin. Colloid Interface Sci.* **7**, 298 (2002).
- [10] *The Aqueous Phase Behavior of Surfactants*. R. G. Laughlin (Academic Press, London, 1994).
- [11] D. Attwood. *Adv. Colloid Interface Sci.* **55**, 271 (1995).
- [12] N. H. Hartshorne, G. D. Woodard. *Mol. Cryst. Liq. Cryst.* **23**, 347 (1973).
- [13] C. Tschierske. *Curr. Opin. Colloid Interface Sci.* **7**, 355 (2002).
- [14] S. A. Hudson, P. Maitlis. *Chem. Rev.* **93**, 861 (1993).
- [15] *Metallomesogens*. J. L. Serrano (VCH, Weinheim, 1996).
- [16] B. Donnio. *Curr. Opin. Colloid Interface Sci.* **7**, 371-394 (2002).
- [17] V. Percec, M. Glodde, T. K. Bera, et al., *Nature* **419**, 384 (2002).
- [18] T. Kato, N. Mizoshita, and K. Kanie, *Macromol. Rapid Commun.* **22**, 797 (2001).
- [19] C. Mauguin, *C.R.A.S.* **156**, 1246 (1911).
- [20] M. G. Tomlin, *J. Opt. Technol.* **64**, 458 (1997)
- [21] J. L. Janning, *Appl. Phys. Lett.* **21**, 173 (1972).
- [22] D. Berreman, *Phys. Rev. Lett.* **28**, 1683 (1972).
- [23] W. Urbach, M. Boix, E. Guyon, *Appl. Phys. Lett.* **25**, 479 (1974).
- [24] *Electro-optical and magneto-optical properties of liquid crystals*. L. M. Blinov (John Wiley and Sons Ltd., Singapore, 1983).
- [25] K. Ichimura, Y. Suzuki, T. Seki, A. Hosoki, K. Aoki, *Langmuir*, **4**, 1241 (1988).



## References

---

- [26] W. M. Gibbons, P. J. Shannon, T. S. Sun, B. J. Swetlin, *Nature*, **351**, 49 (1991).
- [27] K. Ichimura, H. Akiyama, N. Ishizuki, Y. Kawanishi, *Macromol. Rapid Commun*, **14**, 813 (1993).
- [28] X. T. Li, A. Natansohn, P. Rochon, *Appl. Phys. Lett.*, **74**, 3791 (1999).
- [29] A. Dyadyusha, V. Kozimkov, T. Marusii, Y. Reznikov, V. Reshetnyak, A. Khizhnyak, *Ukr. Fiz. Zh.* **36**, 1059 (1991).
- [30] M. Schadt, K. Schmitt, V. Kozinkov, V. G. Chigrinov, *Japan. J. Appl. Phys.* **31**, 2135 (1992).
- [31] M. Hasegawa, Y. Taira, *J. Photopol. Sci. Technol.* **8**, 241 (1995).
- [32] M. O'Neil, S. M. Kelly, *J. Phys. D: Appl. Phys.* **33**, R67 (2000).
- [33] K. Ichimura, *Chem. Rev.* **100**, 1847 (2000).
- [34] O. Yaroshchuk, A.D. Kiselev, Y. Zakrevskyy, J. Stumpe, J. Lindau, *Eur. Phys. J. E* **6**, 57 (2001).
- [35] I. K. Iverson, S. M. Casey, W. Seo, S.-W. Tam-Chang, *Langmuir* **18**, 3510 (2002).
- [36] I. K. Iverson, S.-W. Tam-Chang, *J. Am. Chem. Soc.*, **121**, 5801 (1999).
- [37] S.-W. Tam-Chang, W. Seo, I. K. Iverson, S. M. Casey, *Angew. Chem. Int. Ed.* **42(8)**, 897 (2003).
- [38] L. Ignatov, P. Lazarev, N. Ovchinnikova, *Society for Information Display, Int. Symp. Digest of Technical Papers*, Long Beach, California May 16-18, **XXXI**, 834 (2000).
- [39] A. Dembo, A. Ionov, P. Lazarev, A. Manko, V. Nazarov, *Mol. Cryst. Liq. Cryst.* **14**, 275 (2001).
- [40] K. Kawata. Abstract book of *ILCC-2002*, Edinburgh, UK, 30 June-5 July, I 17, (2002).
- [41] T. Sergan, J. Kelly, *Liq. Cryst.* **27(11)**, 1481 (2000).
- [42] A. Tracz, J. K. Jeszka, M. D. Watson, W. Pisula, K. Müllen, T. Pakula, *J. Am. Chem. Soc.* **125**, 1682 (2003).
- [43] J. M. Lehn. *Supramolecular Chemistry: Concepts and perspectives* (WILEY-VCH, Weinheim, 1995).
- [44] O. Ikkala, G. ten Brinke, *Science* **295**, 2407 (2002).
- [45] J. S. Moore. *Curr. Opin. Solid State Mater. Sci.* **1**, 777 (1966).
- [46] J. C. Macdonald, G. M. Whitesides, *Chemical Reviews* **94**, 2383 (1994).
- [47] J. M. Lehn, *Angew. Chem. Int. Ed.* **29**, 1304 (1990).
- [48] M. W. Hosseini, *Coordination Chemistry Reviews* **240**, 157 (2003).
- [49] C. F. J. Faul, M. Antonetti, *Adv. Mater.* **15(9)**, 673 (2003).
- [50] E. D. Goddard, *Colloids Surf.* **19**, 301 (1986).

## References

---

- [51] C. F. J. Faul, M. Antonetti, *Chem. Eur. J.* **8**, 2764 (2002).
- [52] K. Binnemans, *Chem. Rev.* **105**, 4148 (2005).
- [53] S. Ujiie, K. Imura, *Macromolecules* **25**, 3174 (1992).
- [54] C. G. Bazuin, A. Tork, *Macromolecules* **28**, 8877 (1995).
- [55] A. F. Thünemman, D. Ruppelt, S. Ito, K. Müllen, *J. Mater. Chem.* **9**, 1055 (1999).
- [56] Y. Guan, C. F. J. Faul, M. Antonetti, *Langmuir* **18**, 5939 (2002).
- [57] <http://www.mpikg-golm.mpg.de/kc/faul/>
- [58] O.V. Yaroshchuk, A. D. Kiselev, Y. Zakrevskyy, T. Bidna, J. Kelly, L.-C. Chien, and J. Lindau, *Phys. Rev. E* **68**, 011803 (2003).
- [59] D. W. Berreman, *J. Opt. Soc. Am.* **62**, 502 (1972).
- [60] *Ellipsometry and Polarized Light*. R. M. A. Azzam, N. M. Bashara (Elsevier Science Publishers B. V., Amsterdam, 1999).
- [61] T. S. Perova, J. K. Vij, and A. Kocot, *Adv. Chem. Phys.* **113**, 341 (2000).
- [62] V. D. Neff, L. W. Gulrich, G. H. Brown, *Mol. Cryst.* **1**, 225 (1966).
- [63] G. Kruk, A. Kocot, R. Wrzalik, J. K. Vij, O. Karthaus, H. Ringsdorf. *Liq. Cryst.* **14(3)**, 804 (1993).
- [64] S. Chandrasekhar, B. K. Sadishiva, and K. A. Suresh, *Pramana* **9(5)**, 471 (1977).
- [65] M. L. Bushey, A. Hwang, P. W. Stephens, and C. Nuckolls, *J. Am. Chem. Soc.* **123**, 8157 (2001).
- [66] T. Q. Nguyen, M. L. Bushey, L. E. Brus, and C. Nuckolls, *J. Am. Chem. Soc.* **124**, 15051 (2002).
- [67] M. L. Bushey, A. Hwang, P. W. Stephens, and C. Nuckolls, *Ang. Chem. Int. Ed.* **41**, 2828 (2002).
- [68] L. Eshdat, R. E. Hoffman, A. Fechtenkoetter, K. Muellen, and M. Rabinovitz, *Chem. Eur. J.* **9**, 1844 (2003).
- [69] I. Dierking, *Textures of Liquid Crystals* (Wiley-VCH, Weinheim, 2003).
- [70] P. Mariani, F. Rustichelli, and G. Torquati, in *Physics of liquid crystalline materials*, edited by I.-C. Khoo (OPA B. V., Amsterdam, 1991).
- [71] W. Ruland and B. Smarsly, *J. Appl. Cryst.* **37**, 575 (2004).
- [72] W. Ruland, *Colloid Polym. Sci.* **255**, 417 (1977).
- [73] The small additional maxima around  $\pm 1.5^\circ$  in this experimental setup correspond to reflections originating from the Si wafer.
- [74] *CRC Handbook of Chemistry and Physics*, 80th edition (CRC Press, Boca Raton, 1999-2000).
- [75] D. W. Van Krevelin, *Properties of polymers* (Elsevier, Amsterdam, 1990).

## References

---

- [76] J. B. Lambert, H. F. Shurvell, D. A. Lightner, and R. G. Cooks, *Introduction to organic spectroscopy* (Macmillan Publishing Company, New York, 1987).
- [77] R. M. Silverstein, G. C. Bassler, and T. C. Morrill, *Spectroscopic Identification of Organic compounds* (John Wiley and Sons Inc, New York, 1994), Chap. 3, pp. 91-164.
- [78] H. F. Shurvell, in *Handbook of vibrational spectroscopy*, edited by J. M. Chalmers and P. R. Griffiths (John Wiley and Sons Ltd, Weinheim, 2002), Vol. 3, pp. 1783-1817.
- [79] J. B. Lambert, H. F. Shurvell, D. A. Lightner, and R. G. Cooks, *Introduction to organic spectroscopy* (Macmillan Publishing Company, New York, 1987), Part 2, pp.133-239.
- [80] L. M. Blinov, *Electro-optical and magneto-optical properties of liquid crystals* (John Wiley and Sons Ltd., New York, 1983).
- [81] H. Mori, Y. Itoh, Y. Nishiura, T. Nakamura, and Y. Shinagawa, *Jpn. J. Appl. Phys.* 36, 143 (1997).
- [82] T. Sergan, M. Sontatki, J. Kelly, and L.-C. Chien, *Mol. Cryst. Liq. Cryst.* 359, 245 (2001).
- [83] H. Langhals, *Heterocycles*, **40**, 477 (1995).
- [84] I. K. Iverson, S. M. Casey, W. Seo, S.-W. Tam-Chang, *Langmuir* **18**, 3510 (2002).
- [85] I. K. Iverson, S.-W. Tam-Chang, *J. Am. Chem. Soc.*, **121**, 5801 (1999).
- [86] S.-W. Tam-Chang, W. Seo, I. K. Iverson, S. M. Casey, *Angew. Chem. Int. Ed.* **42(8)**, 897 (2003).
- [87] L. Ignatov, P. Lazarev, N. Ovchinnikova, *Society for Information Display, Int. Symp. Digest of Technical Papers*, Long Beach, California May 16-18, **XXXI**, 834 (2000).
- [88] A. Dembo, A. Ionov, P. Lazarev, A. Manko, V. Nazarov, *Mol. Cryst. Liq. Cryst.* **14**, 275(2001).
- [89] C. W. Strijk, A. B. Sieval, J. E. Dakhorst, M. van Dijk, P. Kimkes, R. B. M. Koehorst, H. Donker, T. J. Schaafsma, S. J. Picken, A. M. Van de Craats, J. M. Warman, H. Zuilhof, E. J. R. Sudhölter, *J. Am. Chem. Soc.* **122**, 11057 (2000).
- [90] C. D. Dimitrakopoulos, P. R. K. Malenfant, *Adv. Mater.* **14**, 99 (2002).
- [91] V. G. Kozlov, G. Parthasarathy, P. E. Burrows, S. R. Forrest, Y. You, M. E. Thompson, *Appl. Phys. Lett.* **72**, 144 (1998).
- [92] L. Schmidt-Mende, A. Fechtenkötter, K. Müllen, R. D. Friend, J. D. MacKenzie, *Phys. E.* **14**, 263 (2002).
- [93] P. Schouwink, A. H. Schäfer, C. Seidel, H. Fuchs, *Thin Solid Films.* **372**, 163 (2000).
- [94] J. Mizuguchi and K. Tojo, *J. Phys. Chem. B.* **106**, 767 (2002).
- [95] M. Kasha. *Spectroscopy of the Exited State*. Plenum Press: New York, 1976, pp. 337-363.
- [96] I. K. Iverson, S. M. Casey, W. Seo, S.-W. Tam-Chang, *Langmuir* **18**, 3510 (2002).
- [97] S.-G. Liy, G. Sui, R. A. Cormier, R. M. Leblanc, B. A. Gregg, *J. Phys. Chem. B.* **106**, 1307 (2002).
- [98] I. Itoh, A. Tanaka, F. Fukuda, T. Miyamoto, *Liq. Cryst.* **9**, 221 (1991).

## References

---

- [99] H. Bock, W. Helfrich. *Liq. Cryst.* **12**, 697 (1992).
- [100] H. Bock, W. Helfrich. *Liq. Cryst.* **18**, 387 (1992).
- [101] I. K. Iverson, S.-W. Tam-Chang, *J. Am. Chem. Soc.*, **21**, 5801 (1999).
- [102] A. Dembo, A. Ionov, P. Lazarev, A. Manko, V. Nazarov, *Mol. Cryst. Liq. Cryst.* **14**, 275 (2001).
- [103] F. Weigert. *Verh. Phys. Ges.* **21**, 485 (1919).
- [104] B. S. Neporent, O. V. Stolbova. *Opt. Spectrosc.* **10**, 146 (1961).
- [105] T. Todorov, L. Nokolova, and T. Tomova, *Appl. Opt.* **23**, 4309 (1984).
- [106] M. Eich, J. H. Wendorff, B. Reck, H. Ringsdorf, *Macromol. Rapid Commun.* **8**, 59 (1987).
- [107] Th. Fischer, L. Läscher, M. Rutloh, S. Czaplá, J. Stumpe. *Mol. Cryst. Liq. Cryst.* **299**, 293 (1997).
- [108] R. Rosenhauer, Th. Fischer, S. Czaplá, J. Stumpe, A. Vinuales, M. Pinol, J. L. Serrano. *Mol. Cryst. Liq. Cryst.* **364**, 295 (2001).
- [109] C. B. McArdle, The application of Side Chain Liquid crystalline Polymers in *Side Chain Liquid Crystalline Polymers*, edited by C. B. McArdle (Balckie, London, 1989).
- [110] A. Natanson, P. Rochon, Photoinduced Motions in *Azobenzene-Based Polymers in Photorefractive Organic Thin Films*, edited by Z. Sekkat and W. Knoll (Academic Press, Amsterdam, 2002).
- [111] M. O'Neil and S. M. Kelly, *J. Phys. D: Appl. Phys.* **33**, R67 (2000).
- [112] D. Demus and L. Richter, *Textures of Liquid Crystals* (Verlag Chemie, Weinheim, 1978).
- [113] T. Fuhrmann, T. Tsutsui. *Chem. Mater.* **11(8)**, 2226 (1999).
- [114] A. Stracke, J. H. Wendorff, D. Goldmann, D. Janietz, B. Stiller. *Adv. Mater.* **12(4)**, 282 (2000).
- [115] V. Chigrinov, E. Prudnikova, V. Kozenkov, H. Kwok, H. Akiyama, T. Kawara, H. Takada, H. Takatsu. *Liq. Cryst.* **29**, 1321 (2002).
- [116] H. Nakano, T. Takahashi, T. Kadota, Y. Shiota. *Adv. Meter.* **14**, 1157 (2002).
- [117] K. Ichimura. *Chem. Rev.* **100**, 1847 (2000).
- [118] M. Kasha, *Spectroscopy of the Exited State*. 337-363 (Plenum Press, New York, 1976).
- [119] J. Billard, *Thesis*. University of Paris (1966).
- [120] S. Teitler, B. Hennis, *J. Opt. Soc. Am.* **60**, 830 (1970).
- [121] D. W. Berreman, T. J. Scheffer, *Phys. Rev. Lett.* **25**, 577-581 (1970).
- [122] D. W. Berreman, *J. Opt. Soc. Am.* **63**, 1374-1380 (1970).
- [123] K. Eidner, G. Mayer, M. Schmidt, and H. Schmiedel, *Mol. Cryst. Liq. Cryst.* **172**, 191 (1989).
- [124] M. Schubert, *Phys. Rev. B* **53**, 4265 (1996).